KfK 4606
Juli 1989

Proceedings of the Coagulation Workshop 16th - 18th March, 1988 Karlsruhe, Federal Republic of Germany

Edited by:
G. Metzig, W. O. Schikarski
Laboratorium für Aerosolphysik und Filtertechnik

Kernforschungszentrum Karlsruhe

KERNFORSCHUNGSZENTRUM KARLSRUHE
Laboratorium für Aerosolphysik und Filtertechnik

KfK 4606

Proceedings of the Coagulation Workshop

16th - 18th March, 1988
Karlsruhe, Federal Republic of Germany

Sponsored by:
Association for Aerosol Research (GAeF)

Hosted by:
Kernforschungszentrum Karlsruhe

Edited by:
G. Metzig and W.O. Schikarski

Kernforschungszentrum Karlsruhe GmbH, Karlsruhe

Kernforschungszentrum Karlsruhe GmbH
Postfach 3640, 7500 Karlsruhe 1

ISSN 0303-4003

FOREWORD

During March 16 - 18, 1988 a workshop on coagulation was held at the Nuclear Research Center at Karlsruhe,Federal Republic of Germany. The workshop was sponsored by the Association for Aerosol Research (Gesellschaft für Aerosol-forschung - GAeF) and hosted by the Laboratorium für Aerosolphysik und Filtertechnik in the Nuclear Research Center Karlsruhe.

The basis for aerosol science was laid down at the turn of the last century by many researchers, mainly physicists. The first theory of the physics of coagulation was published by Smoluchowski seventy years ago (1). Many investigations on coagulation have been carried out experimentally and theoretically, since. In its continuous series of workshops on fundamental problems in aerosol science GAeF provides a forum for discussion of the state-of-the-art. The coagulation workshop was centered around the problems of mathematical formulation (modelling), new experimental results, and future research needs. The following summary report gives the full text of the papers and the summarizing discussion.A short summary report of the workshop is to be published in the Journal of Aerosol Science.

The editors wish to express their thanks to the participants from the various countries for their contribution in making the workshop successful. Special thanks are offered to the sponsoring society, the Association for Aerosol Research (GAeF), and to the host of the workshop, Nuclear Research Center Karlsruhe, for their support and cooperation.

G. Metzig

W.O. Schikarski

(1) Smoluchowski, M.: Z.f. Phys. Chem., 92, 129 - 168 (1917)

Content

Brownian Coagulation:

Chairman: W.O. Schikarski

MEASUREMENT OF THE COAGULATION FUNCTION FOR FINE PARTICLES THE INFLUENCE OF EXPERIMENTAL CONDITIONS AND OBSERVATION TECHNIQUES

P.E. Wagner
Institut für Experimentalphysik
Universität Wien

1. Introduction

Dynamical changes of aerosols are frequently connected with coagulation. Particularly in the atmosphere coagulation of nucleation mode with accumulation mode particles leads to transformations of aerosol size distributions.

The evolution in time of the aerosol size distribution n(v,t) during coagulation can be described under certain idealizing assumptions by the Population Balance Equation

$$\frac{\partial n(v,t)}{\partial t} = \frac{1}{2} \int_0^v K(u,v-u)\, n(u,t)\, n(v-u,t)\, du - n(v,t) \int_0^\infty K(v,u)\, n(u,t)\, du, \tag{1}$$

where K is the coagulation function.

For the special case of the initial stages of coagulation in a monodispersed aerosol with particle radius a, integration of the Population Balance Equation yields the well-known rate equation

$$\frac{dN}{dt} = -\frac{1}{2} K(a,a)\, N^2 , \tag{2}$$

where N is the total particle number concentration.

2. Dynamical Regimes for Brownian Coagulation

The actual physical processes occuring during coagulation and their dependence on the radii a, b of the colliding particles are described by the Coagulation Function K (a,b). A consistent theoretical expression for K, valid over the whole interesting range of particle radii, is presently not available. Particularly for particles in the transition regime some controversy can be observed in the literature. For practical purposes the semiempirical interpolation formula by Fuchs (1964) is most widely used for the description of thermal (Brownian) coagulation. The dependence of K on the radii of both colliding particles is shown in Fig. 1. It can be seen that K exhibits a minimum for equal-sized particles and increases strongly for unequal particles.

Up to now in most experimental investigations the coagulation of equal-sized particles was considered. In order to show the coagulation in the various regimes, K is frequently plotted as a function of the Knudsen-number. This, however, can lead to some ambiguity, because identical values of Kn can be obtained by chosing various combinations of particle radius and carrier gas pressure. In Fig. 2 the coagulation function K for equal-sized particles is plotted vs. particle radius and gas pressure. It can be seen that at constant gas pressure, e.g. atmospheric pressure, with decreasing particle radius, K first increases (slip flow regime) and after passing through a maximum decreases again (free molecule regime). On the other hand, at constant particle size, K again increases with decreasing gas pressure (slip flow regime), but then approaches a constant limiting value (free molecular limit). Thus there is no unique dependence of the Coagulation Function K on the Knudsen number. This has to be kept in mind particularly if coagulation experiments at constant gas pressure (e.g. Shon et al., 1980; Okuyama et al., 1984) are to be compared with data obtained for constant particle size and varying gas pressure (Wagner and Kerker, 1977).

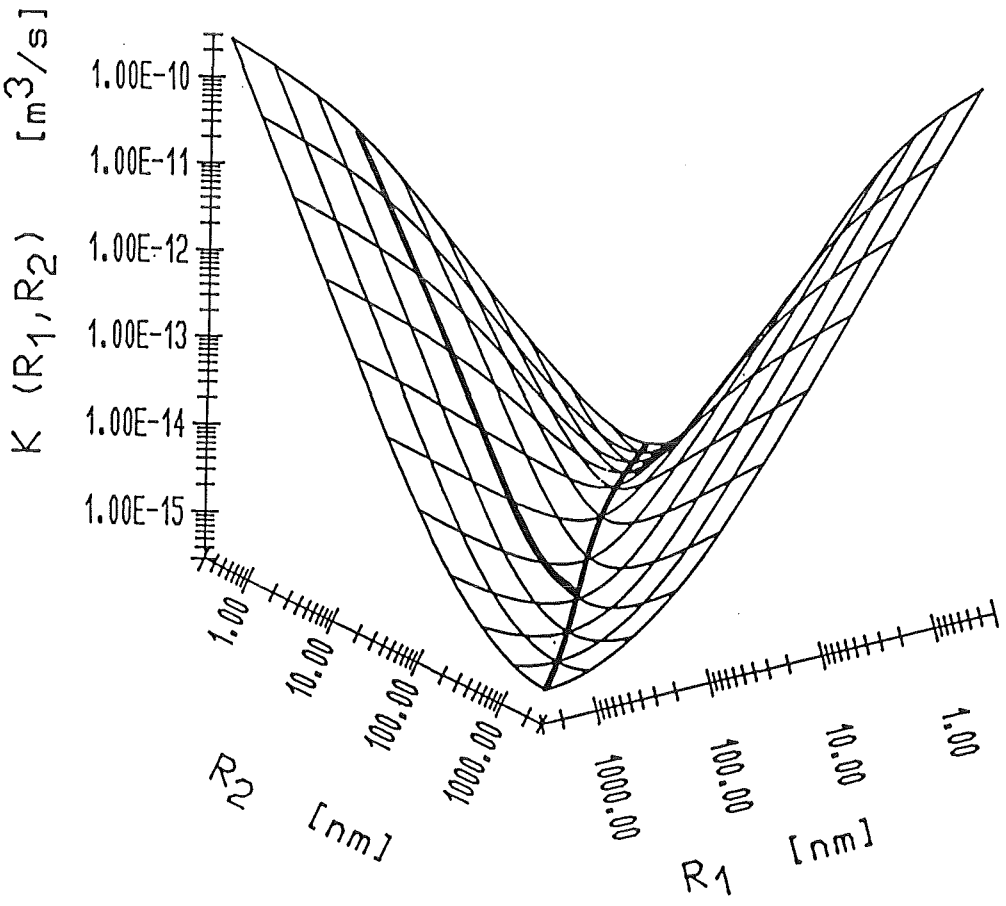

Figure 1. Coagulation function K according to Fuchs (1964) shown vs. the radii of both colliding particles.

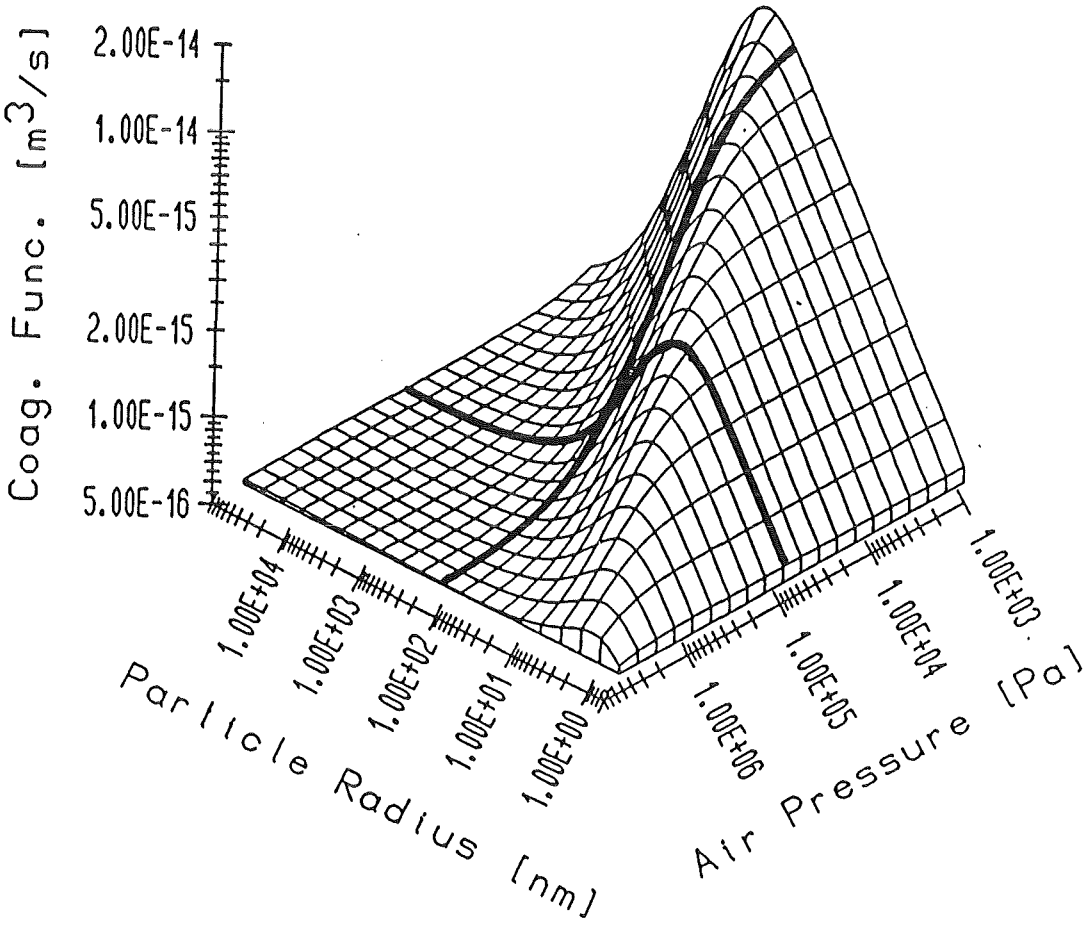

Figure 2. Coagulation function K according to Fuchs (1964) for equal-sized particles shown vs. particle radius and carrier gas pressure. Curves for constant pressure and for constant radius are indicated.

The three-dimensional presentation of K shown vs. particle radius and gas pressure (Figure 3) allows a clear discrimination between the various dynamical regimes for Brownian coagulation. For comparatively large particle radii and gas pressures K is approximately constant and coagulation in the continuum regime (C) is observed. On the other hand, for small particle radii and sufficiently low gas pressures K decreases with decreasing particle radii and is independent of the gas pressure (free molecule regime, FM). Between these limiting regimes a slip flow region (SL) can be observed, where K is uniquely dependent on the Knudsen-Number and increases proportional to the particle diffusivity. The gap between the slip flow region (SL) and the free molecule regime (FM) is bridged by the transition regime (TR), where K exhibits a somewhat more complicated behavior. It should be noted that the slip flow region (SL) is only found below a certain gas pressure, as can be seen in Fig. 3. Beyond this pressure a direct transition from the continuum (C) to the free molecule regime (FM) can be observed.

3. Experimental problems associated with coagulation investigations

Coagulation experiments are generally performed in order to determine the coagulation function K (a,b) for various particle radii a, b. Usually particle number concentrations or size distributions are monitored during coagulation. As can be seen from eq. (1), however, thereby usually only an integral information on the coagulation function K can be obtained. Actual values for K at certain particle radii can only be determined experimentally, if special experimental conditions are chosen so that coagulation of particles with the actually considered sizes is predominant, while coagulation of other particles is of minor importance.

Many phenomena in aerosol science can be studied under conditions, where microphysical (single particle) effects are observed. Under these conditions the aerosol concentration does not directly enter the experimental result and accurate

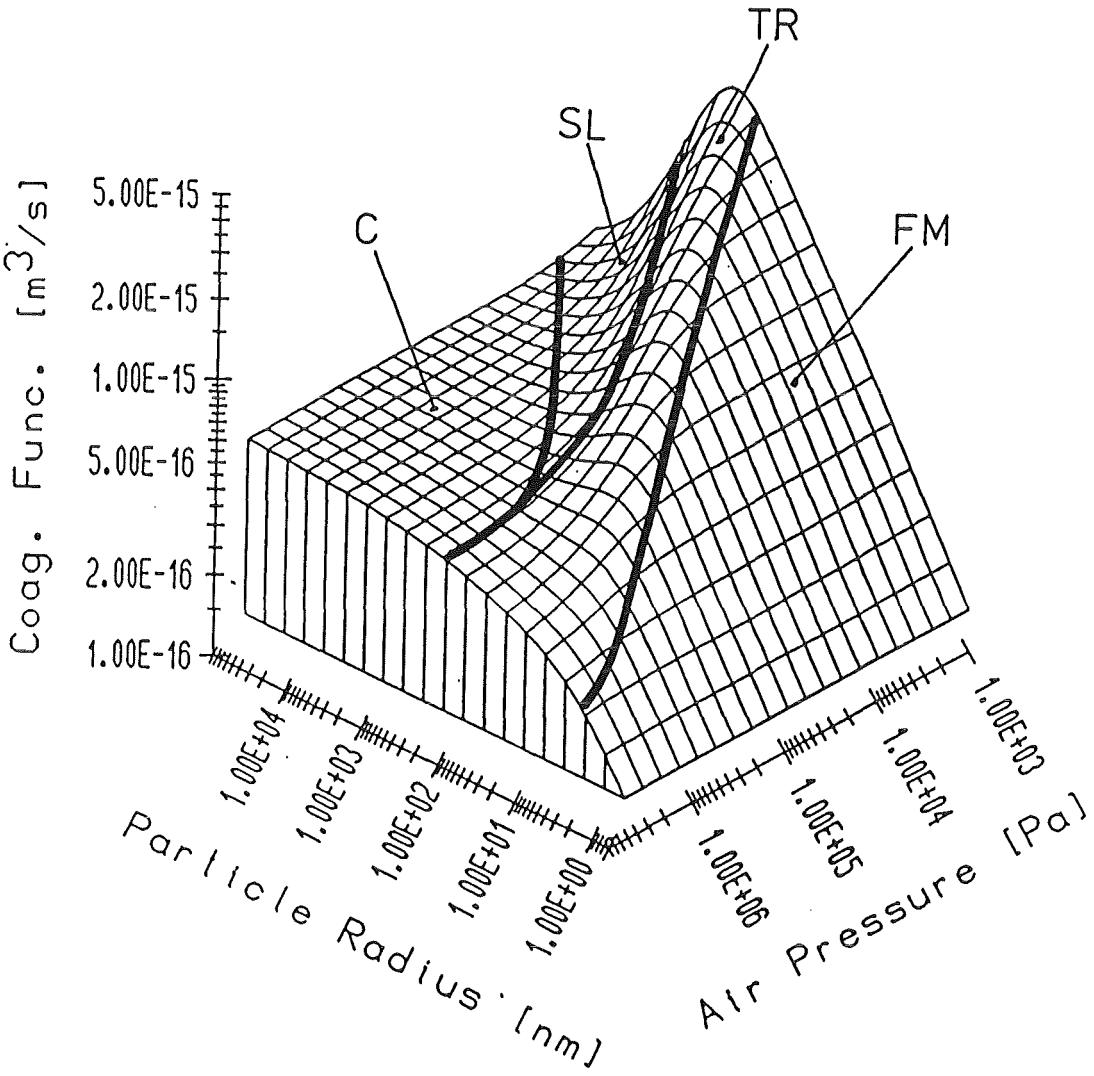

Figure 3. Coagulation function K according to Fuchs (1964) for equal-sized particles shown vs. particle radius and carrier gas pressure. Various dynamical regimes are indicated: C - continuum regime, SL - slip flow regime, TR - transition regime, FM - free molecule regime.

concentration measurements are not required. Coagulation, however, is inherently an aerosol macrophysical (collective) process and accordingly the determination of coagulation functions is directly related to the particle concentration. The accuracy of the experimental results depends on the accurate measurement of particle number concentrations.

As can be seen from eqs. (1), (2), the changes of the particle size distribution depend on the square of the number concentration. As a consequence of this nonlinear dependence spatial inhomogeneities of a coagulating aerosol will generally lead to an increase of the coagulation rate as compared to a corresponding uniform aerosol. Accordingly the occurence of spatial aerosol inhomogeneities can cause an overestimation of the coagulation function.

A typical problem associated with coagulation experiments is caused by the possible simultaneous occurence of other dynamical processes, e.g., diffusion, sedimentation, condensational growth, Ostwald ripening, etc., which have to be taken into account properly. Most of these processes tend to cause similar size distribution changes as coagulation. Accordingly, neglecting these simultaneous processes can lead to a systematic overestimation of the coagulation function.

The theoretical description of aerosol coagulation is frequently restricted to spherical particles, which remain spherical after coagulation has occured. This condition is fulfilled only for liquid particles. In many practically important situations, however, the coagulation of solid particles is observed, which leads to the formation of randomly shaped aggregates. The presence of non-spherical particles, however, is significantly complicating the interpretation of coagulation experiments and the quantitative evaluation of the coagulation function.

4. Conditions for coagulation experiments

In order to facilitate a unique quantitative interpretation of coagulation experiments, a number of conditions should be satisfied. In the following some important conditions are listed.

4.1. Absolute concentration measurement.

As mentioned earlier, the aerosol number concentration is a crucial parameter for coagulation experiments, which enters directly the experimental result. Thus sufficiently accurate absolute concentration measurements are of primary importance. Most of the experimental techniques for absolute number concentration measurement are based on single particle counting and thus restricted to rather low concentrations. Significant coagulation rates, however, are only observed at comparatively high particle concentrations. Therefore a certain dilution of the aerosol considered is usually required before number concentration measurement, which can lead to particle losses and thus introduce significant experimental uncertainties. Absolute concentration measurements can also be performed gravimetrically. The evaluation of the particle number concentration from mass concentration measurement, however, requires accurate knowledge of the particle size distribution, otherwise significant errors may occur. Absolute measurements of aerosol number concentration can be performed by the Constant Angle Mie Scattering (CAMS) method (Wagner, 1985), which is strictly linear over a wide concentration range and does not depend on empirical calibrations relative to external reference standards. The CAMS-method has recently been applied to coagulation experiments (Szymanski et al., 1989).

Particularly for investigations of coagulation in ultrafine aerosols the concentration measurement is complicated by particle losses in the measuring system. If possible particle losses are not properly taken into account, the coagulation function will be systematically overestimated.

4.2. Measurement of particle size distribution.

As can be seen from eq. (1), the coagulation process is sensitively dependent on the particle frequency distribution. Only for the initial stages of coagulation in monodispersed aerosols measurements of the total number concentration are sufficient for determination of the coagulation function (eq. (2)). Usually it is difficult to generate nearly monodispersed aerosols with sufficiently high particle number concentration. Therefore coagulation, particularly in the ultrafine size range, is frequently studied in aerosols with considerably large standard deviations. In this case it is essential to measure the actual frequency size distribution at various stages of the coagulation process. Comparison with corresponding numerical model calculations then yields quantiative information on the coagulation function.

In connection with size distribution measurement it should be emphasized that a unique aerosol size distribution will only be observed, if the coagulating aerosol is spatially uniform. Otherwise the situation will be considerably complicated and non-uniformities will generally lead to an overestimation of the coagulation function. Spatial uniformity of an initially non-uniform aerosol can be achieved by mechanical stirring, however, this will cause velocity gradients and an increase of the coagulation rate due to gradient and turbulent coagulation.

4.3. Absolute measurement of coagulation time.

If the coagulating aerosol is stagnant and contained in a vessel, measurement of the coagulation time is straightforward. However, as mentioned in the next section, it is sometimes advantageous to observe coagulation in a flow system. In this case measurement of the coagulation time requires absolute measurement of the flow velocity of the coagulating aerosol. This measurement should be performed without interfering with the coagulation process. In a steady-state laminar flow system a certain flow velocity profile will develop and hence various residence times will be observed

at different parts of the flow cross section. In order to facilitate a unique interpretation of the experimental results a single, well-defined coagulation time should be considered. Hence the observation of aerosol coagulation in a flowing system should be restricted to a region with nearly constant, uniform flow velocity.

4.4. Narrow size distribution modes.

As mentioned earlier, coagulation experiments generally yield only an integral information on the coagulation function. In order to obtain more specific data on the coagulation function for particular particle sizes, aerosols with comparatively narrow size distributions should be considered. The coagulation function for equal-sized particles can be determined from experiments with monodispersed aerosols. For the determination of coagulation functions for unequal particles coagulation in a mixture of two different nearly monodispersed aerosol fractions can be considered. In this case the evaluation of the coagulation function is simplified if conditions are chosen, under which the coagulation of unequal particles is the predominant effect. Of course, during coagulation in a bimodal aerosol there will always be some contribution by the coagulation of equal-sized particles within each monodispersed fraction. If coagulation within each mode of the bimodal system cannot be neglected, coagulation measurements for each single monodispersed fraction should first be performed in order to determine the corresponding coagulation functions for equal-sized particles. Subsequently a coagulation experiment with the bimodal system will yield a unique information on the corresponding coagulation function for unequal particles.

A meaningful determination of particle size requires knowledge of the particle shape. As mentioned earlier, coagulation of solid particles will generally yield randomly shaped aggregates. Well-defined spherical particles will be obtained for coagulation of liquid particles. However, even for coagulation of solid particles the effect of nonsphericity may be small, if bimodal

systems with strongly different particle sizes are considered, where the coagulation of unequal particles is predominant.

4.5. Suppression of simultaneous processes.

As mentioned earlier, coagulation experiments are generally complicated by various dynamical processes acting simultaneously to coagulation. A unique interpretation of a coagulation experiment can only be achieved, if coagulation is predominant as compared to the competing processes. This condition can generally be fulfilled, if sufficiently high particle number concentrations are chosen, which may, however, lead to some increase of polydispersity. In any case, a detailed analysis of the simultaneous dynamical processes is very important for a valid interpretation of coagulation experiments. In addition to theoretical estimates the simultaneous processes can also be studied experimentally and independent of coagulation. To this end the aerosol considered should be diluted sufficiently with otherwise unchanged conditions, so that coagulation becomes negligible and the combined effect of other processes (diffusion, sedimentation, etc.) can be quantitatively determined.

5. Design of coagulation experiments

Most of the coagulation experiments reported in the literature can be considered either as container or as flow experiments. In container experiments the coagulating aerosol is observed in a vessel at stagnant conditions. Changes of the size distribution during coagulation are monitored by taking aerosol samples at various times. On the other hand, in flow experiments the aerosol considered is passed through a tube at steady-state conditions. Size distributions of the aerosol can be determined for various coagulation times by extracting aerosol samples at different positions along the tube. In the following some important features of container and of flow experiments are discussed.

5.1. Container experiments

The important advantage of container experiments is the straightforward determination of the coagulation time. For the aerosol in the whole vessel there is one absolute and uniform time scale. The time resolution, however, is limited by the actual measuring instrument used. Particularly the measurement of one particle size distribution can take several minutes and thus changes due to coagulation, which are occuring during this time interval, cannot be properly resolved in a container experiment.

In order to prevent significant wall effects during coagulation, usually comparatively large containers are chosen. At large container volumes, however, there is a tendency to spatial non-uniformities of the coagulating aerosol. These non-uniformities can be prevented by sufficient mechanical stirring, however, thereby velocity gradients and turbulence are introduced in the chamber leading to possible changes of the coagulation process.

Another possible disturbance occuring in large vessels is thermal convection. Thereby portions of the aerosol, which are initially adjacent to the walls, can be transported to the center of the vessel causing significant measurement errors.

Finally it should be mentioned that taking of aerosol samples from the vessel will generally lead to a dilution of the aerosol considered. This problem, however, can be avoided at bag experiments.

5.2. Flow experiments

At steady-state flow experiments constant conditions can be observed at each position along the flow tube. This allows a good time resolution regardless of the time required for performing a single aerosol measurement. Furthermore in flow systems usually a good spatial uniformity of the coagulating aerosol can be achieved.

In order to obtain well-defined and uniform coagulation times it is essential that the aerosol samples are only extracted from the axial region of the flow tube in laminar flow. The sample flow must be chosen sufficiently small, otherwise significant disturbances of the aerosol flow would occur. The sampling lines can usually be chosen much shorter than in container experiments and thus significant line losses can be prevented.

For accurate determination of the coagulation time the aerosol flow velocity profile must be measured by an absolute method. In order to prevent disturbances of the aerosol flow, a non-invasive measurement technique, as for example Laser-Doppler velocimetry, should be applied for this purpose.

Finally it should be mentioned that the accuracy of coagulation measurements in a flow system depends on a constant aerosol generation over an extended time period. Therefore it is important to check several times during an experiment, whether the aerosol production remains stable.

6. Summary and comments

Brownian coagulation is one of the most important dynamical processes in aerosols. However, a consistent theory, valid over the entire range of Knudsen-numbers, is presently not available. For most practical applications the semi-empirical flux-matching approach by Fuchs (1964) is used. On the other hand, severe discrepancies between various experimental investigations can be observed in the literature. Some of these discrepancies are probably caused by the fact that coagulation experiments are complicated by various different effects, which can lead to significant experimental errors. In order to minimize systematic experimental errors and to facilitate a unique interpretation of coagulation experiments, a number of experimental conditions should be fulfilled, as dicussed earlier (chapter 4).

Up to now mostly coagulation in monodispersed or nearly monodispersed aerosols has been studied experimentally and thus

the coagulation function has been investigated mostly for equal-sized particles. However, for many practically important applications, e.g., the interaction of nucleation and accumulation mode of atmospheric aerosols, coagulation of particles with different size and chemical composition is of overriding importance.

Much theoretical and experimental work is still required in order to clarify the coagulation of free-molecular aerosols, to determine the quantitative influence of particle interaction forces and to characterize material properties. This topic will be discussed in some detail in the following contribution.

Unfortunately only very little information on the coalescence efficiency for aerosol particles and its possible dependence on particle size and composition is presently available. This situation appears to be similar to the problem of the sticking probability for condensation of vapor molecules to liquid surfaces.

Theoretical treatments of coagulation are, strictly speaking, often restricted to liquid particles, which remain spherical during coagulation. However, in many practically important situations the coagulation of solid particles is encountered, which leads to the formation of non-spherical particles. A theoretical description of these processes, including the influence of shape factors, is complicated and much work remains to be done. Recently the concept of fractal dimension has been used to describe the statistical aggregation of solid particles during aerosol coagulation.

Concluding this review it should be emphasized that a sound basis of accurate experimental data on aerosol coagulation is prerequisite for further theoretical developments.

Acknowledgements

The author is indebted to Mag. A. Majerowicz for his help with the numerical computations.

This work was partly supported by the Fonds zur Förderung der wissenschaftlichen Forschung, Österreich, Proj. Nr. P 7202-PHY and by the Hochschuljubiläumsstiftung der Stadt Wien.

References

FUCHS, N.A. (1964) The Mechanics of Aerosols, Pergamon Oxford, London Edinburg, New York, Paris, Frankfurt,

OKUYAMA, K., KOUSAKA, Y., and HAYASHI, K. (1984) J. Colloid Interface Sci. 101, 98.

SHON, S.-N., KASPER, G., and SHAW, D.T. (1980) J. Colloid Interface Sci. 73, 233.

SZYMANSKI, W.W., MAJEROWICZ, A., and WAGNER, P.E. (1989) "Measurement of Brownian Coagulation in Monodispersed and Bidispersed Liquid Aerosols", Aerosol Sci. Technol., in press.

WAGNER, P.E., and KERKER, M. (1977) J. Chem. Phys. 66, 638.

WAGNER, P.E. (1985) J. Colloid Interface Sci. 105, 456.

LONG-RANGE FORCES AND THE COLLISIONS OF FREE-MOLECULAR AND TRANSITION REGIME AEROSOLS

William H. Marlow*
Texas A and M University
College Station, Texas 77843-3133

I. Introduction

An *aerosol* here is understood to be a two-component system comprised of gaseous and condensed phases with the characteristic that the condensed phase is not an equilibrium subsystem. In contrast to the usual definitions based upon geometrical or mechanical variables (see Ref. 1 for discussion of alternative definitions), this quasi-thermodynamic formulation is framed to emphasize the dynamical behavior of aerosols by allowing for coagulation and other aerosol evolutionary processes as natural consequences of the interactions and state variables appropriate to the system. As will become clear later, it also provides a point of departure for distinguishing aerosol particles from unstable gas-phase cluster systems.

The question of accommodation in particle collisions must be addressed as a prelude to the discussion of the role of long-range forces. Microscopic reversibility is frequently assumed for molecular collisions with either molecules or solid surfaces. In the case of aerosol collisions, the implication of this assumption is that collisions are elastic, which is contrary to the evidence from coagulation experiments and the conventional operational assumption of sticking upon collision. Gay and Berne[2] have performed computer simulations of the collision of two clusters consisting of a total of 135 molecules interacting via Lennard-Jones potentials. That work showed that complete accommodation, accompanied by overall heating of the unified cluster, occurred. Since heating represents an irreversible degradation of the kinetic energy of the collision, the hamiltonian of the two-cluster system should be considered as dissipative and therefore microscopic reversibility does not apply.

Intermolecular forces have long been acknowledged to be of importance in atomic and molecular collisions and therefore in the equations of state for real gases. The best-known such equation of state is the van der Waals equation

$$\left(P + \frac{a}{V^2}\right)(V - b) = NkT, \qquad (1)$$

where P is pressure, V is gas volume, N is number density of molecules, T is temperature, k is Boltzmann's constant, a and b are constants, and the a/V^2 term

accounts for attractive intermolecular forces. A form commonly used to fit experimental data which are dependent upon molecular force paramenters is the "Lennard-Jones" or "6-12" potential:

$$\Phi_{L\text{-}J}(r) = 4\varepsilon\left[\left(\frac{r_0}{r}\right)^{12} - \left(\frac{r_0}{r}\right)^{6}\right] \qquad (2)$$

In this formula, r is the intermolecular separation with ε and r_0 fitting constants determined by the data. The implications of this intermolecular potential for gas-phase collisions can be treated qualitatively by determining the distance of separation r_k between molecules at which the potential is equal to the thermal energy, $\Phi_{L\text{-}J}(r_k) = -kT$. This distance is to be compared with the minimum distance of separation r_m (or hard-sphere radius) which follows from the condition $\frac{d\Phi_{L\text{-}J}(r_m)}{dr} = 0$. Then the ratio r_k/r_m is qualitatively the enhancement of the collision radius due to the long-range (i.e. the r^{-6} part of the potential) and $(r_k/r_m)^2$ is the corresponding enhancement of the collision cross section. These calculations for selected data based upon gas viscosity measurements[3] imply that even for rare gas atoms, almost an order of magnitude enhancement in the collision rates can be expected over what would follow from purely hard-sphere collisions as illustrated in Table 1.

TABLE 1
ENHANCEMENTS OF THERMAL CAPTURE RADII FOR SELECTED RARE GASES(T=300°K)

Species	(rk/rm)	$(rk/rm)^2$
Ne	2.13	4.5
Ar	2.56	6.56
Kr	2.69	7.2
Xe	2.83	8.0

Macroscopic objects also are subject to intermolecular forces (see Ref. 4 for brief review of experimental data) and play a major role in adhesion of particulate matter to surfaces[5,6]. In contrast to molecular collisions, however, there is no evidence that atmospheric continuum regime aerosol particle collision rate densities are in any way affected by the long-range, intermolecular forces. Therefore, particle transport as determined by background gas and other factors override the effects of the long-range intermolecular forces in continuum particle collisions. The situation is not so clear for submicrometer particulate matter, however. There is substantial experimental evidence in the transition and free-molecular regimes[7,8,9,10] that collisions rates exceed those which are calculated based solely upon brownian or thermal motion of hard-sphere particles (i.e. no long-range attraction between equivalent-sphere particles) and that the magnitude of those collision rate enhancements is inversely

related to the physical size of the colliding particles. Since incomplete accommodation of the particles upon collision can never give an enhancement of the collision rate, the conclusion must be drawn that long range, interparticle forces are required to fully describe experimental data.

II. Nature of Long-Range Forces

In the last section, the necessity of introducing long-range forces into transition and free-molecular regime particle collisions was argued without explicitly defining what is meant by long-range forces in the aerosol context. Let Φ be the potential for the long-range force. Then $|\Phi(R)|>kT$ when $(R-r_{ij})>2\text{Å}$ (R=center-of-mass separation and r_{ij}= sum of radii of spheres i and j) is taken here to define a long-range force. Physically, this means that beyond the orbital overlap or "jellium" leakage range,[11,12] the potential well depth is greater than thermal energy.

Long-range, intermolecular forces arise from the specific atomic, molecular, and structural properties of individual molecules and molecules-in-aggregate in condensed matter[4,6]. While permanent multipole moments make important contributions at the molecular level, in most cases for condensed matter, even at low levels of aggregation, they tend to "average out" leaving only the dipole-induced-dipole force as present in all matter.

The simplest form of the induced-dipole force arises from the London-van der Waals interaction potential[13,14]

$$\Phi_{Lon}(R) = -\frac{3\hbar}{\pi R^6}\int_0^\infty d\xi\,\alpha_1(i\xi)\alpha_2(i\xi) \qquad (3)$$

In the most general case, a tensor coupling of polarizability tensors must be considered and involves both electric and magnetic polarizabilities. Here, $\alpha_j(i\xi)$ is electric polarizability of spherically symmetric molecule j at frequency $\omega=i\xi$, R is separation of point molecules 1 and 2, $i=\sqrt{(-1)}$, and $\hbar$ is Planck's constant divided by 2π. Eq.(3) gives the R^{-6} factor in the 6-12 potential, eq. (2), that is characteristic of the dipole-induced dipole interaction. Because the intermolecular coupling employed in eq. (3) assumes that the electric fields at the positions of the two molecules are equal, this potential is strictly valid only in the electrostatic limit.

In contrast, if the propagation speed, c, of the photons coupling the interacting molecules is taken into account, the Casimir-Polder form for the van der Waals interaction results:

$$\Phi_{C\text{-}P}(R)= -\frac{\hbar}{\pi R^2}\int_0^\infty d\xi\alpha_1(i\xi)\alpha_2(i\xi)e^{-2\xi R/c}\left(\frac{\xi^4}{c^4}+\frac{2\xi^3}{c^3R}+\frac{5\xi^2}{c^2R^2}+\frac{6\xi}{cR^3}+\frac{3}{R^4}\right) \quad (4)$$

In this equation, *retardation* is included explicitly, and has the effect of diminishing the strength of the interaction relative to its nonretarded form, eq. (3). The effect of retardation is not uniform but is dependent upon the frequency, or wavelength, of the electromagnetic field coupling the molecules. In the limiting cases, when the wavelength $\lambda=2\pi c/\omega >>R$, then $\Phi_{C\text{-}P}(R)\text{-->}\Phi_{Lon}(R)$ and the full electrostatic coupling R^{-6} is recovered. In the other limit, for $\lambda << R$, $\Phi_{C\text{-}P}(R)\text{-->}\Phi_{ret.}(R)$ where

$$\Phi_{ret.}(R) = \frac{-23\hbar c\alpha_1(0)\alpha_2(0)}{4\pi R^7} \quad (5)$$

is the retarded interaction potential. In general, retardation is unimportant for molecular collision rates because at intermolecular separations large enough that the nonretarded energy is significantly larger than the retarded energy, both energies are much less than thermal energies, i.e. when $[\Phi_{C\text{-}P}(R)/\Phi_{Lon}(R)]<<1$, $|\Phi_{Lon}(R)|<<kT$. One significant aspect of eq. (5) is that the transition in the functional dependence of the potential which accompanies retardation, the change from R^{-6} to R^{-7}, lessens the attractive energy and prevents scaling of any physical interaction which is dependent upon constant integral powers of radius.

Long-range, attractive interactions of condensed matter arise from the intermolecular interactions discussed above and their appropriate generalizations. By far the most generally used form for these interactions is the sum-over-pair-interactions, $(\Phi_{pr})_{AB}$ which can be expressed as

$$(\Phi_{pr})_{AB}= -\int_{V_A} d\tau_a \int_{V_B} d\tau_b \frac{\Lambda_{ab}\rho_a(\mathbf{r}_a)\rho_b(\mathbf{r}_b)}{|\mathbf{r}_a-\mathbf{r}_b|^6} \quad (6)$$

Here, Λ_{ab} is a constant related to $\Phi_{Lon}(|\mathbf{r}_a-\mathbf{r}_b|)\cdot|\mathbf{r}_a-\mathbf{r}_b|^6$ for molecules at locations $\mathbf{r}_a$ and $\mathbf{r}_b$, V_A is the volume of body A, $d\tau_a$ is a volume element of A containing $\mathbf{r}_a$ and $\rho_a(\mathbf{r}_a)$ is the number density of oscillators (i.e. molecules) at $\mathbf{r}_a$. The constant Λ_{ab} is customarily computed from molecular parameters[12] and is related to the widely-used Hamaker[6] constant A_{AB} by

$$A_{AB}= \pi^2\Lambda_{ab}\rho_a\rho_b \quad (7)$$

With this characterization of the interaction energy, the long-range forces can be computed quite easily for particles of a number of different geometries[14].

Unfortunately, the sum-over-pair interactions approach has not proved to be either reliable or necessarily accurate. It does not include the effects on the

interparticle energy of either the collective behavior (e.g. conduction band in metals) or the mutual interactions of the atoms and molecules comprising the condensed matter. The role of retardation, though unimportant for molecules, is known[4] to play an important role for condensed-matter interactions but again the naive pair-summation energy does not take this into account.

A highly successful theory by Lifshitz[15] has been developed for the long-range "intermolecular" interactions of condensed matter. In the same manner that London's theory of the van der Waals interaction arises from fluctuating molecular dipoles and is based upon the dipole polarizability $\alpha(\omega)$ of the molecules, Lifshitz's theory is parameterized by the frequency-dependent dielectric permeability, $\varepsilon(\omega)$ (as well as the corresponding magnetic permeability $\mu(\omega)$ which in most cases makes no appreciable contribution to the interaction energy). Consequently, Lifshitz theory accounts for the collective nature of the intermolecular interactions of condensed matter, though it does assume local dissipation, meaning that ε is independent of wavenumber. In its original form for the interaction energy of two half-spaces separated by an infinite slab, the theory includes the effects of retardation and in this form has had extensive experimental confirmation[4]. Since Lifshitz's original derivation, the conceptual foundations of the theory have been established by use of the methods of quantum mechanical perturbation theory[16], alternative, simplified derivations of the theory have been given, expressions applicable to several different geometries have been derived, and highly accurate, greatly simplified, formulas which facilitate application of the theory have appeared (see Refs. 6, 13, and 14 for reviews of many of these developments).

III. Long-Range Forces in Aerosol Collision Rate Densities

In the van der Waals potentials discussed above, the mathematical form of the interaction energies diverges as the particles approach to the point of contact, i.e. $\Phi(R) \dashrightarrow -\infty$ as $R \dashrightarrow r_{ij}$, meaning that they are to be described as *singular, attractive contact potentials.* The brownian collision rate densities, or collision kernals, of continuum regime aerosol particles interacting via such interparticle potential energies can be computed from the well-known formula

$$K^c(\Phi)_{ij} = \frac{4\pi D_{ij}}{\int_{r_{ij}}^{\infty} \frac{dR}{R^2} \exp\left(\frac{\Phi(R)}{kT}\right)} \qquad (8)$$

where $D_{ij}=D_i + D_j$, with D_i the diffusion coefficient for i and $r_{ij}=r_i + r_j$ with r_i =radius of particle i. However, in the free-molecular regime, the customary form from gas molecular kinetic theory,

$$K_{ij} = \left(\frac{8\pi kT(m_i+m_j)}{m_i m_j}\right)^{1/2} r_{ij}^2 \exp[-\Phi(r_{ij})] \qquad (9)$$

is not well defined as $\Phi \to -\infty$. This complication can be resolved by describing the collision process by the use of the impact parameter for each collision[17]. While suitable for computation of a single trajectory, this approach requires finding the root of a possibly nonpolynomial function for *each* collision and consequently involves assumptions of how the ensemble of trajectories should be averaged in the computation of the thermal collision rates where pairs of colliding particles initially have a Boltzmann distribution of center-of-mass energies. Also, how to reformulate the impact parameter solution for utilization in models of transition regime collisions is not at all clear, a requirement that cannot be overlooked because of the difficulties associated with rigorous transition regime kinetic theory.

An exact computation of the free-molecular collision rate which resolves these difficulties can be written as[18]

$$K^{fm}(\Phi)_{ij} = \pi\left(\frac{8kT(m_i+m_j)}{\pi m_i m_j}\right)^{1/2} \int_{r_{ij}}^{\infty} d\sigma \; \frac{1}{2kT}\left(\frac{d\Phi(\sigma)}{d\sigma} + \sigma\frac{d^2\Phi(\sigma)}{d\sigma^2}\right)\sigma^2$$

$$\cdot\exp\left(-\frac{1}{kT}\left(\frac{\sigma d\Phi(\sigma)}{2d\sigma} + \Phi(\sigma)\right)\right) \qquad (10)$$

The derivation of eq. (10) is based upon the following assumptions: (1) the potential $\Phi(R) \leq 0$, (2) is monotonically increasing, (3) and approaches minus infinity as the particles come in contact; also, (4) a Boltzmann distribution of velocities holds for the colliding particles; (5) collisions between particles occur when the centrifugal force in the center-of-mass system equals the attractive force due to the potential and the relative radial velocity of the particles is less than or equal to zero. In practice, what this means is that for $R-r_{ij}<4$Å, the potential $-\Phi(R) \gg kT$ which assures convergence of the integral. A particular strength of this approach is that it can readily be generalized to apply to the calculation of transition regime collision rates by the utilization of a suitable transport model as well as potentials which are not monotonic[19].

Equation (10) has been used[18] to generalize Fuchs' interpolation method for transition regime collision rates. Since this Generalized Fuchs Formula (K^{GFF})is the only general formula in the literature which computes the effects of long-range forces on transition regime coagulation rates, its usefulness must be carefully evaluated. Measurements of electrical charging of neutral aerosol particles provide a useful test

of the formula for two reasons: the electrostatic image potential satisfies the conditions on the potential assumed for eq. (10); reliable data on the charging rates of neutral particles are much less difficult to obtain than those on aerosol coagulation. Recognizing that the aerosol particle mass is much larger than the mass of the charging ion suggests that treating the aerosol particle as stationary in the ion-aerosol coagulation problem will introduce little error. Recently, this approach has been used to fit experimental data[20] and the results[21] are displayed in Figures 1 and 2.

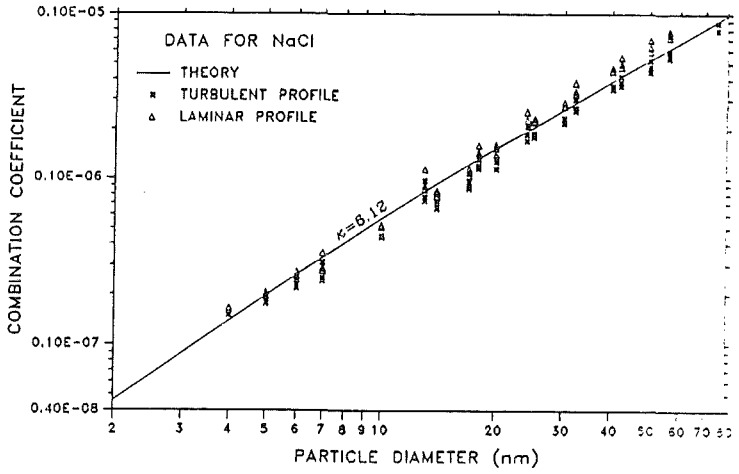

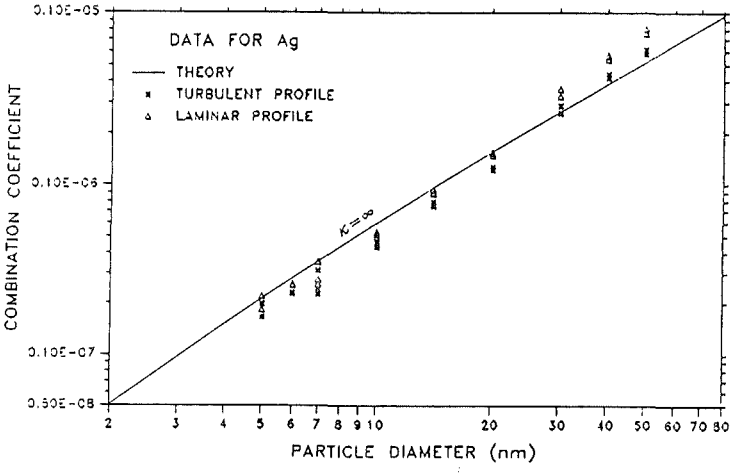

Figures 1 and 2

Collision rate densities of atmospheric cluster ions with aerosol particles. Turbulent and laminar profiles indicate range of experimental uncertainties.

The long-range intermolecular interaction energy (i.e. Lifshitz-van der Waals energy) of a pair of aerosol particles is the only attractive energy that is present under all conditions. For particles (represented as spheres), a highly accurate approximation[22] to the nonretarded interaction energy is a useful starting point for calculations of aerosol brownian or thermal collision rates. As suggested above, retardation is expected to play a major role. Qualitatively, this importance can be understood based upon the fact that the nonretarded energy for identical spheres of

radius r which are separated by a distance r is comparable to thermal energy, $\Phi(3r)_{nonret} \approx -kT$. If r<1 nm, then retardation causes only a minor change in the attractive energy (i.e. $\lambda=2\pi c/\omega>r$ at wavelengths where the contribution to the energy is greatest). For r=10 nm, this is no longer true so that retardation must therefore be included for the calculations to be meaningful. While an expression by Langbein[14] for the retarded energy of two spheres is in the literature, it is not suitable for utilization in expressions based on eq. (10). Consequently, a point-dipolar approximation has been used[23]

$$\Phi_{ret}(R) = \int_0^\infty d\xi \Phi_{nonret}(R,\xi) e^{-2\xi R/c} \left(1 + \frac{2R\xi}{c} + \frac{5R^2\xi^2}{3c^2} + \frac{2R^3\xi^3}{3c^3} + \frac{R^4\xi^4}{3c^4}\right) \qquad (11)$$

which is an obvious adaptation of the exact molecular formula [see eq. (4)] for the interactions of condensed matter. In Figure 3 from Reference 24, results of two sample calculations based on eq. (11) are given. Note how $|\Phi(R)|>>kT$ for $R-r_{ij}\approx 1-2$Å implying convergence of integrals related to eq. (10) and physical capture of the two particles (assuming dissipation of collisional energy) without chemical bonding. Note also that the relative strength of attraction is dependent on particle sizes, an effect directly attributable to the fact that "retardation damping" of the interaction energy is dependent upon frequency and therefore affects different materials in different ways. Had retardation not been included, the 100 nm curves would have moved to become coincident with the 1 nm curves.

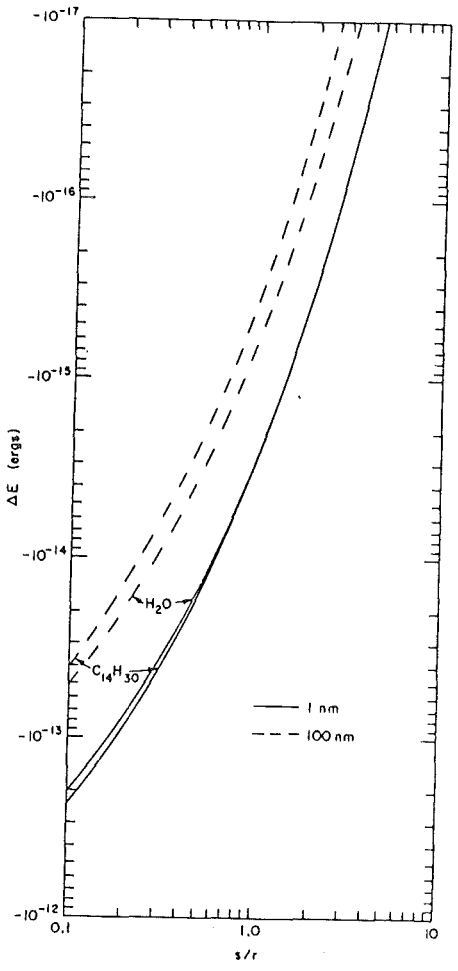

Figure 3
Lifshitz-van der Waals attractive potential well depth as a function of ratio (s/r) of surface-to surface separation, s, to radius, r. Radii of water and tetradecane spheres indicated on graph.

What is of interest here is the role that the long-range forces play in aerosol collision rates. The example of water droplet collisions has been treated in detail[23] with the long-range energies computed according to eq. (11) and used in K^{GFF}. For the purpose of establishing relative effects, the results are presented in Table 2 as the ratio K^{GFF}/K^{F} where K^{F} is the

collision rate as determined by Fuchs' interpolation method without long-range forces.

TABLE 2
COLLISION RATE ENHANCEMENTS FOR WATER: K^{GFF}/K^{F}
including retardation
(excluding retardation)

Radii (nm)	Pressures (atm) 0.1	1.0	10.0
1;1	2.44 (2.46)	2.44 (2.46)	2.37 (2.38)
10;10	2.26 (2.45)	1.94 (2.02)	1.21 (1.22)
100;100	1.31 (1.42)	1.07 (1.15)	1.07 (1.17)
1;10	1.55 (1.59)	1.54 (1.57)	1.30 (1.30)
10;100	1.35 (1.50)	1.09 (1.11)	1.02 (1.03)
1;100	1.09 (1.12)	1.05 (1.07)	1.01 (1.01)

The radii on the left are of the colliding pair of particles. Note that the effect of the long-range forces is greatest where the radii of the particles is comparable and least where the ratio of the radii is greatest as well as where particle sizes approach the continuum regime. These calculations also clearly indicate that retardation has little effect for the collisions of the smallest particles (1 nm) but that its importance increases substantially with size.

Calculations of collisions rates[25] have also been performed to explain qualitative measurements of ultrafine lead aerosol particle coagulation[9]. Those measurements implied a factor of approximately 4 enhancement of the particle collision rates over the hard-sphere rates. To interpret their experimental data, the authors adapted the free-molecular self-preserving size distribution[26] to incorporate the effects of collision rate enhancement due to nonretarded, sum-over-pair interaction energy between the colliding particles. Because of the form of the nonretarded interaction, the interaction energy scales with the particle size (e.g. see discussion of Fig. 3 above) to give a constant enhancement factor, thereby enabling it to be incorporated into the self-preserving distribution. Their calculations gave an enhancement of 2.2, a value that is inconsistent the the error bars on the data that can be inferred from the original paper. In contrast, application of K^{GFF} with the retarded

Lifshitz-van der Waals energy in the approximations discussed above gave a size-dependent enhancement which bracketed the measured enhancement and lay within the error bars of the data. When retardation was dropped from the energy calculations, the resultant size-independent enhancement lay above the error bars for the data.

Detailed measurements of the size distribution evolution of sodium chloride and silver aerosols have been published[10] with the Generalized Fuchs Formula used to the explain the data. Figure 4 taken from the original paper presents both the data points and the collision rate enhancement curves calculated by use of pair-summation energy without retardation.

Figure 4

β is the ratio of the coagulation rate to the rate computed according to Fuchs' formula. The points are experimental data and the lines are computed from K^{GFF} using sum-over-pairs potentials

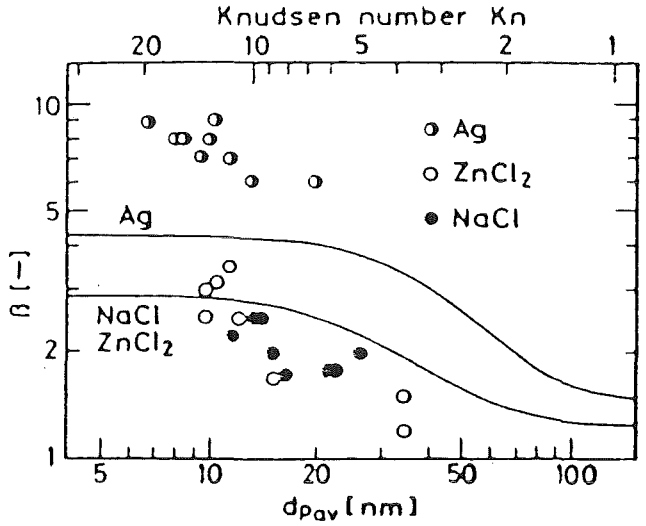

FIG. 9. Coagulation enhancement factor.

Journal of Colloid and Interface Science, Vol. 101, No. 1, September 1984

For the salts in Fig. 4, where pair summation theory has been found to be useful in other contexts, the theoretical and experimental data agree reasonably well for the smaller particles and disagree for larger particles exactly where retardation would have suppressed the calculated collision rates had it been incorporated into the energy calculation. In the case of silver, the rates are far too high to be explained by

the energy expression used; nevertheless, the onset of a fall-off, with increasing diameter, in the collisional enhancements again points to the importance of retardation.

The evidence discussed above implies that the effects of both long-range forces and their retardation must be included in calculations of the collision rates of free-molecular and transition regime aerosols and therefore has implications for the validity of the free-molecular self-preserving size distribution[26]. In its derivation, this distribution requires that the collision kernal scale with the radii of the colliding particles, a property that is adequately fulfilled by the nonretarded interaction[9]. However, retardation breaks scaling because it is dependent solely upon the wavelengths, not upon geometry of the colliding particles. Therefore, as measurement methodology for aerosol size distributions continues to improve, there is the likelihood that deviations from the free-molecular, self-preserving size distribution will continue to be found.

IV. Collision Rates of Clusters

A conceptual question exists of the distinction between ultrafine aerosol particles and atomic or molecular clusters. In the current literature, "cluster" can refer to atomic or molecular aggregates of greater than ten thousand units or to small clusters of two or three units. At the larger end of this spectrum, the clusters have nominal diameters of several nanometers which most aerosol scientists would consider to be aerosol particles while the smaller end of this scale they would relegate to chemistry. This distinction is most pronounced for homogeneous nucleation resulting in the formation of stable "particles" (which may be in the 50-100 monomer-unit range or smaller) from the gas via a build-up of unstable clusters. In other environments, gas phase clusters of the same size (i.e. same number of monomeric units) as these unstable ones are stable and participate in equilibrium thermodynamic processes that result in well-defined, "magic number" distributions (Ref. 12 reviews aspects of the subject).

To provide some characteristics of cluster systems for the determination of which should be encompassed in aerosol considerations, the following properties which are consistent with the thermodynamic characterization provided earlier for an aerosol, may be useful: Only in equilibrium does microscopic reversibility apply to all cluster collisions occurring in the gas phase; thus, if a cluster-cluster collision can be

treated as equilibrium processes, the clusters may be treated as an equilibrium subsystem and would not satisfy the characteristics of an aerosol. Consequently, if there is (effectively) no equilibrium vapor pressure of m-mers over the surface of an n-mer ($m \leq n$), then we may take the coagulation event, m + n ->(m+n) to be irreversible, implying the interaction hamiltonian is dissipative and the collisional behavior is identical to an aerosol. When local equilibrium of the clusters with the gas does exist, though not among the clusters as a subsystem, the distribution of clusters must reflect their relative free energies of formation from the "monomer" of the system.

These properties satisfy the requirements both that the definition of aerosol cluster have meaning for the range of phenomena commonly encompassed by clusters and that it is consistent with known aerosol characteristics. Magic number cluster distributions have been observed in a variety of supersonic jet beam and gas agglomeration experiments where vapor equilibrium is clearly established. Both an overall equilibrium thermodynamic calculation[12] and a calculation based on the (equilibrium) Becker-Döring theory of nucleation have been shown capable of accounting for these distributions[27]. Conversely, for manifestly nonequilibrium systems, these same, well-ordered distributions are not evident. The formation of these distributions may well be heavily influenced by the dissipation of energy upon collision which is characteristic of aerosol systems and is implicit to the aerosol cluster properties discussed here.

To calculate the collision rate densities of clusters, adequate expressions for the long-range interaction energies of the clusters are needed. The Lifshitz theory calculations upon which larger aerosol particle interaction energies were based assume a continuum model of condensed media, a picture which clearly does not apply to clusters. As an alternative, the pair-summation energy is also inadequate because it does not take the collective nature of the interaction energy into account. Langbein[14] has given a derivation of the nonretarded Lifshitz energy based upon the iterated sum over induced-dipole interactions. Instead of taking the limit of a large number of molecules in calculating the coupling energy as is done in the original calculation, Langbein's energy expressions can be truncated to apply only to the molecules comprising the clusters, thereby yielding the cluster interaction energy, a procedure that has been used in the derivation of the collision rates for carbon dioxide clusters[28]. In those calculations, the inability to define a radius for small clusters (13 or fewer molecules) required the utilization of a heuristic method which averages over the four orientations wherein the clusters are in contact at the points of their surfaces which are the greatest and least distances from their centers-of-mass. When the

collision rate calculations were performed without the interaction energy, the results were little different from what is determined via the liquid drop model (which assumes a spherical cluster whose radius is proportional to the cube root of the number of molecules). With the interaction energy included in these model calculations, the collision rates were enhanced as much as a factor of 19 over their values without the attractive energies included.

V. Future Work in Aerosols

Understanding the roles and quantifying the effects of long-range forces on aerosol collisions are studies that are only in their earliest stages. As is clear from the qualitative, thermodynamically-based characterizations of aerosols and aerosol clusters presented above, considerable improvement is still required in even defining the nonequilibrium thermodynamic characteristics of these systems. Apparently, the desirability of dropping the assumption of microscopic reversibility in particle collisions has not been suggested before this paper, so its broader implications have not been explored. From the viewpoint of the observed behavior of aerosols, framing a definition about this specific nonequilibrium characteristic has a value beyond simply restating what is already well-understood in different terms: it provides the vehicle for defining which clusters can reasonably be included under the domain of aerosol studies as was done above. In turn, one can speculate that this may contribute to rigorously defining the boundary of aerosol studies with homogeneous nucleation theory by providing an alternative approach to the Szilard boundary condition that is needed to formulate the solutions that arise from the classical theory of nucleation[29].

Long-range forces, taken by themselves, are of interest solely in nonequilibrium collisions. In equilibrium, where microscopic reversibility pertains, the long-range part of the interaction potential energy is an arbitrarily-selected component of the total potential and makes a generally indistinguishable contribution to the thermodynamic functions that determine equilibrium evolution. However, when there is dissipation of the kinetic energy of collision, then microscopic reversibility is destroyed and the magnitude of the "incident" transport becomes a significant factor because it is no longer part of a balanced (i.e. time reversible) process. In this case which encompasses aerosols, the long-range potential plays a central role in the evolution of the system.

In this review, only the original Lifshitz theory of the van der Waals interaction has been discussed for aerosol collisions. Due to the disagreement between the data on coagulation of ultrafine silver[10] aerosol and the calculations[24] of the enhancement of the collision rates for silver, further work is clearly needed on the long-range interaction potential for nonlocal materials (as silver is known to be).

Only a small number of experiments of aerosol coagulation have been performed which have the precision required to discriminate among collision rates. This is particularly important in the 1-100 nm range of particles where severe, unresolved problems exist for the rigorous treatments of both retardation and transition regime collision rate density.

An important problem with the treatment of retardation provided by eq. (11) is that it describes the retardation of the interaction between two extended bodies as if they were point dipoles. As a result, retardation is the same between all points of the two spheres, a result with clear problems whenever the separations or the radii of the spheres are comparable with wavelengths at which retardation would be expected. One approach for the improvement of the treatment of retardation which is under investigation by the author is to replace eq. (11) by

$$\Phi_{ret}(R) = \int_0^\infty d\xi \Phi_{nonret}(R,\xi) \int_{V_A} d\tau_a \int_{V_B} d\tau_b e^{-2\xi|r_a-r_b|/c} \cdot\left(1 + \frac{2|r_a-r_b|\xi}{c} + \frac{5|r_a-r_b|^2\xi^2}{3c^2} + \frac{2|r_a-r_b|^3\xi^3}{3c^3} + \frac{|r_a-r_b|^4\xi^4}{3c^4}\right) \qquad (12)$$

This is essentially a "sum-over-pairs" approach where now only the effect of retardation between pairwise interactions and not the interactions themselves is treated. In this form, the energy can be computed only for homogeneous spheres, each of the same composition.

While all calculations and measurements of long-range interaction enhancement discussed above have referred to spheres, there is a distinct possibility that the van der Waals forces may promote end growth for rod-like particles. Calculations have been made of the van der Waals sum-over-pair interactions for two spheroids as a function of their surface-to-surface separation and orientation.[30] They showed that for a given separation, the ratio of the attractive energy to the energy for a pair of spheres was considerably greater than unity for "end to end" approach and much smaller than unity for side to side approach.

Finally, the effect of polarizability upon the collisions of electrically charged aerosol particles has apparently not been investigated. This could be of particular interest at high temperatures and in the transition regime. There, thermal or brownian motion is still the transport process driving coagulation. For such particles, two similar-

polarity particles may have sufficient translational energy to penetrate their Coulomb barrier and become attracted by the force of mutual polarization.

---

* This work partially supported by the United States Department of Energy under Grant DE-FG05-87ER60550

[1] Marlow, W. H. (1980) Chapter 1. Introduction:The domains of aerosol physics, in Aerosol Microphysics, I: Particle Interaction ed. W. H. Marlow, Springer-Verlag(Berlin, Heidelberg, New York).

[2] Gay, J. G., and Berne, B. (1986) Energy accommodation in collisions of small particles J. Colloid Interface Sci. 109(1), 90-100.

[3] Clifford, A. A., Gray, P., Platts, N. (1977) Lennard-Jones 12:6 parameters for ten small molecules. J. Chem Soc. Farad. Trans. I 73, 381-2.

[4] Marlow, W. H. (1980) Chapter 5.Survey of aerosol interaction forces, in Aerosol Microphysics, I: Particle Interaction ed. W. H. Marlow, Springer-Verlag(Berlin, Heidelberg, New York).

[5] Zimon, A. D. (1982) Adhesion of Dust and Powder, translated by R. K. Johnston, Consultants Bureau(New York, London).

[6] Israelachvili, J. N., (1985) Intermolecular and Surface Forces with Applications to Colloidal and Biological Systems, Academic Press(London, New York).

[7] Wagner, P. E., and Kerker, M. (1977) Brownian coagulation in rarefied gases. J. Chem. Phys. 66, 638-646.

[8]Fuchs, N. A., and Sutugin, A. G. (1965) J. Colloid Interface Sci. 20 ,492.

[9]Graham, S. C., and Homer, J. B. (1973) Coagulation of molten lead aerosols, Discuss. Farad Soc. 7 ,85-103.

[10]Okuyama,K., Kousaka,Y., and Hayashi,K. (1984) Change in size distribution of ultrafine aerosol particles undergoing brownian coagulation. J. Colloid Interface Sci. 101, 98-109.

[11]Zaremba, E., Kohn, W. (1976) Van der Waals interaction between an atom and a solid surface, Phys. Rev. B13, 2270-2285, discusses the reference plane beyond which Lifshitz theory is useful.

[12] de Heer, Walt A., Knight, W. D., Chou, M.Y., Cohen, M.L.(1987) Electronic shell structure and metal clusters, Solid State Physics 40 , 94-182, ed. Ehrenreich, H, and Turnbull, D. Academic Press(New York), gives references to calculations showing extent of electron density beyond jellium edge.

[13] Mahanty, J., and Ninham, B. W. (1976) Dispersion Forces, Academic Press(London, New York, San Francisco).

[14] Langbein, D., (1974) Theory of Van der Waal Attraction, Springer-Verlag(Berlin, Heidelberg, New York).

[15]Lifshitz, E. M. (1956) Theory of molecular attractive forces between solids, Sov. Phys. 2, 73-83.

[16]Dzyaloshinskii, I.E., Lifshitz, E. M. , Pitaevskii, L. P., (1961) "The general theory of van der Waals forces" (trans. Priestley, M. G.) Adv. Phys. 10, 165-209.

[17]Fuchs, N. A., and Sutugin, A. G. (1965) Coagulation rate of highly dispersed aerosols. J. Colloid Sci. 20. 492-500.

[18]Marlow, W. H. (1980) Derivation of aerosol collision rates for singular attractive contact potentials. J. Chem. Phys. 73, 6284-6287.

[19]Zhu, X.-W., and Marlow, W. H. (1988) in preparation.

[20]Pui,D.Y.H., Fruin,S., McMurry, P.H. (1988) Unipolar diffusion charging of ultrafine aerosol particles, Aerosol Sci. Tech. 8, 173-188.

[21] Marlow, W. H., and McFarlane, D. L., (1988) A theoretical fit of charging data: Comments on "Unipolar diffusion charging of ultrafine particles", Aerosol Sci. Tech. (in press).

[22]Kiefer, J.E., Parsegian, V. A., and Weiss, G. H. (1978) Some convenient bounds and approximations for the many body van der Waals attraction between two spheres. J. Colloid Interface Sci. 67, 140-153.

[23]Marlow, W. H.(1980) Lifshitz-van der Waals forces in aerosol particle collisions. I. Introduction: Water droplets. J. Chem. Phys. 73, 6288-6295.

[24] Marlow, W. H. (1981) Size effects in aerosol particle interactions: the van der Waals potential and collision rates. Surface Sci. 106,529-537.

[25]Marlow, W. H.(1982) Lead aerosol brownian collision rates at normal and elevated temperature:theory. J. Colloid Interface Sci. 87, 209-215.

[26]Lai, F. S., Friedlander. S. K., Pich,J., and Hidy, G. M. (1972) The self-preserving particle size distribution for brownian coagulation in the free-molecule regime. J. Colloid Interface Sci. 39,395-405.

[27]Yang, S.-N., and Lu, T.-M., (1987) Ar-cluster-size distribution in a supersonic jet beam. Phys. Rev. B 35, 6944-6949.

[28] Marlow, W. H. (1986) Thermal collision rate densities of small clusters. J. Phys. Chem. 90, 2302-2305.

[29]Abraham, F. F. (1974) Homogeneous Nucleation Theory, Academic Press(London).

[30]Vold, M. J. (1957) The van der Waals interaction of anisomeric colloidal particles., Proc. Ind. Acad. Sci. A46, 152-166.

COAGULATION OF SUBMICRON PARTICLES IN AN AEROSOL SAMPLING VESSEL

G. Schwientek
H. Fissan

Submitted to:
Nuclear-Research-Center, Karlsruhe
Coagulation Workshop Proceedings
March 16-18, 1988

Bericht Nr. 207
Disk. AMT2, Dok: B207

Universität GH Duisburg
Prozeß- und Aerosolmeßtechnik
Bismarckstr- 81
D-4100 Duisburg 1

1. Introduction

An aerosol is a dynamic system. Changes occur because of chemical and physical processes within the aerosol as well as by interaction with surrounding walls. In this report we only consider physical processes. The investigated system is an aerosol contained in a rigid vessel. This system is used for instance for aerosol sampling, conditioning and storage for successive measurement. Any uncontrolled change in the aerosol will lead to errors in the measurement. Theoretical models, which allow the description of the dynamics of aerosols in a given situation, may be a powerful tool to estimate and reduce errors during the sampling and conditioning procedure of aerosols. In the reported investigation the applicability of modified codes for error analysis of aerosol handling in a vessel was checked especially considering coagulation.

2. Operation of the vessel

During handling processes aerosols may be stored in a vessel. The purpose of a vessel can also be to condition the aerosol. The aerosol properties are adjusted to the measurement ranges of the aerosol measurement instruments in a controlled way. Conditioning may include such processes as mixing to eliminate fluctuation in the aerosol concentration as well as dilution and/or temperature decrease by mixing the aerosol with cold particle free gas in the vessel. Since most measurement instruments need atmospheric conditions in the vessel, the starting point is particle free gas at atmospheric pressure in the vessel. The aerosol is added at a certain flow rate. To maintain atmospheric pressure gas has to exit the vessel at the same flow rate. If the instruments take samples from the vessel the aerosol has to be replaced by particle free gas. In both cases dilution processes take place.

3. Description of ideal behavior of an aerosol in a vessel

In handling processes we wish to have no or at least a defined change in aerosol properties. Therefore, processes as coagulation, condensation or evaporation and particle deposition onto walls have to be avoided or at least minimized. Also the mixing should be ideally.

The temperature adjustment can be described by an energy balance. Often only a small volume of aerosol is mixed with a large volume of particle free gas in the vessel. Then the temperature in the vessel stays almost constant.

In an ideal case the particle number concentration does not change during storage of an aerosol. In case of dilution the change in number concentration can be described by the following differential equation:

$$/1/ \qquad dC_N = \frac{\dot{V}}{V_B} C_{NG}\, dt - \frac{\dot{V}}{V_B} C_N\, dt$$

In this equation C_N is the number concentration at time t, C_{NG} is the number concentration of the input aerosol (generator), $\dot{V}$ is the aerosol flow rate and V_B is the volume of the vessel. The first part describes the changes due to the aerosol input flow, the second part describes the reduction of aerosol concentration due to the aerosol output flow necessary to maintain atmospheric conditions. The solution of equation 1 with C_{NO} equal to the initial concentration at t = 0 is:

$$/2/ \qquad C_N(t) = C_{NG} - (C_{NG} - C_{NO}) \exp(-(\dot{V}/V_B)t)$$

If only sampling occurs the number concentration as a function of time is:

$$/3/ \qquad C_N(t) = C_{NO} \exp(-(\dot{V}/V_B)\,t)$$

In fig. 1 relative concentrations as a function of time for different ratios $\dot{V}/V_B$ are shown. It demonstrates how the ratio $\dot{V}/V_B$ can be used to adjust the concentration in the vessel under ideal conditions during aerosol sampling from a vessel and dilution of an aerosol.

4. Description of real behavior of an aerosol in a vessel

During storage and conditioning of an aerosol additional physical effects occur, which change the aerosol. If no mass transfer between gas- and particle phase takes place, still unwanted changes by coagulation and by particle deposition onto the surrounding walls have to be considered. In recent papers (Fissan et al., 1987, 1987a; Turner et al., 1988) we describe the particle transport from a turbulently mixed gas to walls, including effects such as diffusion, sedimentation, electrical forces and thermophoresis. The energy balance for our system showed that the temperature change in the vessel for aerosol temperature up to 200°C is rather small. Thus only a small temperature gradient occurs at the walls and thermophoresis can be neglected. The vessel itself is metallic and grounded. Therefore Coulombic forces, the most important electrical forces, can also be excluded. The "General Dynamic Equation (GDE)" (Friedlander 1977; Gelbard et al., 1979) describes the changes in an aerosol. There is no general analytical solution available. Several numerical solutions can be found in literature. In most cases the aerosol in a containment of a nuclear power plant after an accident is considered. A comparison of the developed codes (Schwientek, 1988) reveals that most of the codes allow any initial particle size

distribution. Some use the moment method based on a certain type of distribution. Detailed investigations of different programs (NEA, 1979; Fermandjian et al., 1986; Seigneur et al., 1986) showed good agreement even with codes assuming a log-normal size distribution. We also observed good agreement between our code ASTA (Schwientek, 1988) based on MAEROS (Gelbard, 1982) and MAD (Whitby, 1986), which assumes a log-normal distribution. The codes differ also with respect to the considered effects. Before using a code it is therefore necessary to check whether the important effects are included or not. Differences also occur because of differences in the coefficients used in the GDE. There is still basic research needed to establish a correct set of coefficients for all conditions.

The results described further on were gained using ASTA which is an expanded MAEROS version including sources and sinks in the vessel. The used equations are comparable to those given in NEA, 1979. The effects which are uncertain in literature like coagulation due to sedimentation and turbulence, thermophoresis and diffusiophoresis (NEA, 1985) are unimportant in our case, because submicron particles in a vapour free gas are considered, small flow and only very small temperature gradients occur in the vessel. Ideal mixing is assumed. Experimentally a fan was used to achieve good mixing. To check the assumption of ideal mixing the particle number concentration as a function of time in the vessel challenged with nearly monodisperse aerosols with D_p = 0,1 µm (small losses at the walls) and of low concentration to avoid coagulation was measured for different numbers of fan revolutions per minute. Above 280 rpm the measured values compared very well with the ideal ones. With increasing mixing the thickness of the diffusion boundary layer should change. This is a system dependent parameter which has to be introduced into the code. A literature search revealed different thicknesses of the

diffusion boundary layer (Schwientek, 1988). Therefore these parameters had to be determined for our system as a function of particle size. The diffusion boundary layer thickness for different numbers of revolution was determined as a function of particle size by measuring the particle number concentration in a filled vessel as a function of time. Monodisperse neutralized NaCl-particles of low concentration with 25 nm < D_p < 150 nm were used. Thus diffusion was the only effect. In case of pure diffusion with an aerosol sink the relative number concentration as a function of time is:

$$/4/ \qquad C_N/C_{NO} = \exp(-(\beta + \dot{V}/V_B) \cdot t)$$

with β the diffusion constant.

The diffusion boundary layer thickness is derived using the relationship

$$\beta = DA/(\delta V_B)$$

with D diffusion coefficient and A surface of vessel.

In fig. 2 the thickness of the diffusion boundary layer is plotted for different numbers of revolution as a function of particle size. Above D_p = 0,16 µm the thickness does not change very much. It was found by extrapolation.

In the particle size range D_p < 0,1 µm model and experiment were adjusted via the diffusion layer thickness. For particles with D_p > 0,1 µm sedimentation becomes more and more important. Because diffusion and sedimentation are coupled and the extrapolated diffusion layer thickness was used, an experimental check in this size range was performed. With increasing particle number concentration changes occur because of coagulation. Aerosols with high number concentrations were

also included in the experimental verification of the model because of the uncertainties in the coagulation coefficients and effects.

5. Experimental verification of the model

Polydisperse Dioctylphatalat (DOP) aerosols (D_{pg} = 0,8 µm and σ_g = 1,3) were produced (see fig. 3). The aerosol generator (MAGE) produces a highly concentrated aerosol which was diluted step by step (factor 10 per step; maximal 1000). The aerosol flow rate into the mixing vessel (315 l) was 5 l/min. The aerosol was mixed in the chamber (280 rpm) with particle free air saturated with DOP to avoid evaporation of aerosol particles. An Aerodynamic Particle Sizer (APS) sampled from the vessel with the same flow rate. The APS determined the changes in the number concentration as well as the size distribution as a function of time. The diluters were moved one after the other from the place in front of the chamber to the place in front of the APS. By this procedure the generator concentration was increased step by step. The APS is challenged with almost the same aerosol. Differences occur only, if effects which are depending on number concentration (coagulation) are important. This procedure reduces measurement errors quite a bit.

Fig. 4 and 5 show the relative concentration as well as geometric mean diameter and geometric standard deviation changes as a function of time during sampling and dilution from the filled vessel. The dots refer to the measured, the full lines to the calculated results. The calculations were performed using the code ASTA. The theoretical results have been confirmed using the code PARDISEKO (Bunz, 1988). The observed relative concentration changes are mainly due to dilution and to a small amount to particle losses at the wall for small number concentrations (compare with fig. 1). At

higher number concentrations coagulation becomes important. The changes in number concentration increase. Only small changes in the geometric mean diameter and standard deviation (at most 15 %) occur. The shown discrepancy between theoretical and experimental results in the case of the geometric mean diameter is probably due to lack in the size resolution of the APS. This is obvious from fig. 6, which shows the size distribution measured at the beginning and after 120 min of filling the vessel. One needs a very accurate measurement technique with respect to sizing and concentration measurement to detect the differences in size distribution.

The comparison of experimental and theoretical results leads to the conclusion that the code (ASTA) can be used to predict the changes occurring in aerosols with liquid particles during handling in a vessel. It can be used therefore for error estimations.

In case of DOP this recommendation is limited to particles with $D_p > 0{,}1$ µm in a saturated chamber, because small changes in the rate of saturation will cause evaporation of or condensation on particles. For conditioning (f. i. dilution) or investigation of coagulation processes of very small liquid particles a mixing chamber should not be used. A laminar tube flow with short residence times seems to be more appropriate in this case (Wagner, 1988).

To study the changes in an aerosol with small solid particles especially at high concentrations (coagulation) nearly spherical sodium-chloride particles in the size range $D_p < 0{,}15$ µm were produced (Bartz et al., 1985). The concentration was measured with a condensation nuclei counter (CNC). Fig. 7 gives an example of the measured and calculated concentration ratio as a function of time during sampling. The code shows results (dotted line) which are far above the measured values.

Using a factor of 3 in the coagulation function yields a good comparison of measured and calculated results. There are several reasons for the discrepancy. First of all during coagulation non-spherical aggregates are formed. Therefore an aerodynamic and coagulation shape factor has to be introduced into the coagulation function (Zeller, 1985). Also in the investigated size range uncertainties exist with respect to the coagulation function of spherical particles (for instance the role of Van der Waals-forces). Therefore the interpretation of the data is reconsidered at the present time (Schwientek, 1988).

6. Summary

The dynamic changes of an aerosol in a mixing chamber caused by particle losses to the walls (diffusion, sedimentation) and coagulation were investigated theoretically and experimentally. It was demonstrated that the developed code ASTA based on the code MAEROS can be used for error estimation when using a mixing vessel in the handling procedure of an aerosol. This recommendation is limited to large liquid particles (D_p > 0,1 µm for DOP; no condensation or evaporation). Also the system specific diffusion boundary layer thickness has to be known. It was determined by observing the changes in an aerosol with solid particles in the size range D_p < 0,15 µm and at low concentrations. In case of solid particles at high concentrations (coagulation) the present code has to be extended to be applicable to non-spherical particles. Specific informations about aerodynamic and coagulation shape factors are needed.

Acknowledgement

The authors are grateful to the Deutsche Forschungsgemeinschaft (Special Research Program 209, University of Duisburg, FRG).

7. Literature

Bunz H. (1988)
"Persönliche Mitteilung",
Kernforschungszentrum Karlsruhe/LAF,
Postfach 3640, D-7500 Karlsruhe/FRG

Fermandjian J., Bunz H., Dunbar I.,
Benio-Brocchier F. (1986)
"Comparison of European Computer Codes Relative to
Aerosol Behaviour in PWR Containment Buildings During
Severe Core Damage Accidents",
Aerosols: Formation and Reactivity,
Proceedings of the Second International Aerosol Conference
Berlin, September 1987, 1087-1091

Fissan H. J. (1987)
"Partikeltransport zu Produktoberflächen",
VDI-Berichte No. 654, 173-187

Fissan H. J., Turner J. R. (1987a)
"Particle Deposition from Turbulently-Mixed Gases",
Tagung der Gesellschaft für Aerosolforschung,
Hannover, September 1987,
J. Aerosol Science 18, 623-626

Friedlander (1977)
Smoke, Dust and Haze,
John Wiley & Sons, New York

Gelbard F. (1982)
MAEROS User Manual,
Sandia National Laboratories, NUREG/CR-1391,
Sand 80-0822, R7, Albuquerque, New Mexico

Gelbard F., Seinfeld J. (1979)
"The General Dynamics Equation for Aerosols",
J. Coll. Int. Sci. 68, 363-382

NEA (1979)
Nuclear Aerosols in Reactor Safety,
A State-of-the-Art Report by a Group of Experts of the
NEA Committee on the Safety of Nuclear Installations,
Nuclear Energy Agency Organisation for Economic
Cooperation and Development, OECD, Paris

NEA (1985)
Nuclear Aerosols in Reactor Safety,
Supplementary Report, Report to CSNI by an NEA Group
of Experts, Nuclear Energy Agency Organisation for
Economic Cooperation and Development, OECD, Paris

Schwientek G. (1988)
Dissertation Universität Duisburg, in Vorbereitung

Seigneur C., Hudischewskyj A. B., Seinfeld J. H.,
Whitby K. T., Whitby E. R., Brock J. R.,
Barnes H. M. (1986)
"Simulation of Aerosol Dynamics; A Comparative Review
of Mathematical Models",
Aerosol Sci. Technol. 5, 205-225

Turner J. R., Fissan H. J. (1988)
"Convective Diffusion of Particles in External Force
Fields: The Role of Electrostatics on Particle Removal
from Turbulently Mixed Gases",
eingereicht bei Chemical Engineering Science

Wagner P. (1988)
"Measurement of the Coagulation Function of Fine
Particles - The Influence of Experimental Conditions
and Observation Techniques",
erscheint im Tagungsband "Coagulation Workshop"
Kernforschungszentrum Karlsruhe (KFK), März 1988

Whitby E. (1986)
"The Modal Aerosol Dynamics Model",
Aerosols: Formation and Reactivity, Proceedings of the
Second International Aerosol Conference,
Berlin, September 1986

Zeller W. (1985)
"Direct Measurement of Aerosol Shape Factors",
Aerosol Sci. Technol. 4, 45-63

8. Figures

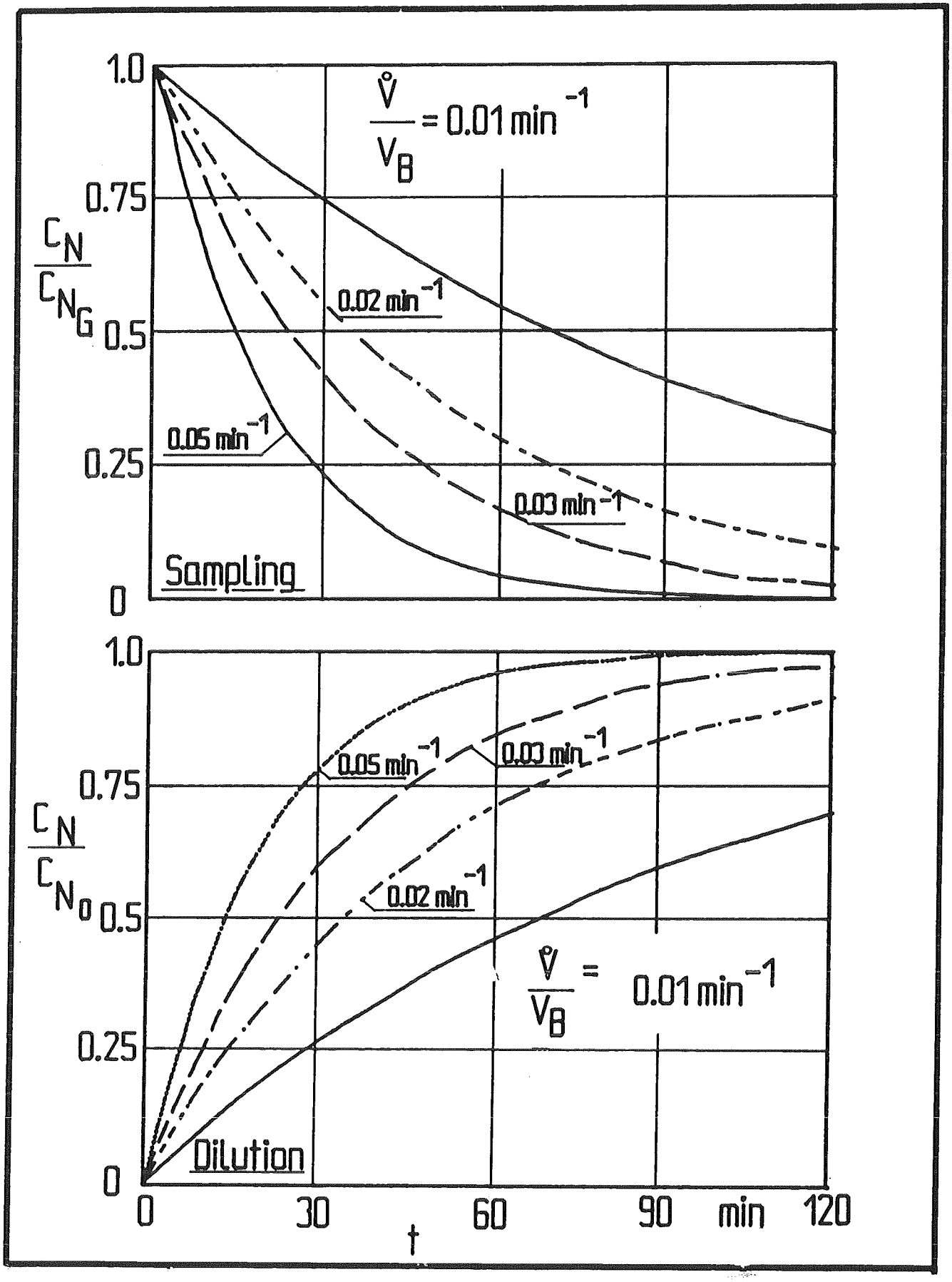

Fig. 1.: Ideal concentration changes in a vessel during sampling and dilution

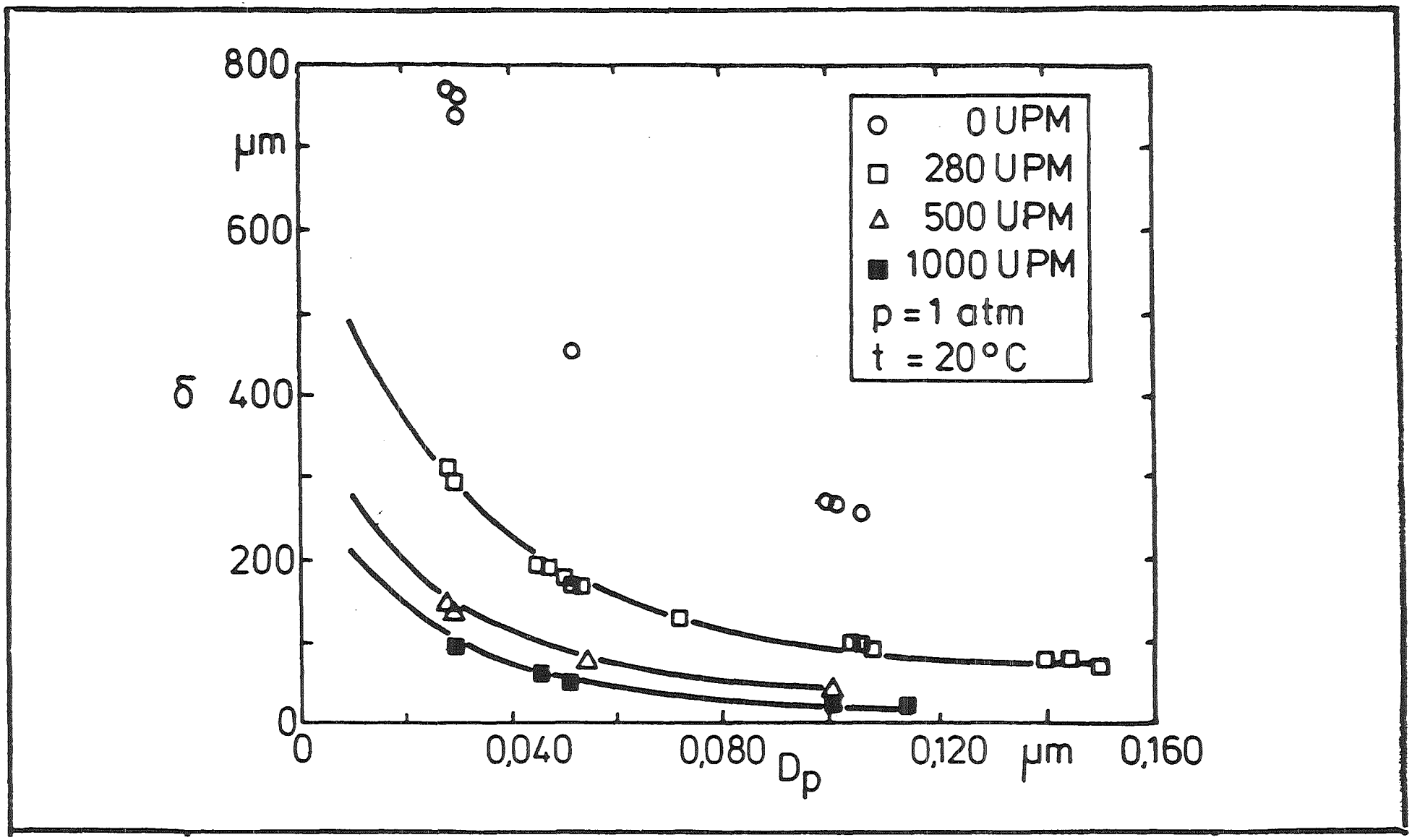

Fig. 2.: Diffusion boundary layer thickness as function of particle diameter

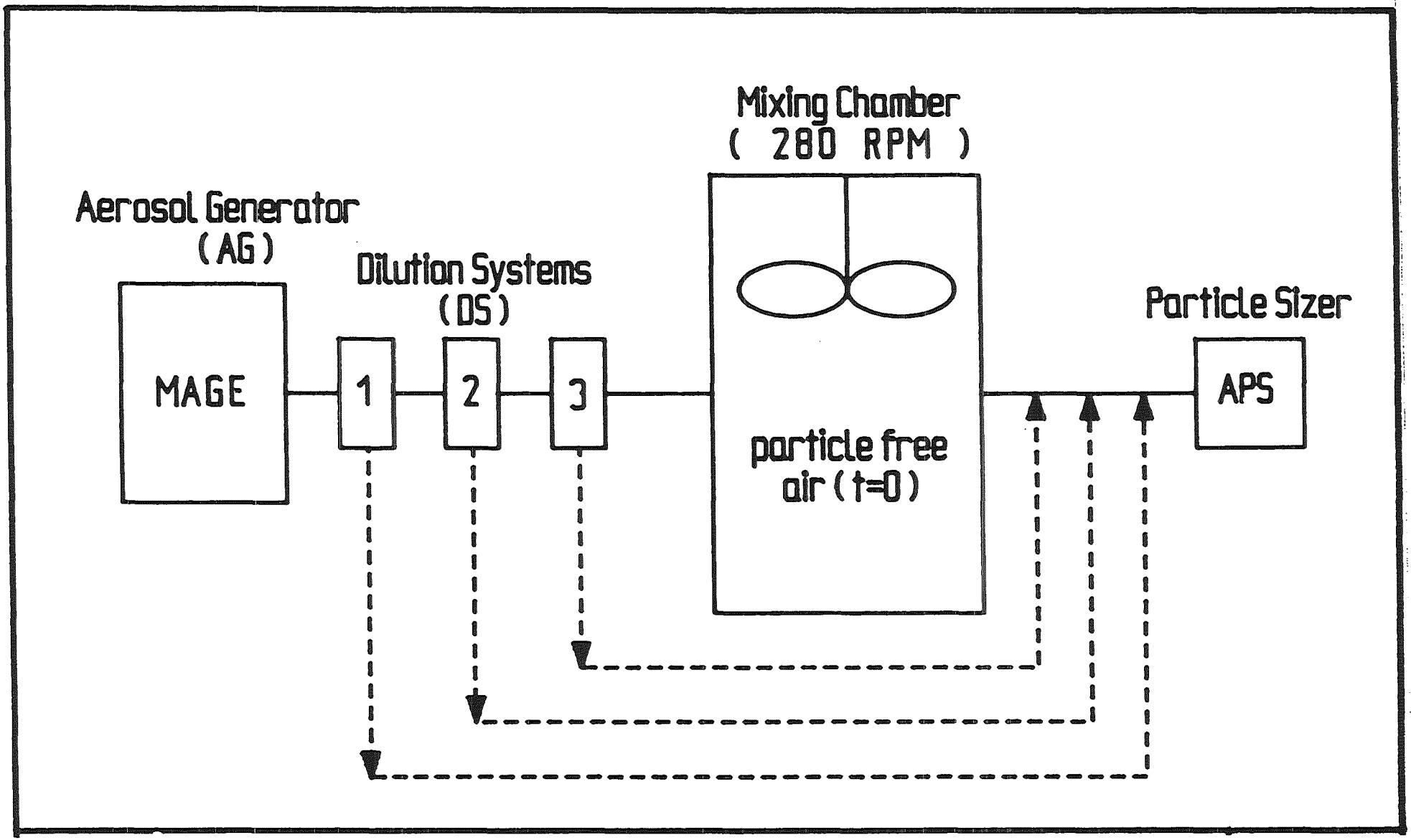

Fig. 3: Experimental set-up for verification of the used model

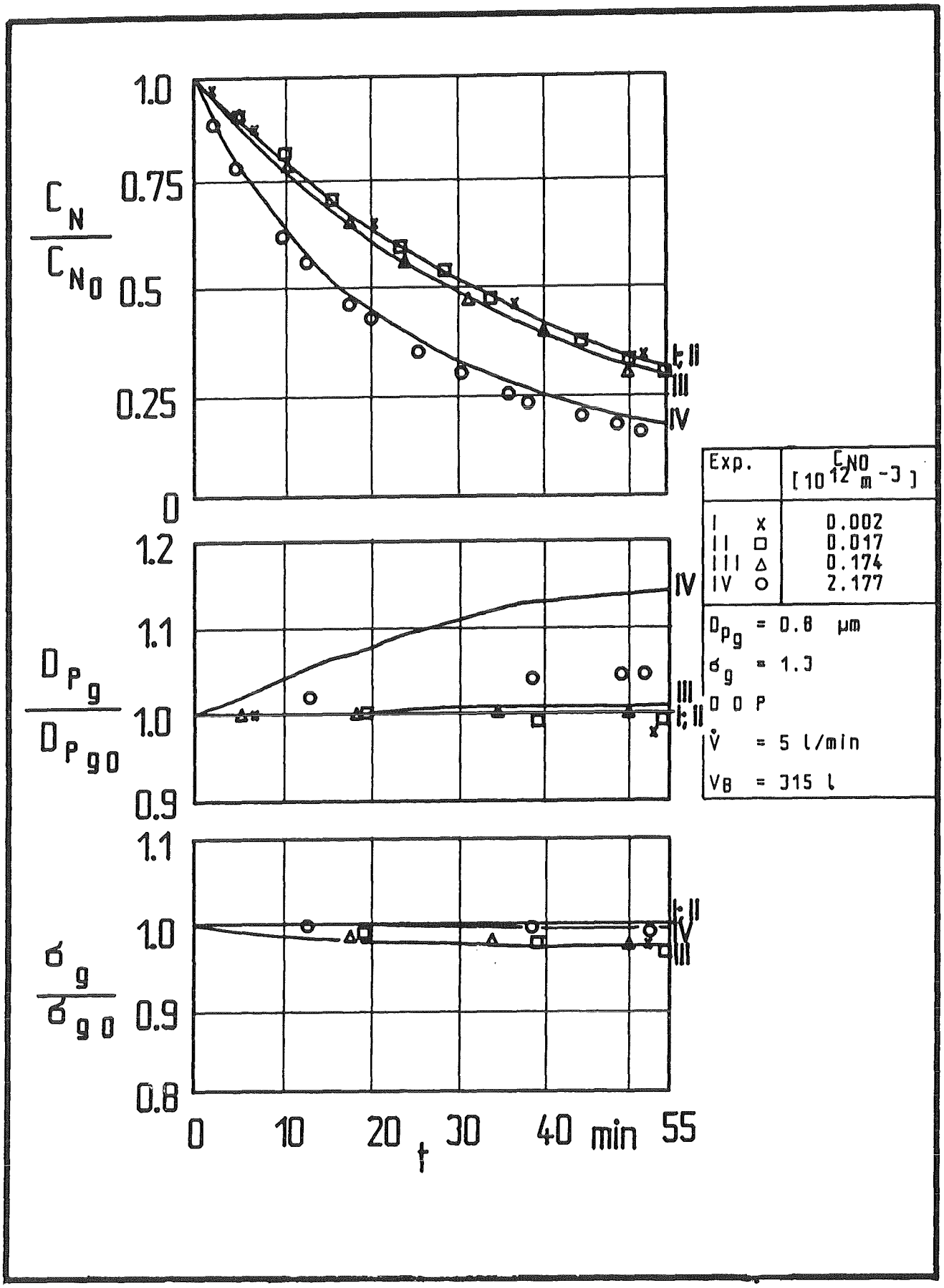

Fig. 4: Aerosol changes during sampling of liquid DOP-particles

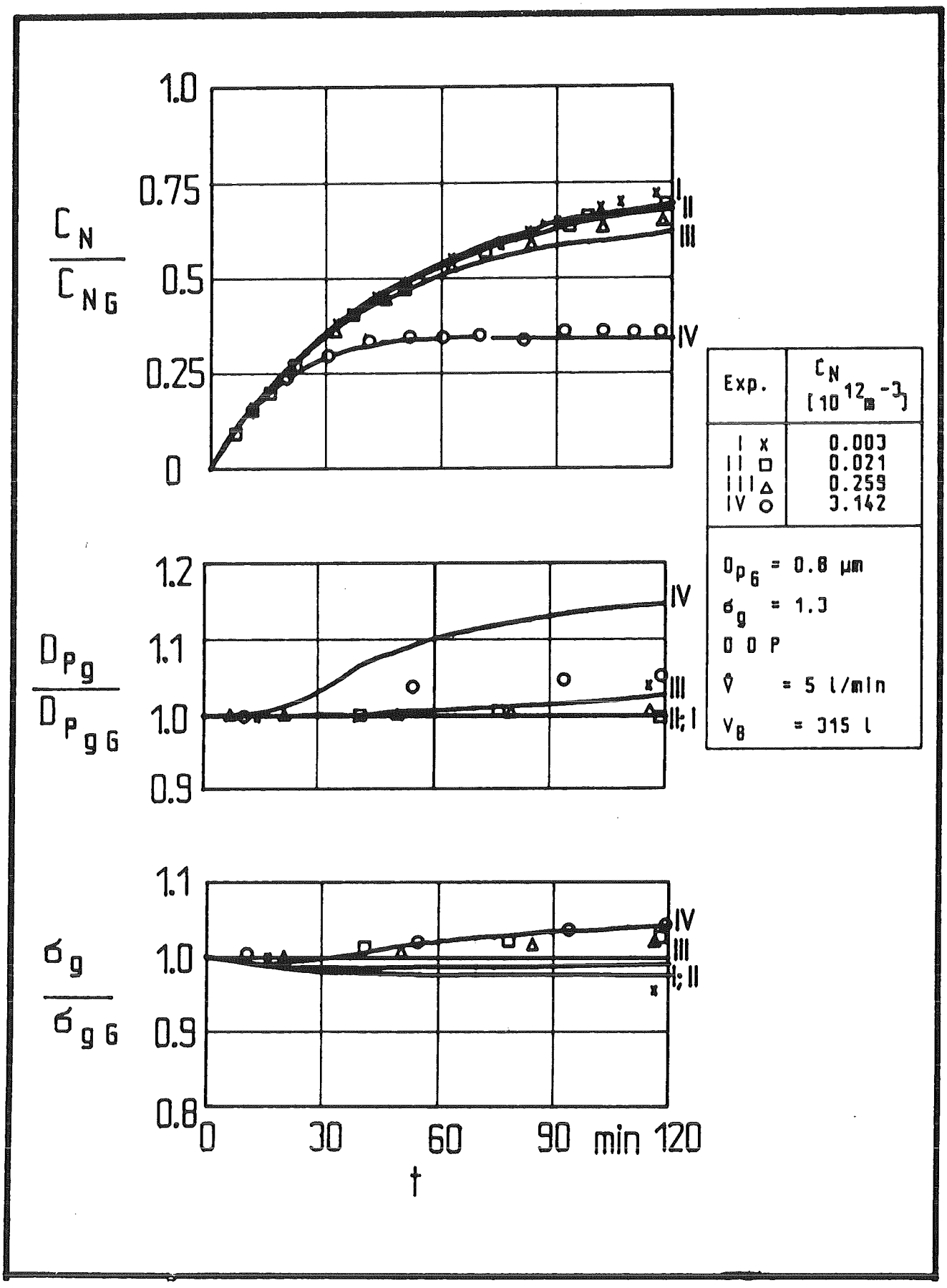

Fig. 5: Aerosol changes during dilution of liquid DOP-particles

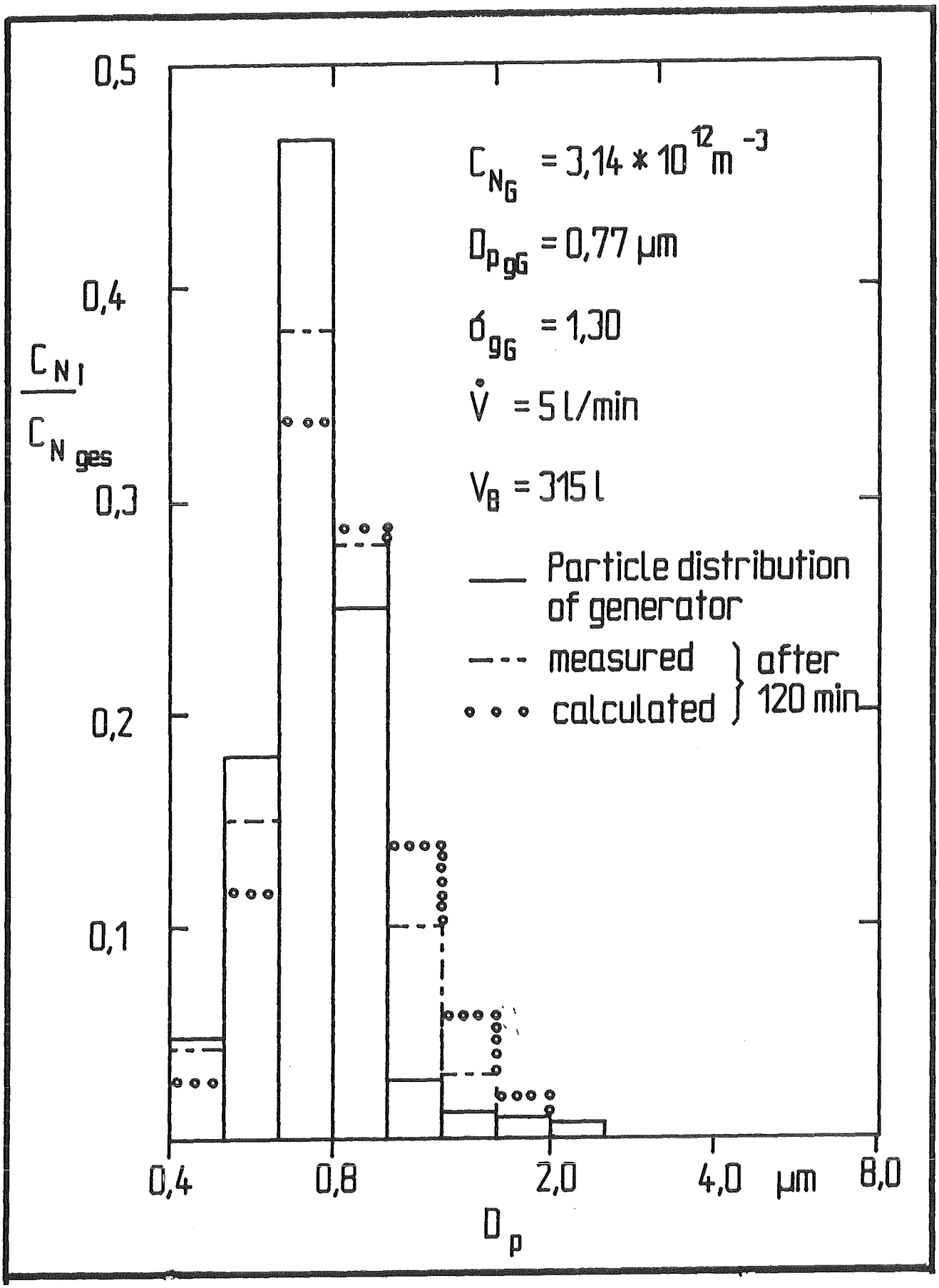

Fig. 6.: Comparison of particle size distributions for dilution processes

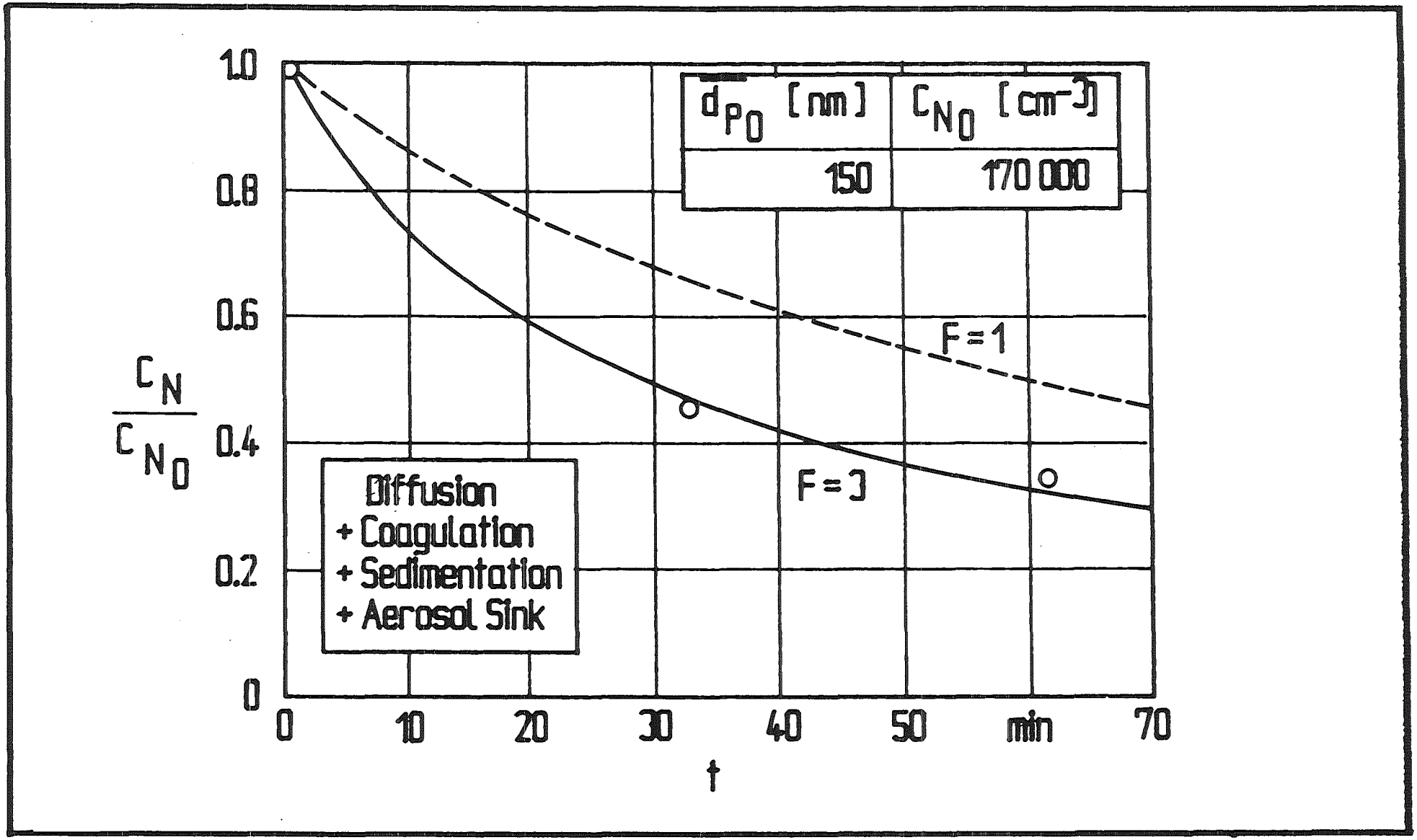

Fig. 7: Aerosol concentration changes during sampling of solid NaCl-particles

The Use of Different Coerrections for the Brownian Coagulation Function in Aerosol Behaviour Modelling

G. Metzig

Kernforschungszentrum Karlsruhe GmbH
Laboratorium für Aerosolphysik und Filtertechnik I
Postfach 36 40, 7500 Karlsruhe, W.-Germany

Abstract:

Smoluchowski`s theory of Brownian coagulation of aerosols in air as well as the corrections from Fuchs and Davies are discussed with respect to Knudsen numbers greater than 1. Own considerations to the coagulation theory are also presented, leading to a correction of Smoluchowski`s theory which pays more attention to the experimental results. PARDISEKO IV calculations were made to demonstrate the consequences when using the different corrections.

Nomenclature:

k	: Boltzmann constant
l	: mean free path
m	: mass of the unit; in air of one so-called "air-molecule"
r	: radius
v	: mean velocity
C	: Knudsen-Weber-(Cuningham) slip correction
D	: diffusion coefficient
K	: coagulation constant
Kn	: Knudsen number
Pe	: Peclet number
T	: temperature in Kelvin
η	: viscosity
ϱ	: density
ϕ	: gas kinetic constant equal 0.491

Subscripts:

g	: gas
p	: particle
SM	: Smoluchowski
F	: Fuchs
D	: Davies
M	: own consideration
GK	: gas kinetic conditions

Introduction

The scientific discussions about the Brownian coagulation constant of spherical monodisperese as well as polydisperse aerosols in air are still going on. Two adapted theories are available to evaluate the Brownian coagulation constant, namely Smoluchowski`s (1916) and the free molecule theory. Each is valid for a limited range of Kundsen numbers only. Which theory is usable depends on the size of the aerosol particles and/or on the mean free path of the carrier gas molecules. Difficulties occur between the two theories in the so-called transition regime. Many investigators (Fuchs, 1964; Hidy and Brock, 1970; Friedländer, 1977; Davies, 1979 etc) tried to find a formula describing the Brownian coagulation constant as a unique function in the whole Knudsen number range. The formulae from Fuchs and Davies are coupled to Smoluchowski`s coagulation constant K_0 but are corrected by a factor. This one from Fuchs is explainable by his concentration jump theory, while Davies interpolates for Knudsen numbers greater than 15 between the values of K_0 and those under gas kinetic conditions. He introduced a function of the Peclet number associating convective and diffusive motion.

In this paper, a new interpolation between Smoluchowski`s theory and the gas kinetic conditions is presented. The new correction factor is not based on an own theory. The correction factor is based on Fuchs` concentration jump theory and under special considerations of the experimental results from Shon (1979) and Fuchs and Sutugin (1965).

On the other side, evaluating the coagulation constant in the transition regime from experiments run into difficulties too, due to problems in measuring ultrafine particles. The dilemma is to exclude other removal processes. In Mercier`s (1978) review the errors which occured in experiments are specified.

The exact knowledge of the coagulation constant over the whole range of Knudsen numbers is for example of importance for simulations of aerosols in closed containments. Especially when ultrafine particles are present, i.e. early state situations with ongoing nucleation, the effect in changing the removal rate is the greatest. The longer the experiment or the simulation runs,

the smaller is the influence of the coagulation constant in the transition regime. It is well known that longtime experiments (atmosphere) produce always the same distribution independent of the initial distribution.

The coagulation constant

Under the well-known assumptions, the rate of coagulation is controlled by the Smoluchowski coefficient of coagulation

$$K_{sm} = \frac{4 \cdot k \cdot T}{3 \cdot \eta} \qquad (1)$$

which is dependent on the properties of the carrier medium but independent of the size and density of the particles. Adapting this expression to gases, the Knudsen-Weber-(Cunningham) slip correction has to be included. The necessary coefficients are taken from Metzig (1983). The resulting equation is valid for small Knudsen numbers ($Kn = l_g/r_p$) and for big particles,

$$K_o = K_{sm} \cdot C = \frac{4 \cdot k \cdot T}{3 \cdot \eta_g} \cdot \left\{1 + 1.2\,Kn + .432\,Kn \cdot e^{-1.039/Kn}\right\} \qquad (2)$$

respectively. Equation (2) has been confirmed by many experiments. However, this is not so in the case of large Knudsen numbers or small particles. The coagulation is now controlled by the gas kinetic theory. The idea is that very small particles have the same behaviour like the gas molecules. According to Jeans' gas kinetic theory (1925), the coagulation constant is:

$$K_{GK} = \frac{4 \cdot \pi \cdot r_p^2 \cdot v_p}{\sqrt{2}} \qquad (3)$$

The coagulation constant is independent on the Knudsen number and independent on the condition of the carrier gas. Involving this, equation (3) becomes:

$$K_{GK} = \frac{4}{\sqrt{2}} \cdot \left(\frac{\eta_g}{Kn \cdot \phi \cdot \rho_g \cdot \sqrt{\frac{3 \cdot k \cdot T}{m_g}}} \right)^2 \cdot \sqrt{\frac{6 \cdot k \cdot T \cdot Kn \cdot \phi \cdot \rho_g \cdot \sqrt{\frac{3 \cdot k \cdot T}{m_g}}}{\eta_g \cdot \rho_p}} \qquad (4)$$

Now the physical and thermodynamical properties of the particles and the carrier gas, respectively, jointly control the coagulation constant under gas kinetic conditions.

It is evident that the coagulation constant increases for small Knudsen numbers (following Smoluchowski`s theory) up to a maximum and decreases when changing to gas kinetic conditions.

If equation (2) and (4) are combined the resulting coagulation constant curve will have a sharp bend. That is in contradiction to processes which happen in nature.

Fuchs` correction

Fuchs tried to find a smooth curve transfering Smoluchowski`s theory into the gas kinetic conditions. He explained the correction with his concentration jump theory. In his opinion the coagulation constant is described by the following equation:

$$K_F = K_{sm} \cdot C \cdot \left(\frac{1}{1 + G_o} \right) \qquad (5)$$

with

$$G_o = \frac{4 \cdot D}{r_p} \cdot \sqrt{\frac{\pi \cdot m_p}{8 \cdot k \cdot T}} \qquad (6)$$

Davies (1979) disagrees with this correction theory. He refuses to believe the analogy between the coagulation of particles and evaporation and condensation of gas molecules. He refers to an underestimation of the rate of coagulation as Kn rises from 0.5 to 15 (see fig. 1).

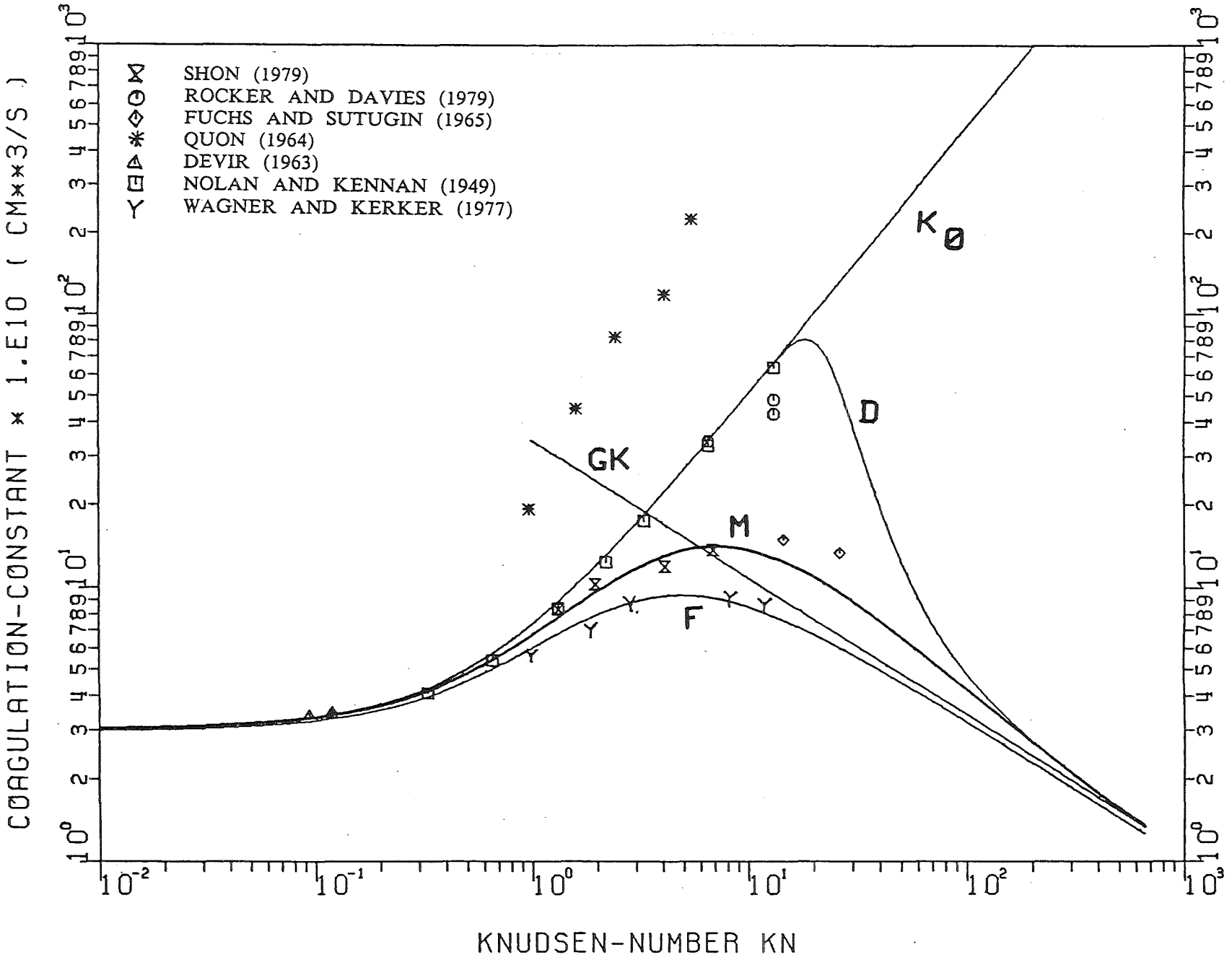

Fig.1:(Air, 293 Kelvin, spherical particles of unit density)

Davies` correction

Davies agrees that the coagulation constant must change to gas kinetic conditions for Knudsen numbers above 15. In his correction the decrease of the coagulation constant is affected

$$Pe = \frac{2 \cdot v_p \cdot r_p}{D} \tag{7}$$

by the Peclet-number which is invariable in problems associating convective and diffusive motion. This can be explained as follows (Davies, 1979): The mean velocity at which a particle passes another particle, with which the possibility of collision exists, is proportional to v_p; during the time of passing, the velocity of approach oo the particles, due to Brownian motion, is proportional to $D/2\ r_p$. Equation (7) is the ratio of the distance travelled at the velocity of translation to the distance diffused on account of Brownian motion, during the same short time interval.

It is nescessary to find a function of Pe which will interpolate between the values of K_o and K_{GK}. According to Davies the interpolation is restricted to Knudsen numbers greater than 15. The coagulation constant due to Davies is now:

$$K_D = K_{sm} \cdot C \cdot \left\{ 1 + \frac{8 \cdot e^{[-9.03 \cdot Pe]}}{2 \cdot Pe} \right\}^{-1} \tag{8}$$

In my opinion the value of 15 is choosen to high. As it will be shown later, there is no difference when using K_o or K_D in PARDISEKO IV calculations. The value of 15 is also higher than a number of experiments are showing. The coagulation constant curve should mark the lower boundary of all coagulation constant values found in experiments. Zeller (1983, 1985) who performed direct measurements of aerosol shape factors had to reduce the coagulation constant K_o to get agreement between measured and calculated size distributions. His maximum in Knudsen numbers was 13.2.

Own considerations

No independent theory exists in the transition regime. An interpolation between gas kinetic and hydrodynamic conditions can be made only. Fuchs and Davies presented different physical conceptions of the coagulation process in the transition regime leading to different descriptions of the coagulation constant curve. Meanwhile, more experiments are available and can be used to find a good approximation to the "true" coagulation constant curve.

The following conditions should be fulfilled:

- For Knudsen numbers smaller than 0.1, the coagulation constant is equal K_o.
- The theoretical coagulation constant curve represents a lower boundary for experiments.
- The coagulation constant curve is of smooth character.
- For very large Knudsen numbers, the coagulation constant values should pass over to the gas kinetic values.

The following expression of the coagulation constant is based on the above statements, on Fuchs` concentration jump theory, and on experimental results:

$$K_M = K_{sm} \cdot C \cdot \left(\frac{1}{.985 + M_o} \right) \tag{9}$$

with

$$M_o = G_o \cdot \left\{ \frac{2 + Kn/25}{1 + Kn/100} \right\} \tag{10}$$

The coagulation constant curves for each theory mentioned above are plotted in figure 1. For better orientation, some experimental results are added. All calculations are done for air, 293 Kelvin, and spherical particles of unit density. The consequences when using the different corrections in computer programms for calculations of the aerosol behaviour are discussed in the next section.

PARDISEKO IV calculations

Adapting the coagulation constant to computer programms, like PARDISEKO IV (Bunz, 1983), the coagulation of particles with different radii has to be taken into account. For that, in all equations the physical properties of single particles must be replaced by an average value of the properties of the two different particles.

For all PARDISEKO IV calculations, the thermodynamic conditions are chosen like those shown in figure 1. Only the Brownian coagulation process is considered, other removal effects are excluded. The mass (figure 2) and the number concentration (figure 3) are plotted versus the mass equivalent radius at three different times (0, 1.2 and 30 seconds after start). The initial distribution is selected for Knudsen numbers between 25 and 230. Within one second, Davies` and Smoluchowski`s coagulation constant, respectively, produce exactly the same number concentration as well as mass distribution. Using Fuchs` correction, the particle growth due to Brownian coagulation is not as fast as observed in experiments. With the own correction, the results are in between. Whether this correction describes the true conditions or not can be checked with experiments only. The observation period in such an experiment must be within a few seconds having initial start distributions like above. During longer observation times, after 10 minutes at the latest, all corrections produce the same final distribution. Therefore in this case, the Smoluchowski`s coagulation constant curve is sufficient. The correction is nescessary for short-term calculations and of importance for source term evaluations and for nucleation processes.

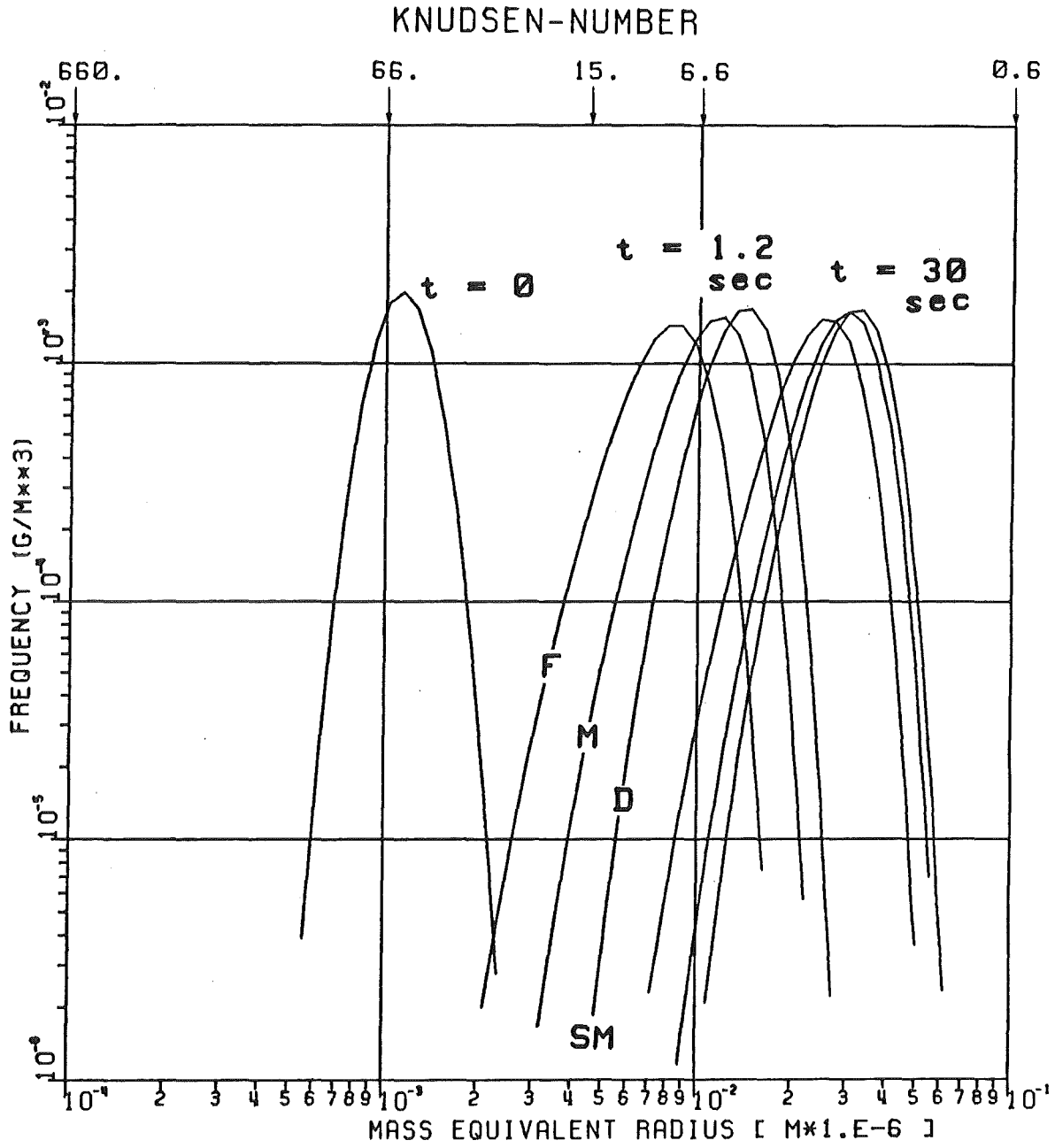

Fig. 2: PARDISEKO 4 calculations

(Air, 293 Kelvin, spherical particles of unit density)

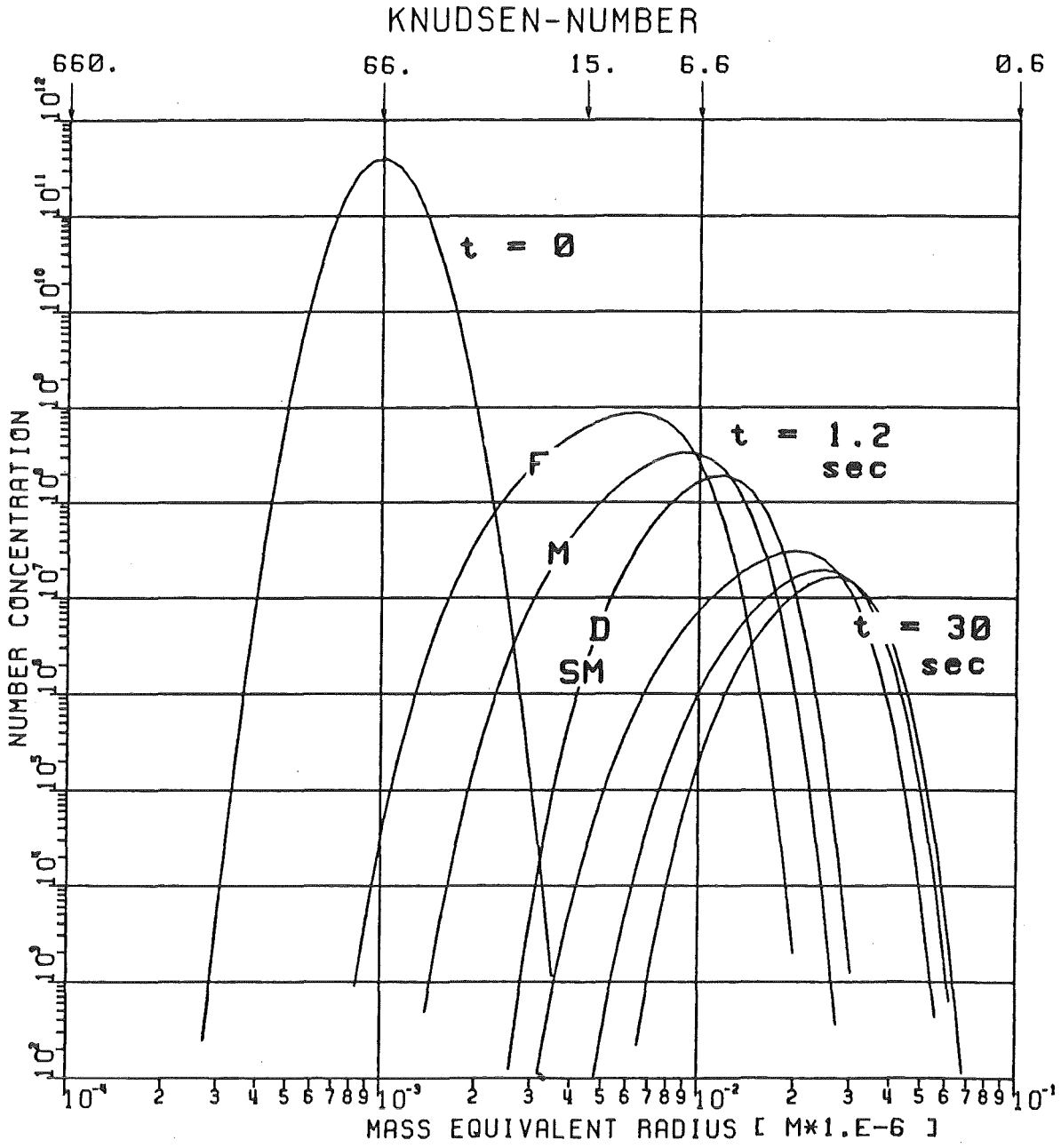

Fig. 3: PARDISEKO 4 calculations

(Air, 293 Kelvin, spherical particles of unit density)

References

Bunz, H., 1983: PARDISEKO IV: Ein Computerprogramm zur Berechnung des Aerosolverhaltens in geschlossenen Behältern, KfK-Bericht 3545, Kernforschungszentrum Karlsruhe

Davies, C.N., 1979: Coagulation of Aerosols by Brownian Motion, J. Aerosol Sci., 10, p 151-161

Devir, S.E., 1963: On the Coagulation of Aerosols (part I). J. of Colloid Sci., 18, p 744-756

Friedländer, S.K., 1977: Smoke, Dust and Haze. In: Atmospheric Aerosols. Ed. by S. Twomey, Elsevier, Amsterdam

Fuchs, N.A., 1964: The Mechanics of Aerosols. Pergamon Press, Oxford

Fuchs, N.A. and A.G. Sutugin, 1965: Coagulation Rate of highly Dispersed Aerosols. J. of Colloid Sci., 20, p 492-500

Hidy, G.M. and J.R. Brock, 1970: The Dynamics of Aerocolloidal Systems. Pergamon Press, Oxford

Jeans, J.H., 1925: The Dynamical Theory of Gases. Dover Publications, New York

Mercer, T.T., 1978: Fundamentals of Aerosol Science. Ed. by D.T. Shaw, Chapt. 2, Wiley, New York

Nolan, P.J. and E.L. Kennan, 1949: Condensation Nuclei from Hot Platinum: Size, Coagulation Coefficient and Charge-distribution. Proc. Royal Irish Academy, 52, (1948-1950), p 171-190

Quon, J.E., 1964: Experimental Determination of the Coagulation Rate Constant for Nuclei. Int. J. Air Wat. Poll., Pergamon Press, 8, p 355-368

Rooker, S.J. and C.N. Davies, 1979: Measurements of the Coagulation Rate of a High Knudsen-number Aerosol with Allowance for Wall Losses. J. of Aerosol Sci., 10, p 139-150

Shon, S.N., 1979: An Experimental Study of the Coagulation of Aerosols by Brownian Motion. Thesis of PH.D. State University of New York at Buffalo

v. Smoluchowski, M., 1916: Drei Vorträge über Diffussion, Brown`sche Molekularbewegung und Koagulation von Kolloidteilchen. Physik. Zeitschrift, XVII, p 557-599

Zeller, W., 1983: Direkte Messung von Aerosolformfaktoren. KfK-Bericht 3560, Kernforschungszentrum Karlsruhe

Zeller, W., 1985: Direct Measurements of Aerosol Shape Factors. Aerosol Science and Technology, 4, No 1, p 45-63

Coagulation by Alternative Forces (Gravitation, Electric Forces, Turbulence, Acoustic)

Chairman: W.H. Marlow

On the state of the art of acoustic coagulation

- Review Paper -

by

D.T. Shaw

"This manuscript was not made available
for printing"

TURBULENT COAGULATION INDUCED BY ACOUSTIC FIELD OF LIQUID AND SOLID AEROSOLS

D. BOULAUD and C. MALHERBE

Laboratoire de Physique et Métrologie des Aérosols
IPSN/DPT/SPIN
Commissariat à l'Energie Atomique
BP 6, 92265 FONTENAY AUX ROSES CEDEX, France

1. INTRODUCTION

The acoustic conditionning of fine particles in an aerosol is a process by which the fraction of particles having the smallest diameters vanishes through agglomeration on large particles ; this phenomenon is induced by an acoustic field. The corresponding variation in the particle size distribution is an important factor as it allows the fraction which is most difficult to filter directly to be eliminated. Conventional equipment located further downstream such as cyclones, granular beds, ... can then be used to eliminated the agglomerates formed.

Increased agglomeration rates leading to these rapid changes in size are due to the increase in particles collision rates through particle and acoustic field interactions.

Acoustic agglomeration has already been successfully used for particle size conditionning. Most of the experiments carried out are summarized in E.P. MEDNIKOV's book (1965) / 1 /. The subject has recently been the object of renewed attention by D.T. SHAW (1976) and K.H. CHOU et al (1981) / 2 /, / 3 /. The latter studies showed the effects of high acoustic intensities of the order of 160 dB (1 W/cm^2) on agglomeration mechanisms.

In this paper after a brief recall on the theoretical background, the first part is devoted to experimental results obtained. On acoustic agglomeration (AA) of liquid and solid aerosols.

The second part concern the study of turbulence induced by strong acoustic field.

And the last part concern the aerosol precipitation due to turbulence induced by strong acoustic field.

2. THEORETICAL BACKGROUND

Generally, the agglomeration equation describing variations in the concentration of particles of volume x over time t can be written :

$$\frac{\delta n(x,t)}{\delta t} = \frac{1}{2} \int_0^x K\,(y,x-y,t)\; n\,(x-y,t)\; n\,(y,t)\; dy - n\,(x,t) \int_0^\infty K\,(x,y,t)\; n\,(y,t)\; dy \qquad (1)$$

The first term of the righthand member of the equation represents the production of particles of volume x through collisions between particles of volume y and (x-y).

The second term represents the vanishing of particles of volume x through collisions with other particles, n (x,t) is the distribution function expressed as a function of the volume of number of particles per unit volume of fluid at time t ; K (x,y,t) is the agglomeration coefficient for particles having volumes x and y.

A knowledge of the coefficient of agglomeration is therefore entirely sufficient to predict n (x,t) behavior when the conditions at the origin are known. Unfortunately, the phenomena intervening in A-A are extremely complex and four types of interactions must be combined :

- orthokinetic,
- hydrodynamic,
- turbulent inertial,
- turbulent diffusional,

in order to define an agglomeration coefficient that can be used in the preceeding integro-differential equation.

2.1. Orthokinetic interactions result from collisions between small particles highly influenced by vibrations and large particles which are virtually stationary.

In this case, the coefficient of coagulation has the following form :

$$K_{oc} = \frac{N_1}{N_t} (a_1 + a_2)^2 E_{oc} \mu_{12} U_g \qquad (2)$$

where N_1 is the large particle concentration, N_t the total concentration, a_1 and a_2 the radii of the large and fine particles, μ_{12} the relative entrainment factor, E_{oc} the collision efficiency and U_g the vibrational velocity of the gas-medium. μ_{12} is a function of the vibrational frequency and the relaxation time of the particles. U_g is a function of the acoustic intensity, velocity of sound and density of the gas-medium.

2.2. Hydrodynamic interaction

This type of interaction is mainly resulting from mutual distorsion of the flow fields around interacting particles. In this case the agglomeration coefficient has the following form :

$$K_{IH} = \pi (a_1 + a_2)^2 E_{IH} V_{rel} \qquad (3)$$

E_{IH} is the collision efficiency and V_{rel} the relative velocities between interacting particles. V_{rel} has a complex analytical form which is a function of the vibrational velocity of the fluid, the relative entrainment factor, the size of the particles an vibrational frequency.

2.3. Turbulent interactions

When the acoustic intensity increases (I > 160 dB), interactions due to turbulence in the fluid become very important and lead to increased particles agglomeration. This type of interaction can be divided into two categories : turbulent diffusional and turbulent inertial. In these interactions, the agglomeration process occurs in small eddies whose sizes are characterized by the Kolmogorov microscale :

$$d \cong (\nu^3/\varepsilon)^{1/4} \qquad (4)$$

where ε is the time rate of energy dissipation of turbulence per unit mass and ν is the kinematic viscosity of the gas-medium.

In the case where particles are completely entrained by the fluid, the agglomeration process can be treated by an approach identical to the diffusional approach of Smoluchowski : In the opposite case the relative velocities of particles must be taken into account as a result of their different inertias ; collision likelihoods are increased in consequence.

2.3.1. Turbulent diffusional interaction

The hypothesis of particles being completely entrained leads to a coefficient of agglomeration of the following form :

$$K_{DT} \cong \pi \, (a_1 + a_2)^3 \, E_{DT} \, (\varepsilon/\nu)^{1/2} \qquad (5)$$

where E_{DT} is the collision efficiency, often taken as unit for particles of the same size.

2.3.2. Turbulent inertial interaction

The hypothesis of different degrees of entrainment for particles of different size leads to a coefficient of agglomeration of the following form :

$$K \cong \pi \, E_{IT} \, (a_1 + a_2)^2 \, (1 - \frac{\rho_g}{\rho_p}) \, (\tau_1 - \tau_2) \, (\varepsilon^3/\nu)^{1/4} \qquad (6)$$

where ρ_g and ρ_p are the respective densities of the gas and particles, τ_i the relaxation time of particles i and E_{IT} the collision efficiency.

A knowledge of the analytical forms of the different agglomeration coefficients enables their variations to be predicted as a function of the conditions imposed. In the K.H. CHOU et al article (1981), a parametric study as a function of particle concentration, aerosol median diameter, standard deviation, acoustic intensity and frequency, temperature and pressure is presented / 3 /.

However, these studies are based on a mainly theoretical approach of particle collisions mechanisms under an acoustic field. Too scarce an amount of exploitable experimental studies are available to confirm theoretical predictions.

This situation led our laboratory to engage in an experimental study of AA in order to determine the sensitivity of this phenomenon to various parameters (acoustic intensities and frequencies, median diameters and standard deviations associated with size distributions of aerosols, residence times in agglomeration chambers).

During these experiments described in a first part of this article, significant particle deposits were observed on the agglomerator wall ; this phenomenon led us to undertake a specific study, described in the last part of this article, of particles precipitation under the influence of acoustic fields.

3. EXPERIMENTAL STUDIES OF ACOUSTIC AGGLOMERATION / 11 /

3.1. Experimental apparatus

The experimental device used, sketched on figure 1, consists of the following elements :

- Agglomeration chamber : this is a 4 liter glass cylinder (diameter 7 cm, length 100 cm). The aerosols produced are fed into the top of the tube at a flow rate of 20 to 100 lpm, corresponding to a residence time between 12 and 2.4 seconds.

- Acoustic source : a 100 W compression chamber (BOUYER 2 R 200) is placed at the top of the agglomeration cylinder. This chamber is powered by a low-frequency signal generator (HEWLETT PACKARD 3310 A) combined with a 200 W amplifier (BOUYER AS 240).

- Acoustic intensity measurement : this is performed by a BRUEL and KJAER measurement line comprising a microphone (BK 4136), a preamplifier (BK 2619) and a reading amplifier (BK 2609). The shape of the acoustic waves is monitored by an oscilloscope.

- Aerosol source : a polydisperse liquid aerosol is produced by pneumatic spraying of dioctylphtalate (DOP) solution. Before entering the agglomeration chamber this aerosol passes through a neutralizer, consisting of a krypton 85 source, to bring the electric charge of the aerosol to Boltzmann's equilibrium.

For the case of solid aerosol an emery powder is produced with a fluidized bed generator.

- Measurement of the aerosol size distribution : samples are taken at the bottom of the agglomeration chamber and measured by a cascade impactor (Andersen Mark II). The impactor calibration and data reduction have been described in earlier articles (D. BOULAUD et al 1981, D. BOULAUD and M. DIOURI 1982) / 4 /, / 5 /.

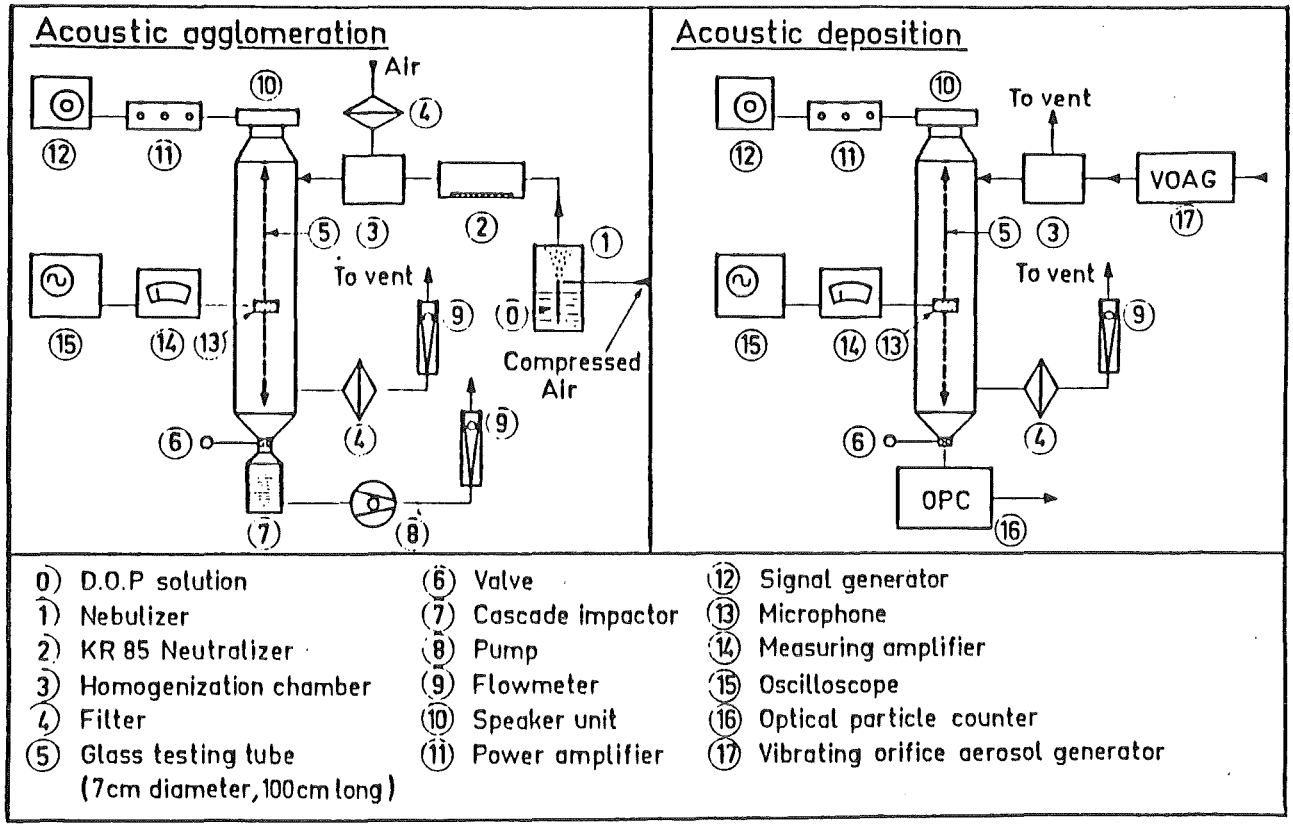

Figure 1 - Experimental set up for acoustic agglomeration and acoustic precipitation experiments

3.2. Experimental procedure

After measurement of the acoustic field in the tube the aerosol is produced and injected into the system. When the stationary state is established a first sampling with the impactor in the absence of acoustic field provides the original size distribution of the aerosol. The measured values of the aerodynamic mass median diameter (AMMD) and standard deviation (σ_g) are reproducible, whatever the residence time chosen (3.8 or 8.6 seconds), which shows that agglomeration phenomena other than acoustic are negligible. The mass concentration value can vary slightly from one experiment to another, remaining within the 0.5 to 1 g/m^3 range whatever the nature of aerosol.

The above operation is then repeated but in the presence of an acoustic field. This measurement gives the new aerosol size distribution after an agglomeration period corresponding to the residence time in the tube.

Figure 2 shows an example of the results obtained with liquid aerosol. Curve 1 represents the original distribution, curves 2 and 3 the change in this

distribution under the effect of an acoustic field of rising intensity, 156.7 and 162.7 respectively, and constant frequency 1 020 Hz, the residence time in the agglomerator remaining constant at 8.6 seconds.

Qualitative analysis of these results shows as expected that the AMMD and σ_g values increase with the sound pressure level. At the same time the mass concentration of the aerosol falls sharply, due to deposition of the particles on the agglomerator walls. This phenomenon, clearly apparent here, is hardly mentioned in the literature except by K.H. CHOU and al (1982) / 6 /.

3.3. Experimental results with liquid aerosols

During these experiments the characteristics of the aerosol introduced in the agglomerator were kept constant, the variables being the residence time in the agglomeration volume, the sound pressure level and the acoustic frequency.

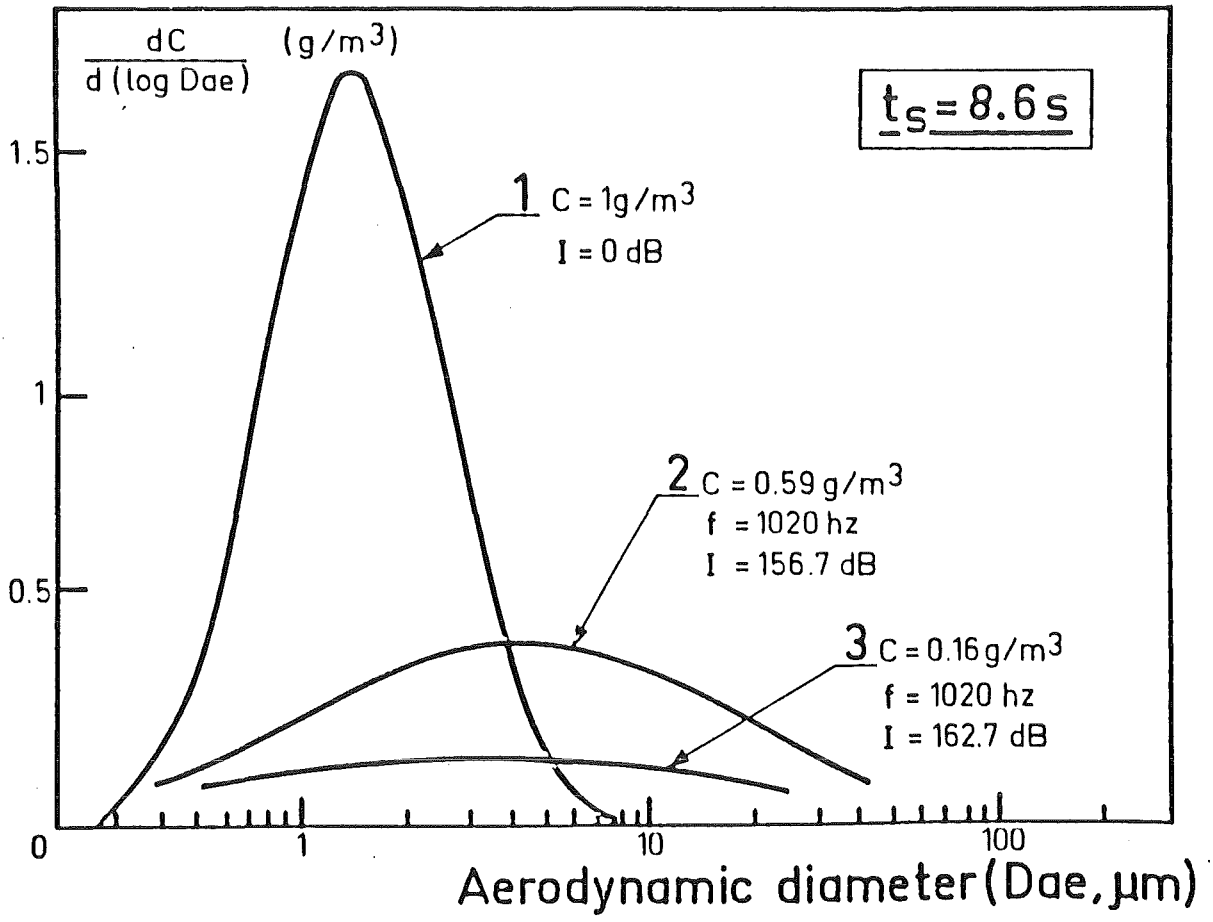

Figure 2 - Variations of the size distributions for different acoustic intensities (residence time t = 8.6 s)

Figures 3 and 4 show the AMMD and σ_g variations after agglomeration as a function of acoustic intensity for two different frequencies (540 and 1 020 Hz) and the same 8.6 seconds residence time. Figure 5 plots AMMD versus acoustic intensity for two different residence times (8.6 and 3.8 seconds) at the frequency 540 Hz.

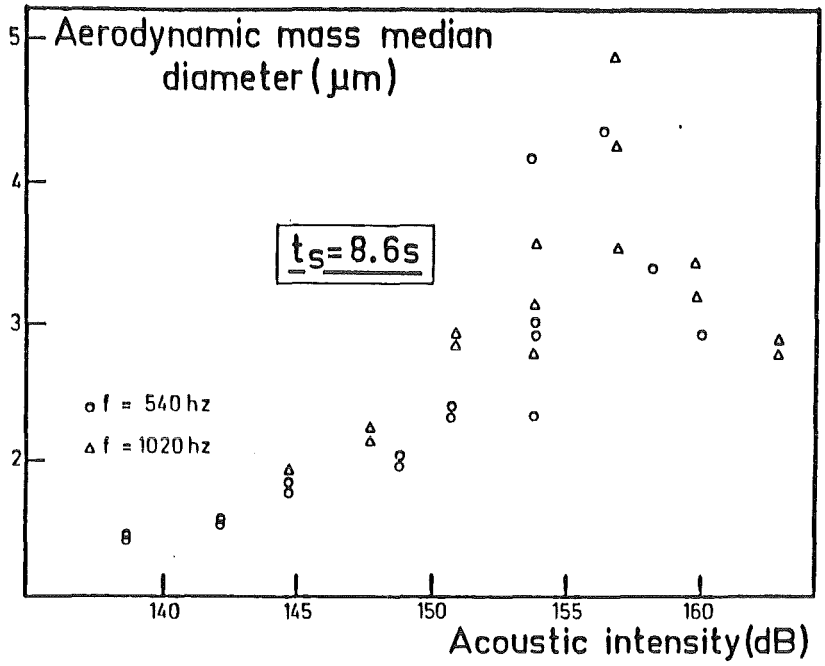

Figure 3 - Aerodynamic mass median diameter after an 8.6 seconds agglomeration time versus acoustic intensity, for two acoustic frequencies (540 and 1 020 Hz)

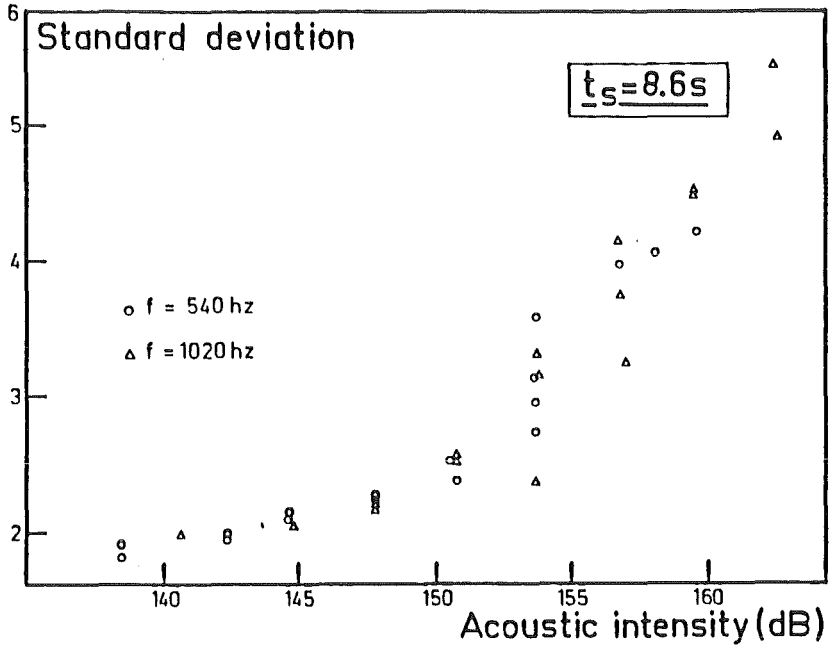

Figure 4 - Standard deviation versus acoustic intensity, for two acoustic frequencies (540 and 1 020 Hz)

From these figures the following conclusions may be drawn :

- little variation in AMMD and σ_g is observed between 100 and 140 dB,
- AMMD increases from 1.5 to 4.5 µm between 140 and 155 dB, reaches a maximum between 155 and 158 dB then drops suddenly when the acoustic intensity is raised further,
- similarly σ_g rises from 1.75 to 5 in the 140 to 160 dB range.

The influence of acoustic frequency on the AMMD and σ_g variations is insignificant in the 500 to 1 000 Hz range, while the effect of residence time on AMMD remains negligible except around the maximum. This tends to prove that agglomeration phenomena are effective mainly during the first few seconds, then diminish as the particles collide and their numerical concentration decreases. This effect is enhanced by heavy particle deposits on the walls as shown on figure 6, where the percentage aerosol mass deposition varies from 0 to 85 % as the sound pressure rises from 130 to 163 dB.

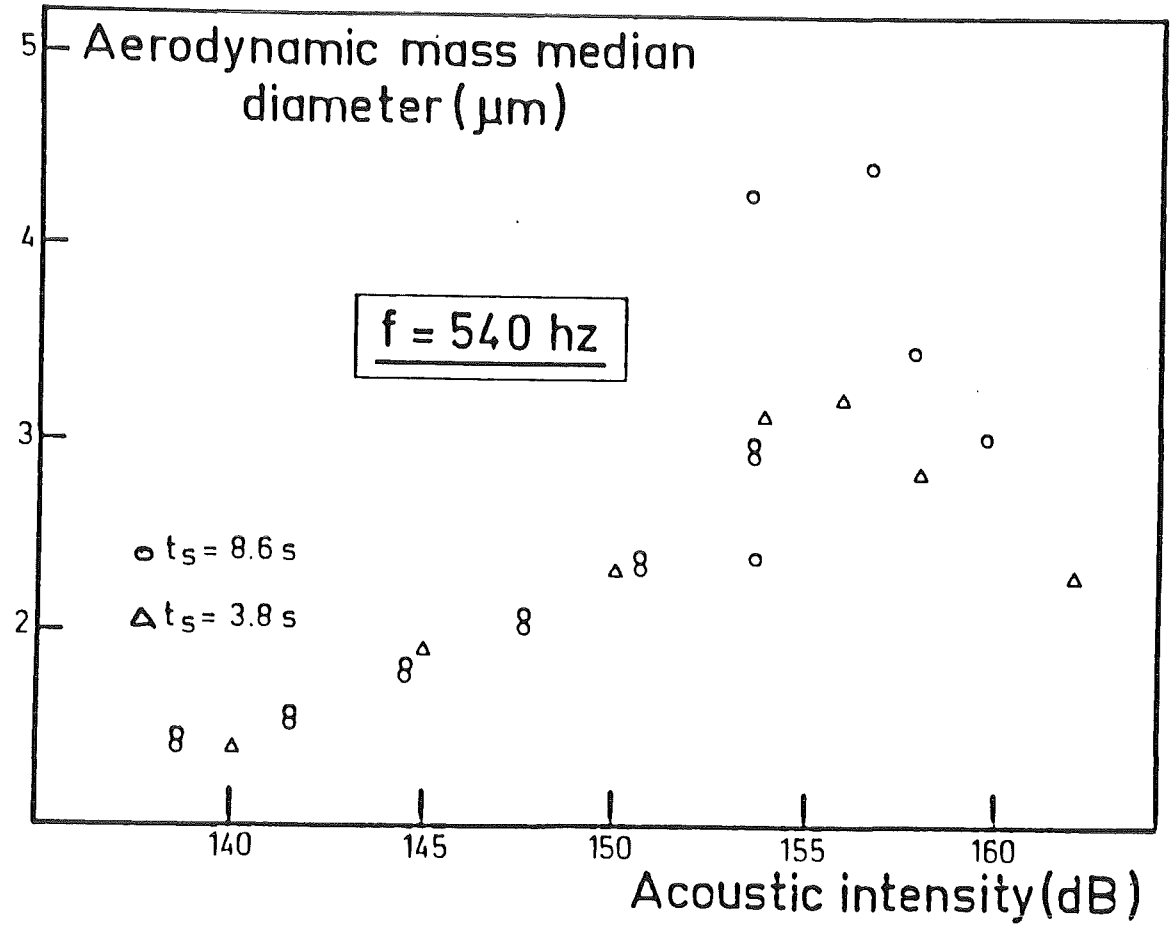

Figure 5 - Aerodynamic mass median diameter versus acoustic intensity for two different residence times (8.6 and 3.8 s) and constant frequency 540 Hz

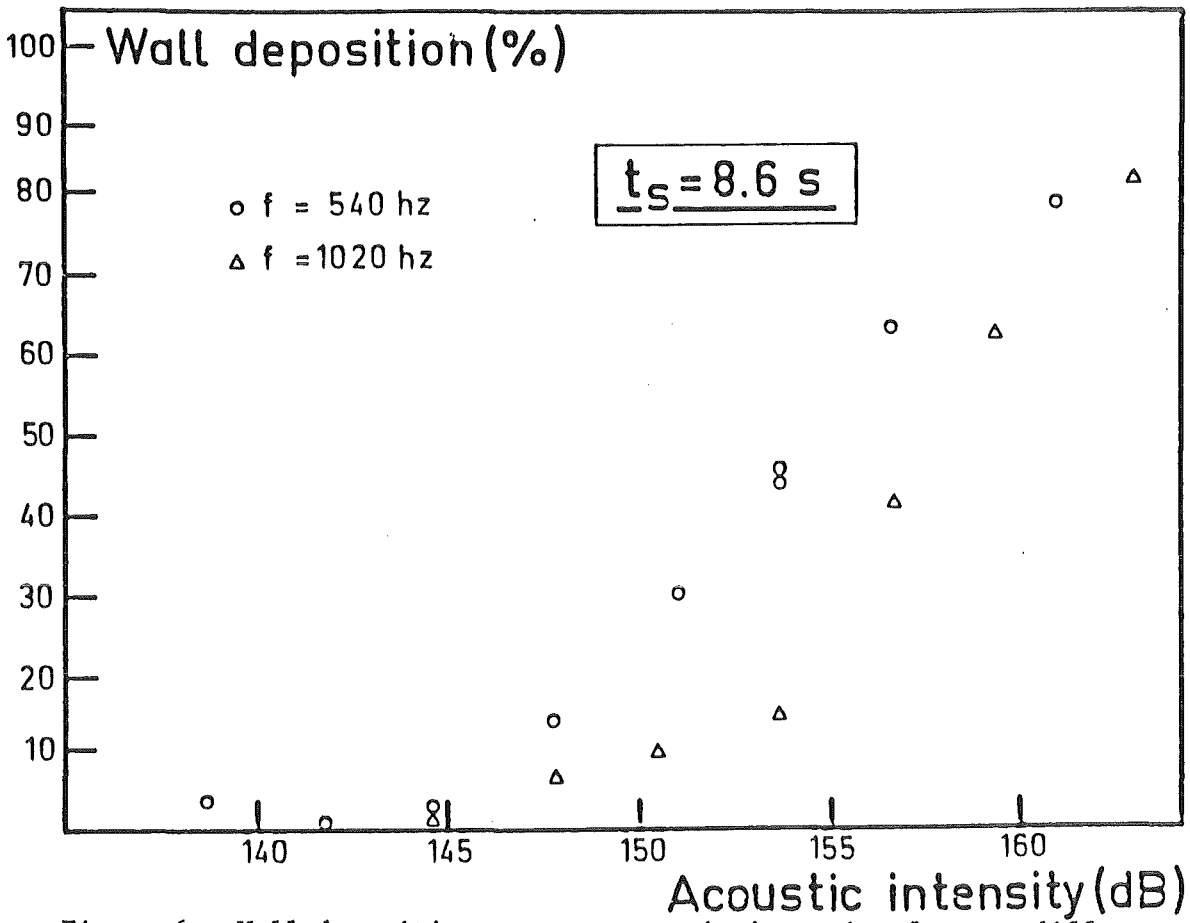

Figure 6 - Wall deposition versus acoustic intensity for two different frequencies (540 and 1 020 Hz). Residence time 8.6 seconds

3.4. Experimental results with solid aerosols

In the same way during these experiments the characteristics of the aerosol introduced in the agglomerator were kept constant, the variable being mainly the sound pressure level in the agglomeration volume.

Figures 7 and 8 show respectively the variations of the AMMD and the deposited fraction with the sound pressure level. Whatever the nature of the aerosol (liquid or solid) the behavior is similar when an acoustic field is applied and the following conclusions could be drawn :

- a mutual agglomeration of particles occurs resulting in an increase in the median diameter of the aerosol and the corresponding standard deviation. These acoustic field effects begin to occur at around 140 dB but only became significant above 155 dB.

- The value of the acoustic frequency has little effect in the 500 to 2 000 Hz range.

- Particles should spent a few seconds in the agglomerator (1 to 3 seconds) depending on the numerical concentration of the aerosol.

- A strong phenomenon of aerosol precipitation on the wall occurs when the sound pressure level increase.

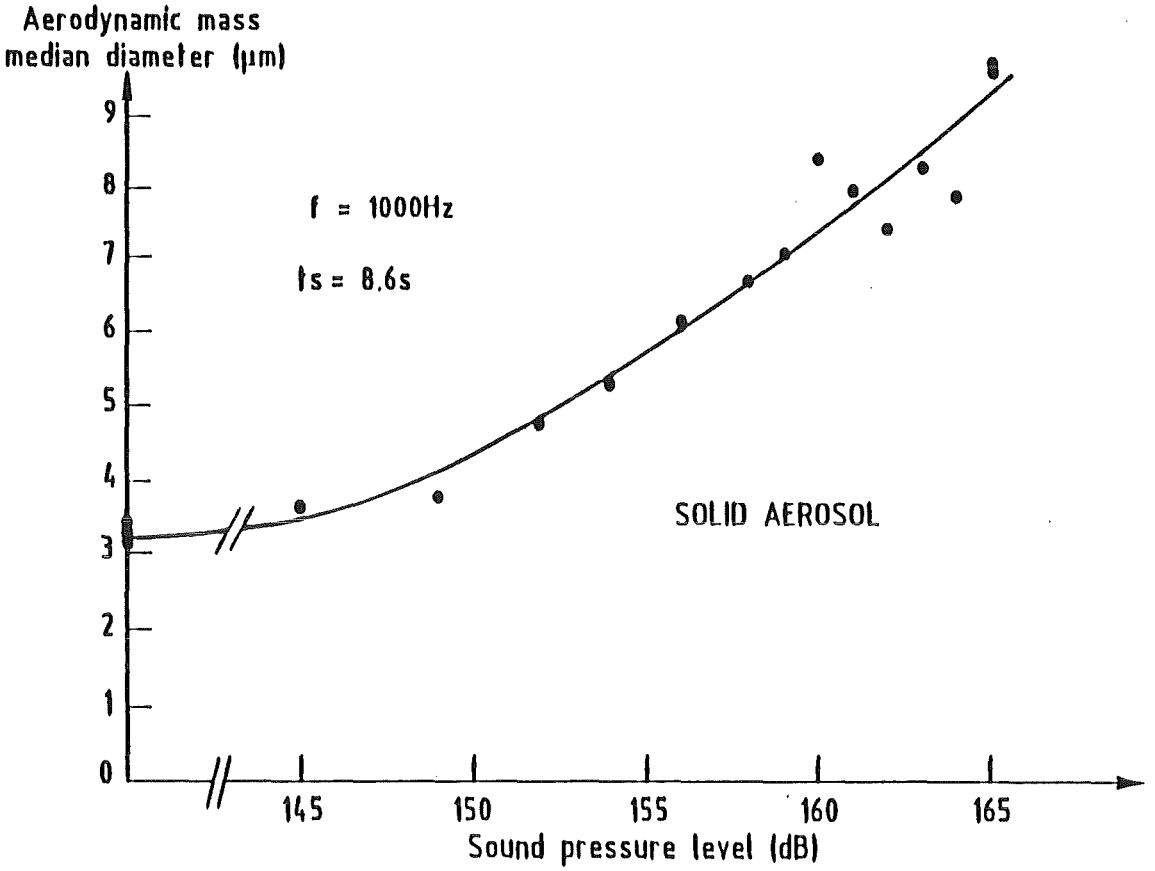

Figure 7 - Variations of the aerodynamic mass median diameter related to the sound pressure level

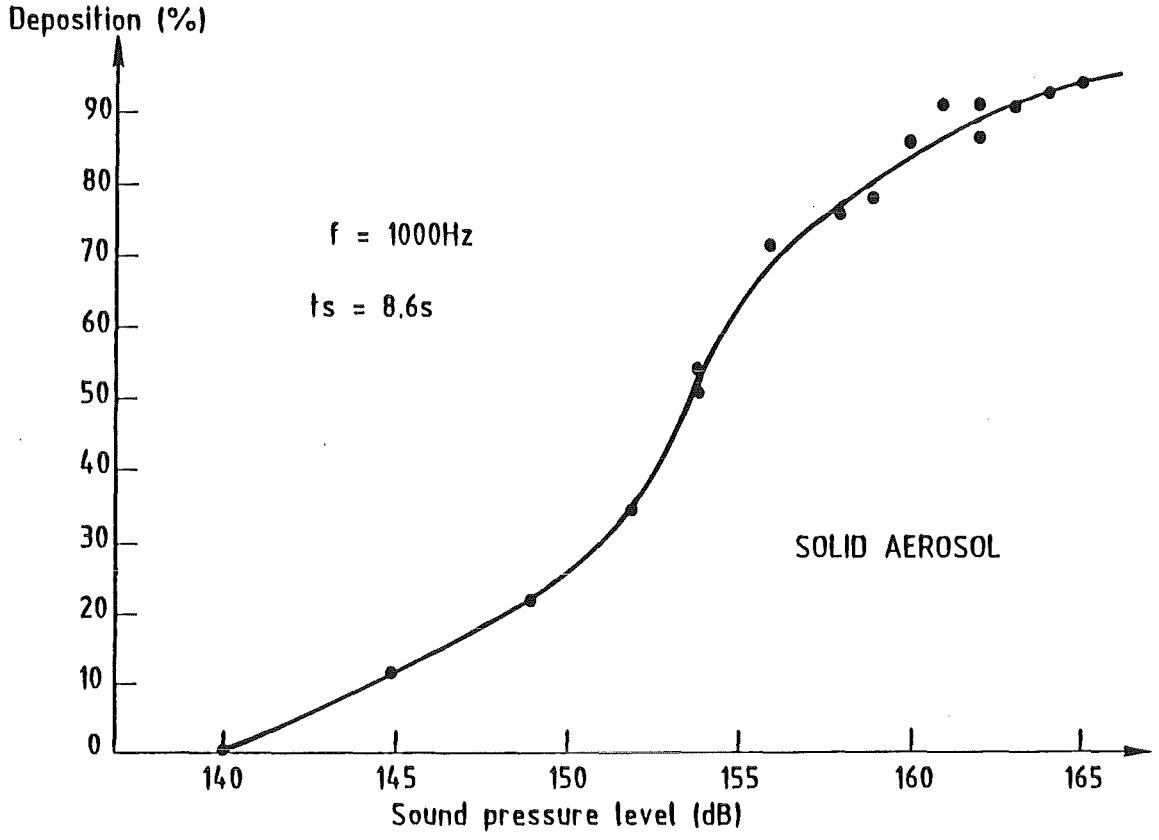

Figure 8 - Variations of the aerosol deposition related to the sound pressure level

4. TURBULENCE INDUCED BY AN ACOUSTIC FIELD

As we have seen hereabove the agglomeration is strongly reinforced and a phenomenon of precipitation is observed above 158 db. (This value could correspond to the great enhancement of acoustic turbulence).

Given the importance of this mechanism the aim of this chapter is to study the aerodynamic behavior of the carrier gas in order to understand the acoustic coagulation in the case of very high sound pressure level. The object is moreover to determine velocity fluctuations of the system, eddies size and finally to evaluate the degree of turbulence by intermediary of the dissipation energy, which is a parameter allowing to calculate agglomeration kernels (see 2.3).

4.1. Velocity fluctuations

4.1.1. Experimental set-up

The experiment consists in determining the effluent velocity of the gas to be processed, as a function of the acoustic energy. Frequency is set at 1 000 Hz.

Velocities are generally measured by laser velocimetry, an optical technique which does not disturb the medium / 7 / (BOUTIER (1979)).

The principle of laser velocimetry with intersected beams is the following : an interference fringe pattern is created by intersecting two beams issued from a laser. When a particle goes successively through the dark and the bright areas of the pattern, it scatters light with a frequency ν. This modulated light is collected by a photomultiplier, which transforms it into a sinusoidal electric signal.

With i as the interfringe, the velocity component of the particle parallel to the bisectrix of the intersected beams is written :

$$v = \nu i \qquad (7)$$

A laser velocimeter was integrated into an experimental device, previously developed in order to study the acoustic agglomeration (see 3.1).

Our device is composed of the following components (see figure 9) :

- agglomeration chamber, acoustic source, acoustic intensity measurement already have been described (see 3.1).

- An aerosols generator : gas is seeded by a monodispersed aerosol of 0.4 µm sized particles (wholly carried along by the fluid) delivered from a generator of the type SINCLAIR-LAMER. Rise to Boltzmann's equilibrium is ensured by a krypton 85 source.

- A pump located downstream the agglomeration chamber supplies a mean flow velocity of 12 cm/s.

- A two-dimensions laser velocimeter capable of measuring simultaneously 2 velocity components.

The emitting part is composed of a laser source (3 W) and some optical devices allowing to split the initial beam into 4. The residual beams are focussed on a limited area in space ; this is the measurement volume (cylinder of some mm in length and diameter 120 μm). Two of the beams (in green) located in a vertical plan allow longitudinal velocity measurements (parallel to acoustic wave propagation). The two other beams (in blue) located in a horizontal plane are concerned with the radial velocity component. The resulting interference fringes create a grid.

Light scattered by particles is collected by two photomultipliers and then transformed into electric signals displayed by an oscilloscope. Finally data are processed by two DISA counters.

Numeric values of instantaneous frequency couples are processed by a micro-computer which calculates mean velocities and parameters characterizing the turbulence.

For each particle passing through the probe volume, the following data are stored :

- the frequency relative to the axial component (green),
- the frequency relative to the radial component (blue),
- the measurement date.

The acoustic signal interval (1 ms) is cut into 100 intervals (windows) of 10 μs. Pairs of frequency measurement, relative to each particle are "classified" according to their date into the different temporal intervals of 10 μs. About 1 000 frequency couples are measured in each interval. For each experiment, the probe volume position along the tube axis and the acoustic energy are established previously.

We thus obtain the following informations.

4.1.2. Mean velocity as a function of the acoustic oscillation phase

For each temporal class of 10 μs, velocity is calculated by averaging instantaneous values by the number of measurements carried out in this class.

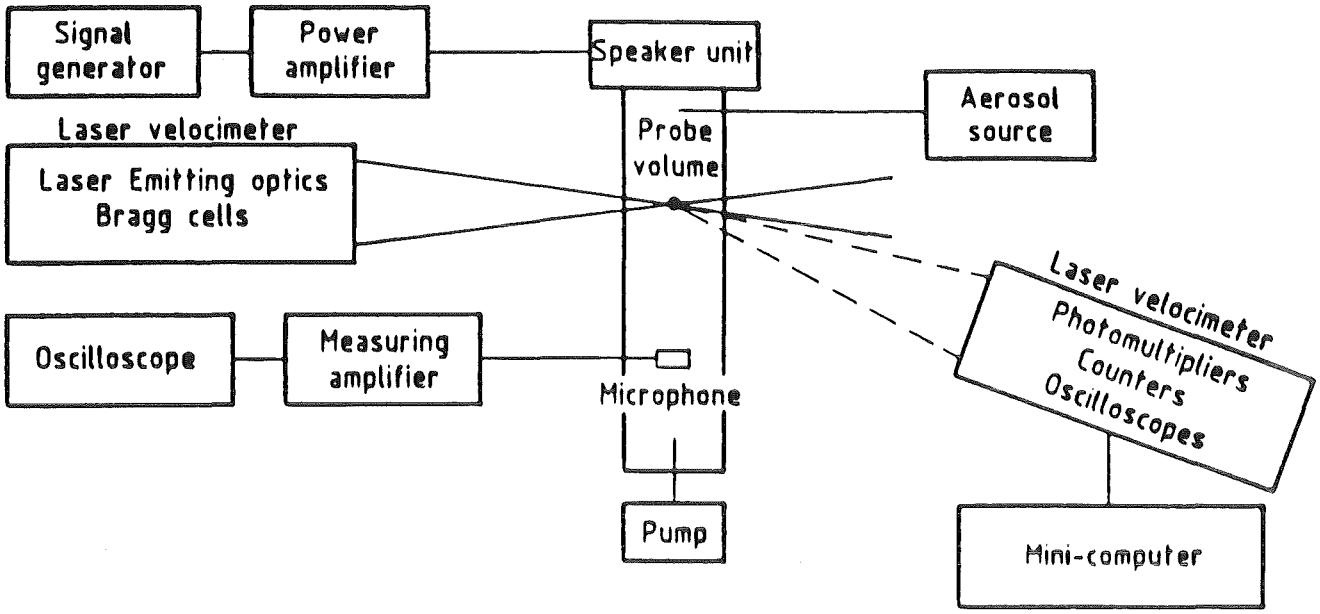

Figure 9 - Experimental apparatus destined to measure the velocity of the fluid inside the agglomeration chamber

$$\overline{v}_j = \frac{\sum_{i=1}^{N_j} v_{ij}}{N_j} \qquad (8)$$

v_j : mean velocity related to the j^{th} temporal class. The longitudinal and transversal components of the velocity are successively calculated,

v_{ij} : velocity dated at time j x 10 µs (modulo 1 ms),

N_j : number of measurements carried out in the j^{th} class.

It should be recalled that each instantaneous velocity verifies the relation :

$v = \nu i$

Where ν : frequency measured by the DISA counter

i : interfringe.

Into our experimental conditions, we get :

i_v : 8.6 µm green interfringe

i_B : 8.2 µm blue interfringe.

4.1.3. Velocity fluctuations (standard deviation of mean velocity distributions)

$$\sigma_j = \left(\overline{v'_j{}^2}\right)^{1/2} = \left(\frac{\sum_{1}^{N_j} (\overline{v_j}^2 - v_{ij}^2)}{N_j}\right)^{1/2} \qquad (9)$$

v'_j : velocity fluctuations relative to the j^{th} class.

For each experiment, acoustic frequency is set at 1 000 Hz. Sound pressure level, adjustable parameter, is limited to 163 db, maximum value allowed by the loudspeaker.

The measurement volume is successively located at a velocity loop, between a loop and a node, and at a velocity node, and acoustic energy is then allowed to vary.

Figure 10 shows mean velocities "stroboscoped" on 10 μs classes.

* Probe volume is located at a velocity loop (pressure node).

* Acoustic intensity, measured at a pressure loop I(P,L), is equal to 163 dB.

* Acoustic intensity, LI measured at the volume location of measurement (local intensity) is equal to 155 dB.

The mean longitudinal motion is oscillating and has a frequency of 1 000 Hz ; the maximum velocity reaches 15 m/s.

We may notice the irregular curve resulting from the presence of turbulent instabilities. The transversal velocity, which does not exceed 30 cm/s, is however higher than measurement uncertainties (5 cm/s).

Figures 11 and 12 show velocity fluctuations as a function of the oscillating phase, at a velocity loop, respectively for a sound pressure level equal to 163 db and 153 dB. At 163 dB, longitudinal velocity fluctuations, of about 2.5 m/s, represent 30 % of the vibration velocity and we may point out peaks exceeding 6 m/s. At 153 dB, turbulence is also present but is less important. Velocity fluctuations don't become higher than 1 m/s. Transversal velocity fluctuations are weaker and do not exceed the order of magnitude of the transversal velocities averaged over 10 μs classes.

The same kind of curves have been drawn for different positions of probe volume and acoustic energies ; we then studied the evolution of velocities as a function of acoustic intensity.

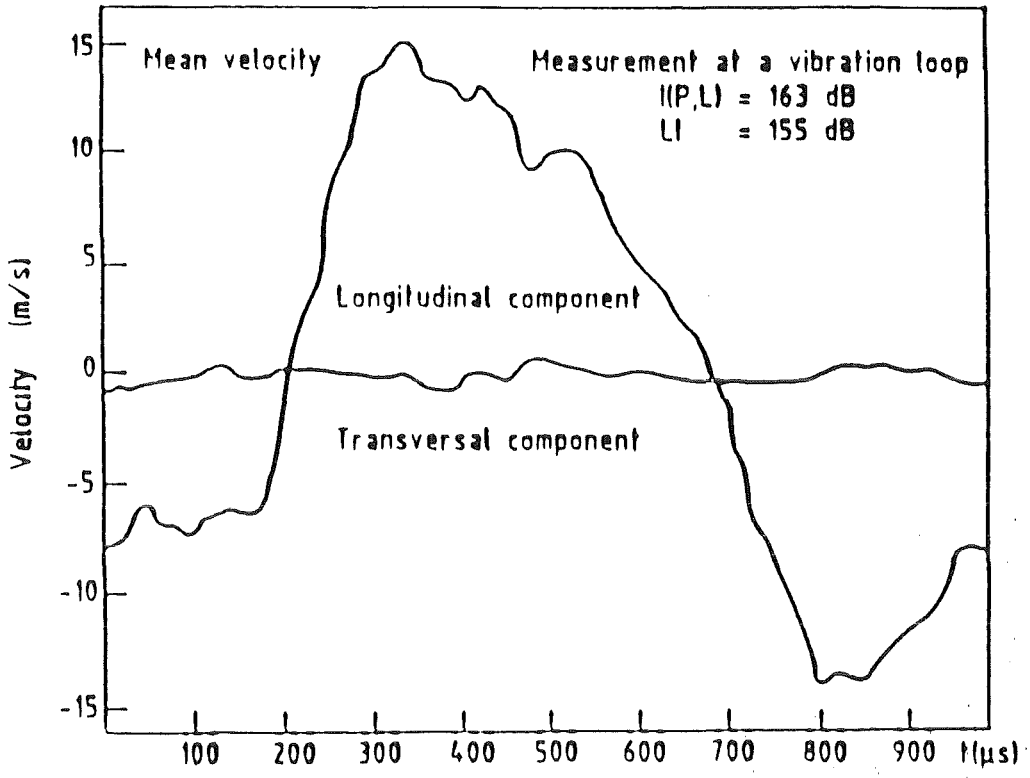

Figure 10 - Mean velocity "stroboscoped" on the classes of 10 µs

Velocity fluctuations appear in a significant way at 152-153 dB (fig. 13) and then quickly increase with acoustic energy above 158 dB. However if the vibration velocity between a loop and a node is reduced by a factor 10 the longitudinal velocity fluctuations are nearly constant ; turbulence is convected. Transversal velocity fluctuations, which appear at about 160 dB, remain weak and only represent a third of the value of longitudinal velocity fluctuations at high intensity. Turbulence is homogeneous (constant in the tube) but it is not isotropic (one direction is favoured).

4.2. Turbulence spectrum

The spectrum corresponds to the decomposition of kinetic energy into waves of different periods and different wave lengths (eddy size). The spectrum value at a given wave number represents the mean energy of this wave (HINZE ; 1959).

From a mathematical point of view, the spatial decomposition of the kinetic energy spectrum is equivalent to the Fourier transform of the autocorrelation function of instantaneous velocities (definition of frequency spectrum according to G.I. TAYLOR / 9 /.

The autocorrelation function represents the correlation existing between the velocities at two points separated by $\vec{r}$.

$$R_i (\vec{x}, \vec{r}) = \overline{v_i (\vec{x}, t)\, v_i (\vec{x} + \vec{r}, t)} \qquad (10)$$

with $v_i (\vec{x}, t)$: i^{th} instantaneous velocity component $(\vec{x})$

$R_{ii} (\vec{x}, \vec{r})$ only depends on $\vec{r}$ in the case of homogeneous turbulence.

The Fourier transform f_{ii} of the autocorrelation function is written as follows :

$$f_{ii} (\vec{k}) = \frac{1}{(2\pi)^3} \int_{-\infty}^{+\infty} \exp (- j \vec{k} . \vec{r}) R_{ii} (\vec{r})\, d\vec{r} \qquad (11)$$

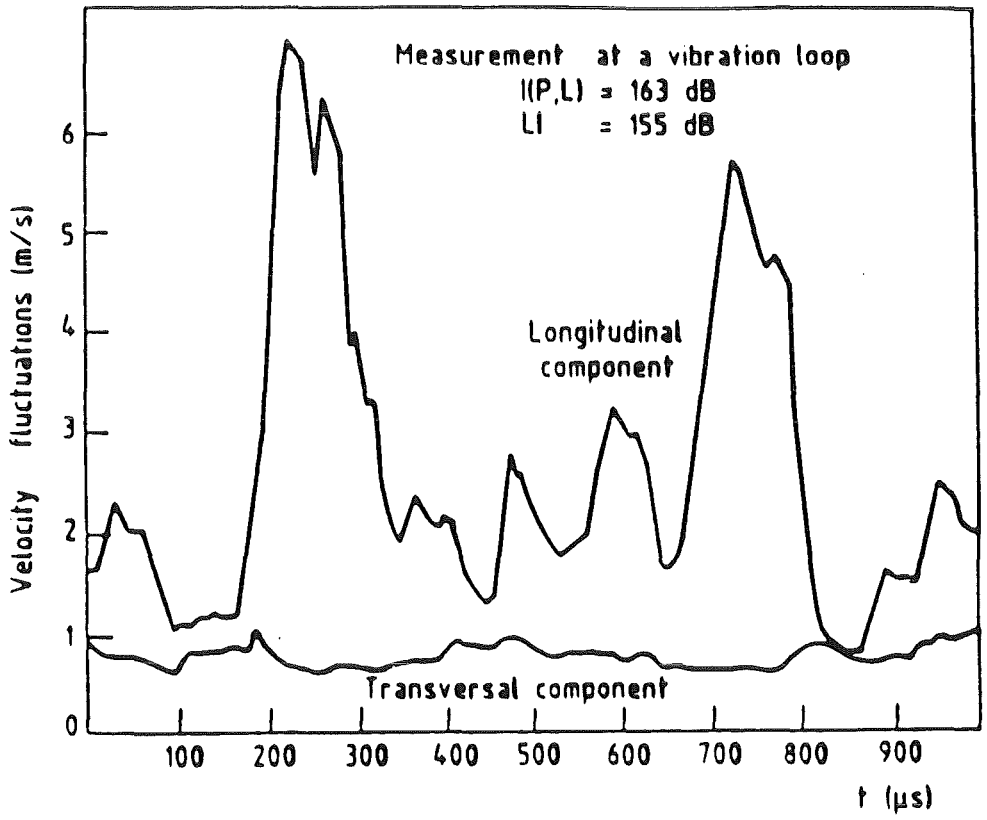

Figure 11 - Velocity fluctuations measured at a velocity loop at 163 dB

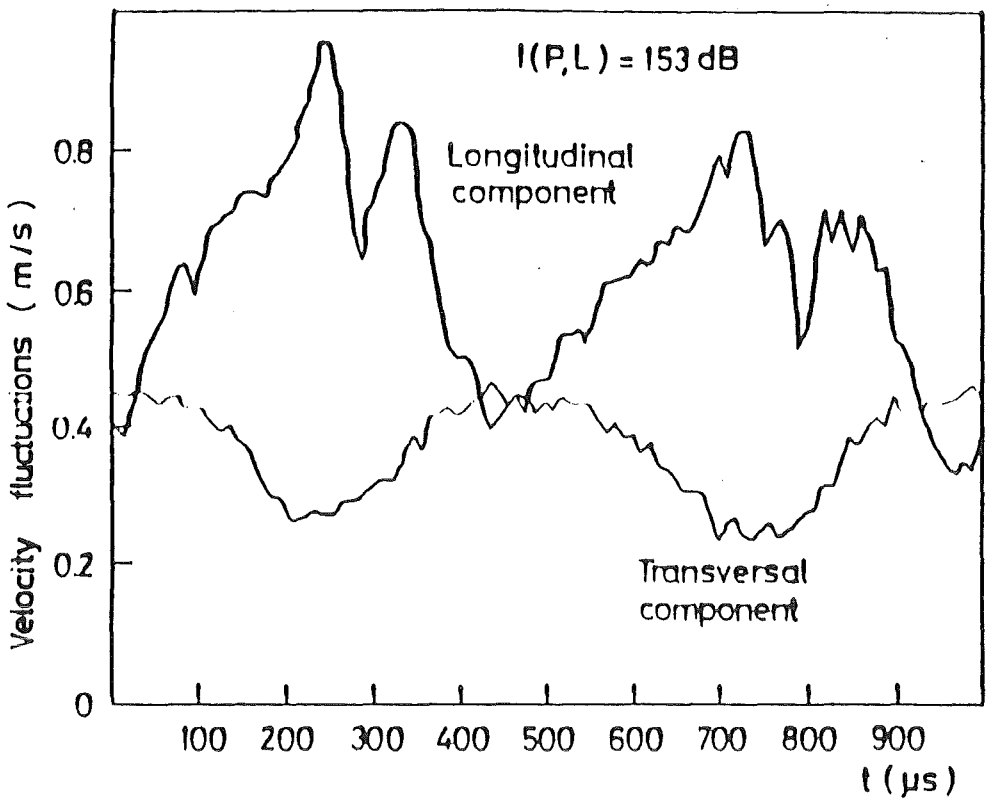

Figure 12 - Velocity fluctuations measured at a velocity loop at 153 dB

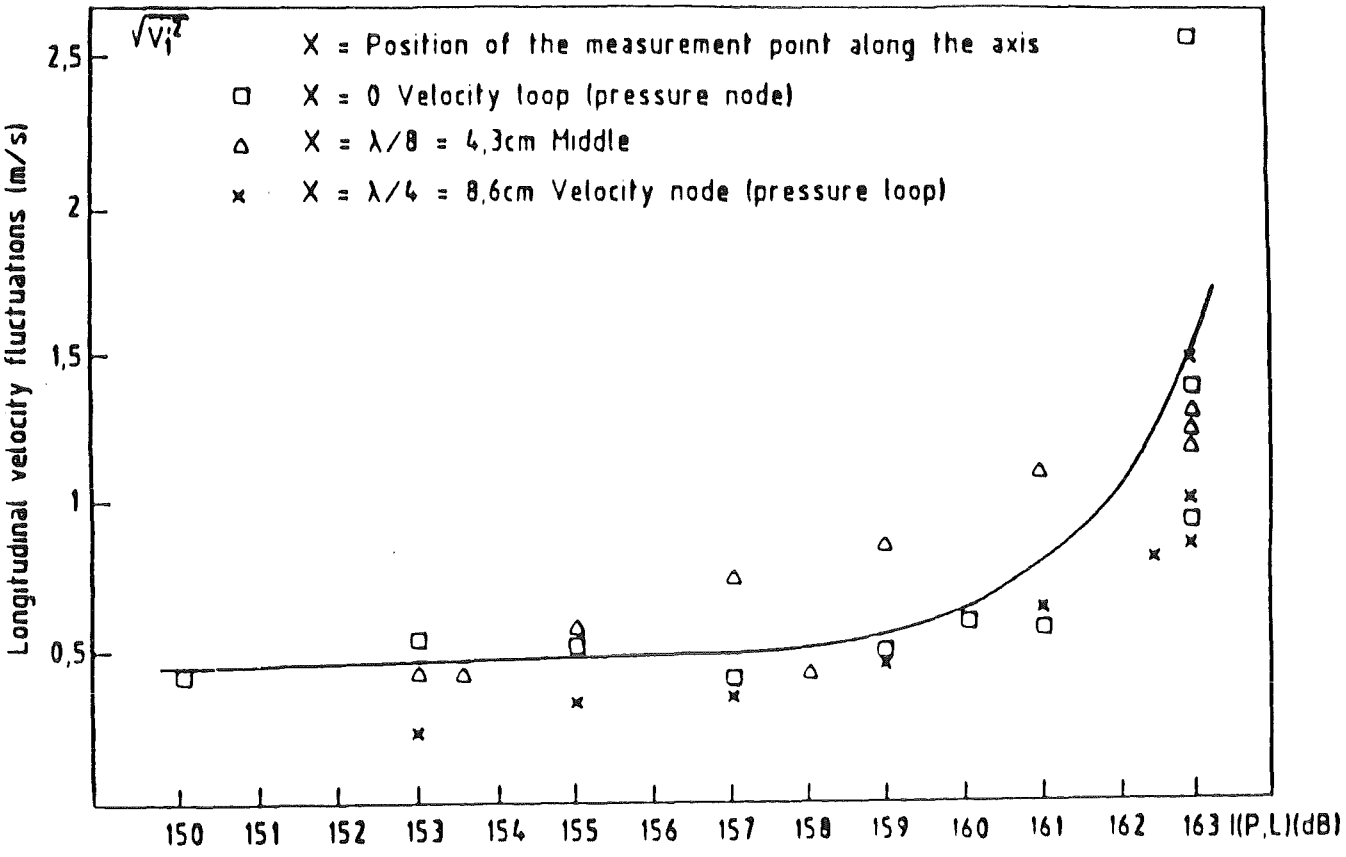

Figure 13 - Longitudinal velocity fluctuations in term of acoustic intensity

Kinetic energy is thus divided into the sum of waves $\vec{k}$.

The turbulence shown in our system arises mainly in the direction of the acoustic wave propagation. This is why the one - dimensional spectrum is of interest to us.

The problem now is to know if the turbulence has enough time to get developed before primary eddies are carried out of the agglomerator by a 12 cm/s mean flow.

The developed turbulence corresponds to the degeneracy of the largest structures into small eddies. The knowledge of the kinetic energy spectrum of fluctuations allows to foresee the evolution of the turbulence. If k_1 is the longitudinal component of the wave vector $\vec{k}$, the spectrum is written as follows :

$$f_{11}(k_1) = \frac{1}{2\pi} \int_{-\infty}^{+\infty} R_{11}(r)\, e^{-jk_1 r}\, dr \qquad (12)$$

Determining f_{11} requires the knowledge of instantaneous velocities, measured on a large number of nearly points. Such a detailed and complete exploration is not possible using the installation utilized. The difficulty can be avoided by determining the spatial spectrum starting from the temporal spectrum, which is easier to obtain experimentally.

In the case of a stationary system, the spectrum density as a function of ν, (temporal frequency) verifies the relation :

$$F(\nu) \propto \left(\int_0^T v_1(x_1 t) \exp(-2\pi j \nu t)\, dt \right) \left(\int_0^T v_1(x_1 t) \exp(2\pi j \nu t)\, dt \right) \qquad (13)$$

In practice, T corresponds to the duration of the experiment and x is the axial position of the point of measurement.

If $T \gg Ta$, Ta being the acoustic period, we can write :

$T \sim n\, Ta$

(n being an integer number).

In such a condition, the phenomenon is stationary during the time T.

Turbulence is fully developed if the largest structures degenerate into smaller size eddies, to reach the Kolmogorov internal scale. One can see on figure 14 the 1 000 Hz peak (corresponding to the acoustic oscillation fundamental mode) and the first harmonic components. A systematic study between 145 and 163 dB allows us to ascertain that below 153 dB, the decrease with $\nu^{-5/3}$ is not maintained.

The developed turbulence is characterized by a spatial spectrum in $k^{-5/3}$, (Kolmogorov law). Up to now, we knew that if the spectrum with ν temporal frequency followed the law in $\nu^{-5/3}$, the spatial spectrum followed the law in $k^{-5/3}$ in the case of a constant velocity flow. Now a recent study (J. TAILLET, 1986, / 10 /) has shown that in the case where scanning is a periodic function of time, both the spatial and temporal decompositions follow the same laws ; as regards our system, the $\nu^{-5/3}$ temporal spectrum decrease is thus representative of the developed character of the turbulence.

In our system, the turbulence is fully developed above 153 dB. Below this value, the turbulence decreases. Under weak acoustic intensity, the degeneracy becomes slow, the latter eddies are ejected out of the system by a mean flow of 12 cm/s before reaching the Kolmogorov scale.

The turbulence frequency corresponds to the frequency at which a same instantaneous velocity is recorded by the sensor (fig. 15).

The experimental device is composed of the elements described in the last section. However, we are only interested in the longitudinal velocity component. Our device for the acquisition and processing of data incorporates a rapid Fourier analyzer.

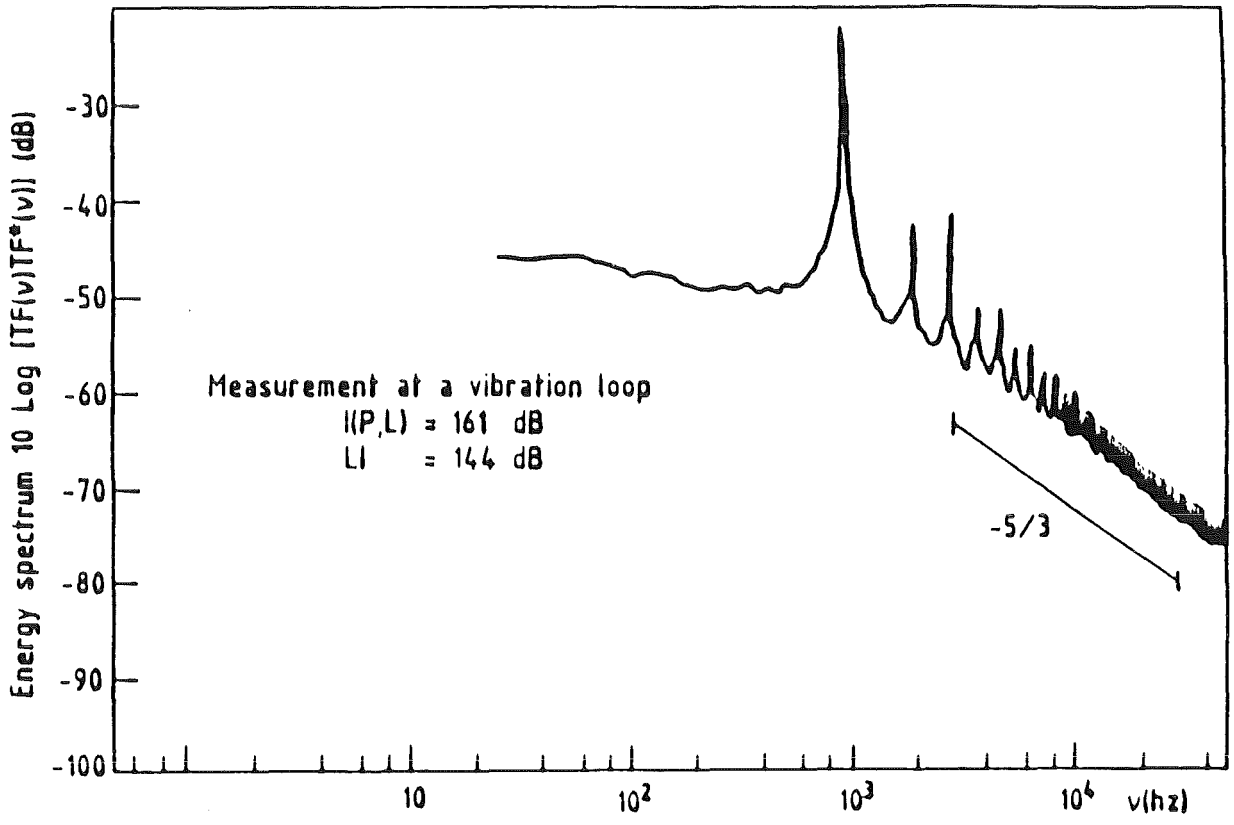

Figure 14 - Typical turbulence spectrum

To determine the turbulence kinetic energy spectrum $F(\nu)$, we sample instantaneous velocities at a point with a rate of 200 kHz, for a function $F(\nu)$ calculated for a ν max value of 50 kHz.

The Fourier analyzer calculates the product :

$TF_v(\nu)\ TF_v^*(\nu)$ with :

$$TF_v(\nu) = \frac{1}{T} \int_o^T V \exp(-2\pi j \nu t)\, dt) \qquad (14)$$

V, being the analog signal transmitted to the Fourier analyzer, is proportional to particles velocity.

Under such conditions :

$TF_v(\nu)\ TF_v^*(\nu) \propto F(\nu)$ represents the temporal turbulence spectrum.

A typical spectrum is represented in figure 14.

The acoustic energy, delivered by the loudspeaker reaches 161 dB at a pressure loop. The spectrum energy assessed in dB is equal to :

$10 \log \left| TF_v(\nu)\ TF_v^*(\nu) \right|$

The turbulent kinetic energy spectrum decreases as $\nu^{-5/3}$. This law of power spectrum density variation as a function of the fluid velocities variation frequency gives information on the turbulence evolution (fully developed or not).

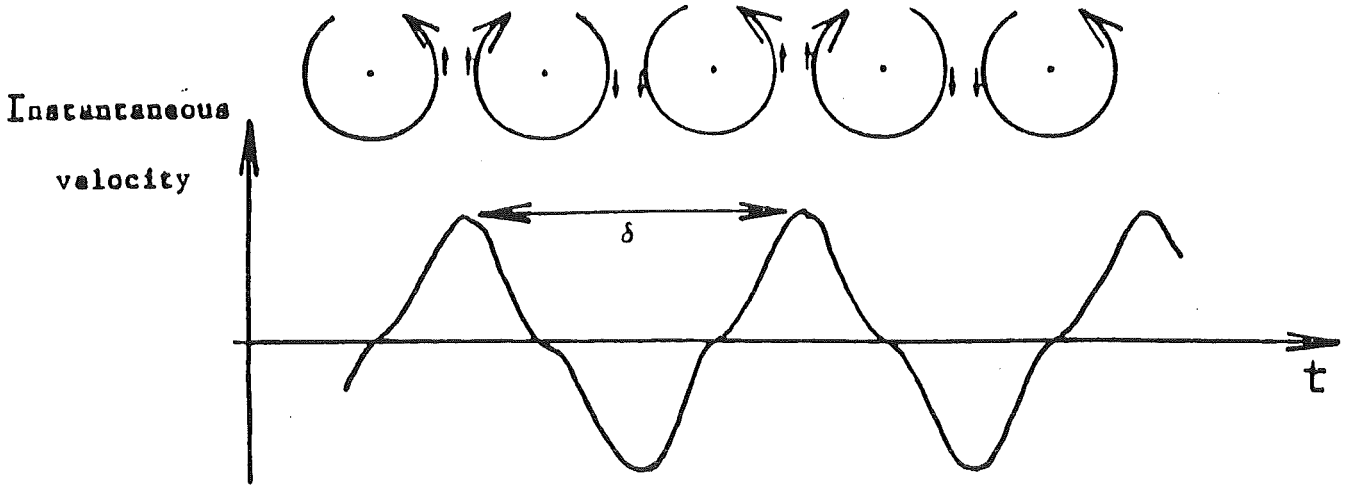

Figure 15 - Illustration of the size of the eddies

δ corresponds to the size of the two eddies.

$\delta = 2\ l$

thus $k = \frac{2\pi}{2\ l}$ and $l = \frac{v}{2\nu}$ (15)

The largest structures sized L correspond to the acoustic frequency where the decrease in - 5/3 begins to be observed (see fig. 14).

If ν min represents the minimal turbulence frequency, we get :

$$L = \frac{v}{2\nu_{min}} \quad (16)$$

however $v < v$ max where v max is the wave velocity amplitude, thus

$$L = \frac{v_{max}}{2\nu_{min}} \quad (17)$$

Figure 14 shows that ν_{min} is equal to the acoustic frequency f.

Let a_{max} be the acoustic wave amplitude :

$$v_{max} = 2\pi f a_{max} \quad (18)$$

$$\text{Let } L = \pi a_{max} \quad (19)$$

The size of the largest structures is of the order of the local amplitude of the acoustic oscillation, peak-to-peak (some mm).

Primary structures degenerate into smaller and smaller eddies until reaching the size lo (Kolmogorov internal scale). Inside these eddies, energy is then dissipated into heat along the time.

The maximum turbulence frequency recorded verifies the relation :

$$lo = \frac{v_{max}}{2\nu_{max}} \quad (20)$$

The Kolmogorov internal scale is about 100 µm.

4.3. Application to acoustic agglomeration

The mean diameter of an aerosol subjected to an acoustic field rapidly increases above 158 dB. This phenomenon corresponds to the sharp increase of the turbulence, induced by acoustic waves, as we have seen in the previous sections.

It is generally admitted that under high sound pressure level, the two main mechanisms responsible for the acoustic agglomeration are directly linked to the dissipation energy of the system (ε) (see 2.3). It is therefore necessary to know this parameter in order to assess the turbulent acoustic agglomeration kernel. Two methods allow to assess ε.

4.3.1. Mednikov formula

E.P. MEDNIKOV / 1 / links, in an empiric way, the energy dissipation per unit of mass and time ε, the acoustic parameters (frequency f and sound pressure level I) and fluid properties (volumic mass ρ_g and wave propagation velocity c_g)

$$\varepsilon = 0{,}53 \frac{I^{3/2} f}{\rho_g^{3/2} c_g^{5/2}} \qquad (21)$$

The dependence of ε thus defined on I(P,L) is shown in the figure 16.

4.3.2. Velocity fluctuations

According to the isotropic homogeneous turbulence, dissipation energy is expressed as follows :

$$\varepsilon = \frac{\overline{(v'^2)}^{3/2}}{L} \qquad (22)$$

v' : velocity fluctuations

L : size of the largest eddies

In our experimental conditions, turbulence is not isotropic. However, comparing our system to a fictitious isotropic system having the same kinetic energy,

ε becomes :

$$\varepsilon = \frac{1/3\ \overline{(v'_1{}^2 + 2v'_2{}^2)}^{3/2}}{L} \qquad (23)$$

v'_1 : longitudinal velocity fluctuations

v'_2 : transversal velocity fluctuations

Turbulence having originated from an oscillatory motion, we formulate the hypothesis that the size of the largest structures is equal to twice amplitude of the wave motion :

$$\text{Let } L = \frac{\overline{v_1}}{4f} \qquad (24)$$

The variation of ε with I(V,P) as evaluated by this method is shown figure 16.

Although obtained with only one frequency (1 000 Hz), the ε determination according to these two methods leads to almost similar results. Dissipation energy is a monotonously increasing function of the acoustic intensity. Above 158 db, ε quickly increases and reaches 500 $m^2\ s^{-3}$ at 163 dB. To calculate the turbulent acoustic agglomeration kernels in which ε interferes, the use of Mednikov's formula is justified with frequencies of about 1 000 Hz.

While ε allows to assess the turbulence, it is also interesting to know the size of the eddies present in the system. At each point of the system, the largest eddies attain twice the acoustic wave oscillation amplitude (at the point, a few mm). In the case of an isotropic homogeneous turbulence, the size of the smallest eddies verifies the following relation :

$$lo = \left(\frac{\nu^3}{\varepsilon}\right)^{1/4} \qquad (25)$$

The microscale, which is not very sensitive to dissipation energy, is about 100 μm (see table 1)

The largest structures derive their kinetic energy from vibrating motion. Then energy cascade corresponds to the energy transfer to smaller and smaller eddies. For the smallest eddies ($\sim$ 100 μm), the energy is transformed into heat along the time.

I(P,L) (dB)	ε (m^2 s^{-3})	lo (μm)
163	471	52
161	186	65
159	98	77
157	65	85
155	45	93
153	35	99

Table 1 - Kolmogorov's internal/scale

As we have seen hereabove the agglomeration of particles subjected to an acoustic field becomes marked above 158 dB. This value corresponds to the sharp increase of velocity fluctuations, representative of an important turbulence.

Starting from our experiments about the study of acoustic turbulence, the following conclusions could be drawn :

Turbulence seems to appear between 152 to 153 dB ; above 153 dB, turbulence (which is revealed by fluctuating velocities) is developed in our system : the largest structures (whose size is about the acoustic oscillation amplitude) degenerate into smaller and smaller eddies to reach the Kolmogorov scale (about 100 μm in our system).

Above 158 dB, the velocity fluctuations sharply increase and could represent up to 30 % of the acoustic wave oscillation velocity under high sound pressure level (163 dB).

Acoustic agglomeration, resulting from agitation in the fluid appears between particles carried out by smallest eddies. The acoustic coagulation coefficient is generally determined from the energy transformed into heat by eddies of size equal to Kolmogorov scale. This parameter was experimentally measured in course of this work ; dissipated energy rises rapidly above 158 dB, thus acoustic agglomeration under high intensity could be related to the sharp increase of turbulence in the system.

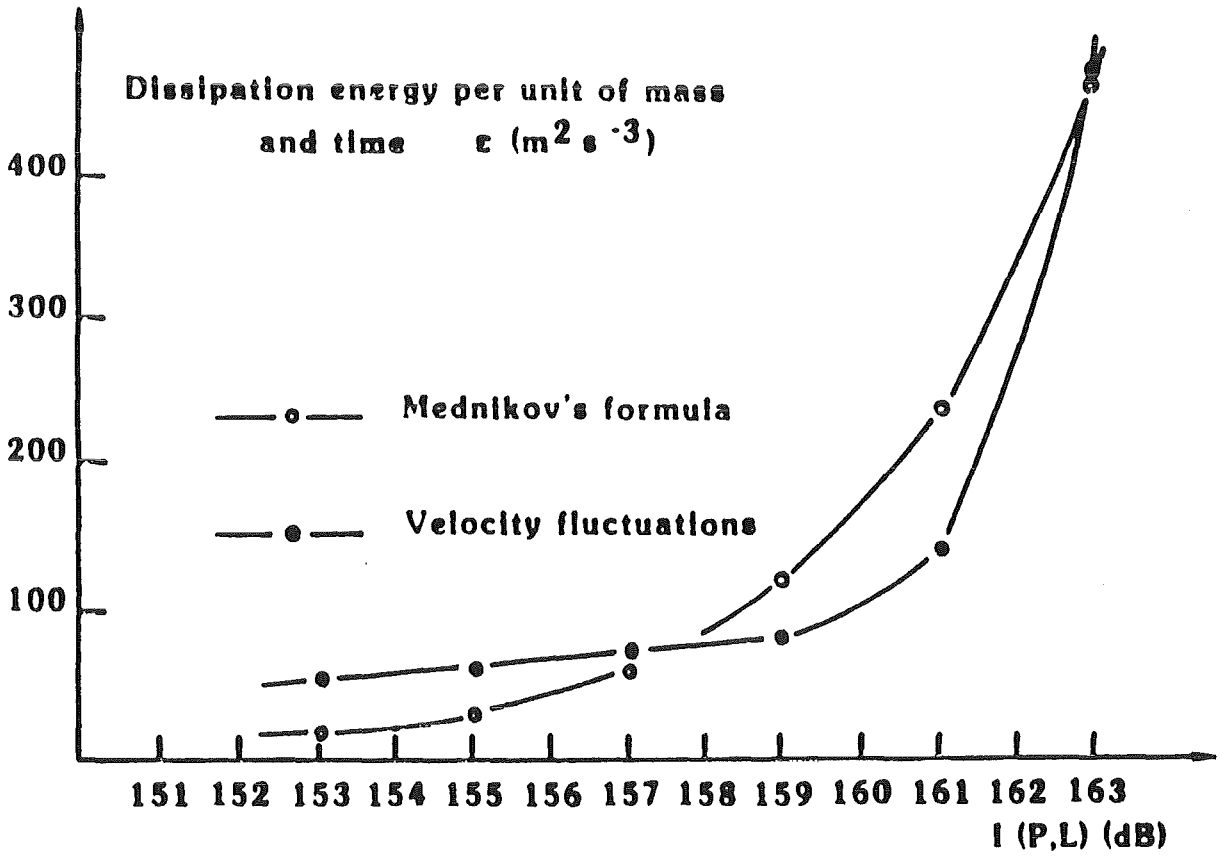

Figure 16 - Dissipation energy in term of acoustic intensity
Validity of Mednikov's formula

5. ACOUSTIC PRECIPITATION

The aim here is to determine the relations between the establishment of an acoustic field and the precipitation of an aerosol on the walls of a pipe. For these experiments therefore, unlike those described in part one, it was decided to keep the characteristic parameters of the aerosol constant (diameter and

standard deviation). For this purpose the aerosol is monodispersed and has a low numerical concentration (under 50 particles/cm^3) to reduce the collision frequency when the acoustic field is applied.

5.1. Experimental apparatus

The device used is represented on figure 1. The components are the same as those of the previous set-up except for the aerosol source and the numerical particle concentration measurement.

- Aerosol source : a monodispersed DOP aerosol is produced by a vibrating orifice generator (TSI 3050). Before entering the precipitation chamber it passes through a krypton 85 source neutralizer to reach Boltzmann's equilibrium.

- Particles concentration measurement : this is accomplished by a "Kratel model 328" type spectrophotometer on samples taken at the bottom of the precipitation tube.

5.2. Experimental procedure

Once the acoustic field has been measured in the tube, the DOP aerosol is injected into the system. When the stationary state is established a first concentration measurement is performed at the base of the tube (C_o), after which the operation is repeated but in the presence of the acoustic field. This measurement supplies the new downstream concentration value (C). Assuming that the liquid DOP particles entering into contact with the wall are not carried away again the particle fraction deposited in the tube is given by the following expression :

$$\text{Deposit } (\%) = 100\ (1 - (C/Co)) \qquad (26)$$

In this way, if the different wall precipitation mechanisms are considered to be independent, the measured deposit can only be due to application of the acoustic field.

5.3. Experimental results

During these experiments the geometry of the precipitation tube and the fluid flow rate inside were kept constant (fluid velocity = 12 cm/s), the variable being the particle diameter, sound pressure level and acoustic frequency.

Figure 17 gives the results obtained for six diameters (0.7, 1, 2, 3, 5 and 7 μm) three sound pressure levels (152, 155 and 158 dB) and two acoustic frequencies (540 an 1 020 Hz), representing 36 experiments altogether. From these curves and for our experimental conditions the first conclusions are the following :

- the wall deposition rate increases with particle size, sound pressure level and acoustic frequency,

- for given acoustic intensity and frequency the deposition rate increases abruptly between 0.7 and 2 μm, then slightly between 2 and 7 μm,

- for given particle size the deposition rate increases steadily with sound pressure level and frequency.

From these wall deposition curves an acoustically induced deposition velocity (K_a) may be deduced, as follows :

$$K_a \quad \frac{-UD}{4L} \text{Ln } (C/C_o) \qquad (27)$$

where U is the mean flow volecity of the fluid in the tube, D the tube diameter and L its length. On figure 17 the K_a values are also plotted as ordinates.

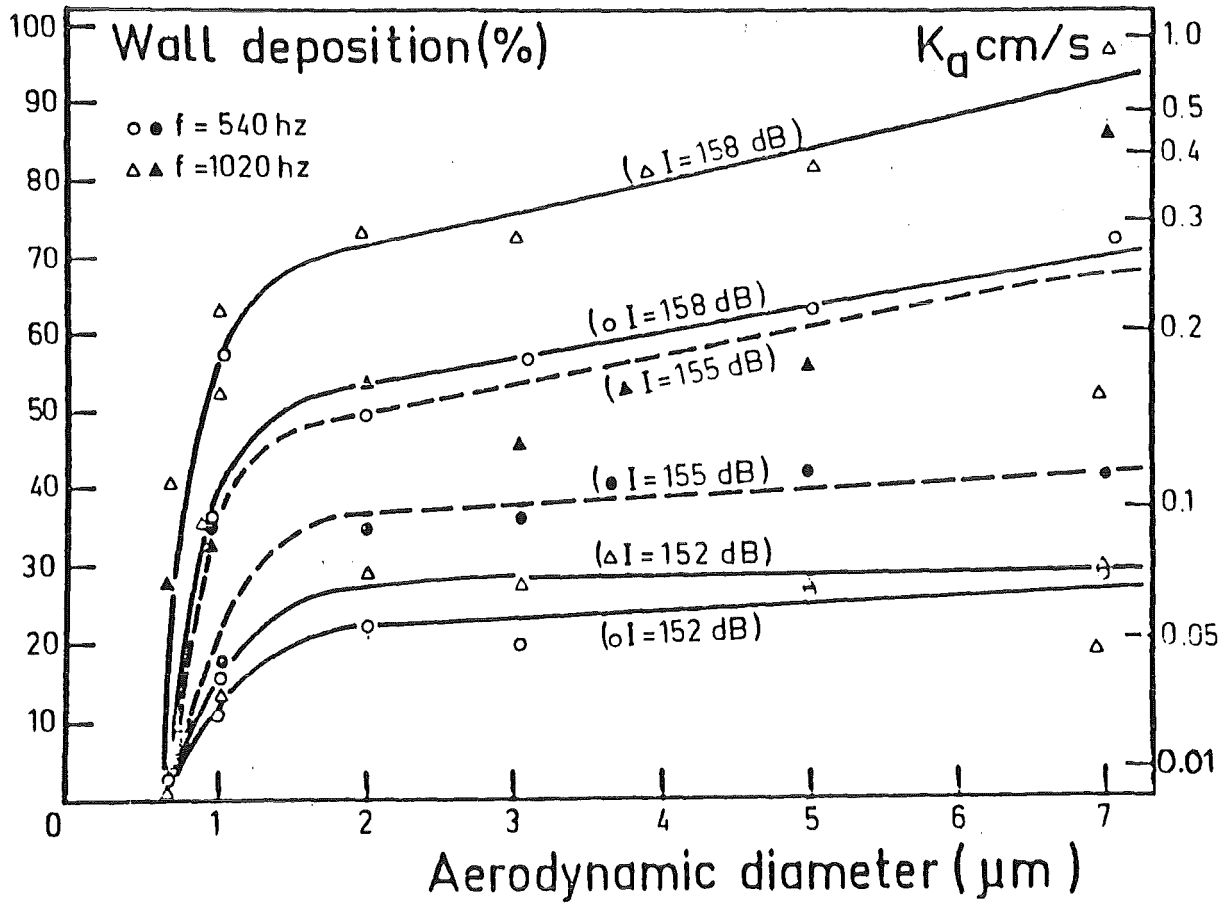

Figure 17 - Percentage wall deposition versus aerodynamic particle diameter, with four acoustic intensities and two frequencies. The residence time being 8.6 s, K_a represents the acoustic deposition velocity

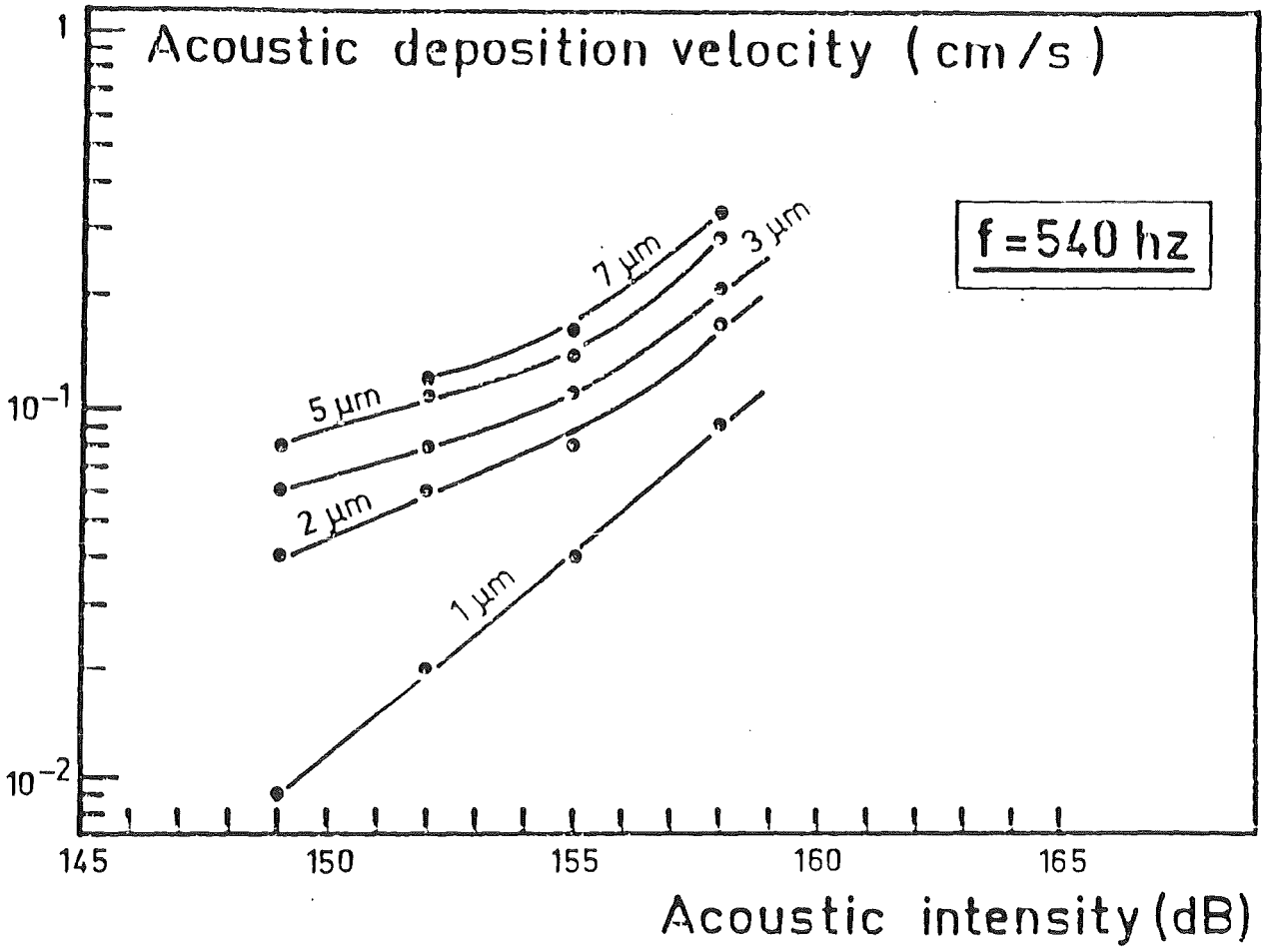

Figure 18 - Acoustic deposition velocity versus acoustic intensity for different diameters. Acoustic frequency is constant 540 Hz

On figure 18 the K_a values are plotted versus the acoustic intensity for different values of particle diameter, in this case the acoustic frequency is maintained constant (540 Hz).

5.4. Interpretation

More generally it is useful to relate acoustic deposition rate to particles diameter through dimensionless quantities. For this purpose a dimensionless acoustic velocity is introduced, defined by :

$$K_a^+ = K_a/(\varepsilon \cdot \nu)^{1/4} \qquad (28)$$

ν being the kinematic viscosity and ε the energy dissipated per unit time and fluid mass due to turbulences induced by the acoustic field.

To describe the inertial behavior of aerosols, caused by acoustically induced turbulences, we introduce a dimensionless relaxation time defined by the expression ;

$$\tau^+ = \tau \cdot (\varepsilon/\nu)^{1/2} \qquad (29)$$

with τ the particle relaxation time being expressed by :

$$\tau = Cu\ D_p^2\ \rho_p/18\ \mu \qquad (30)$$

where Cu represents Cunningham's correction slip factor, D_p the particle diameter, ρ_p its mass per unit volume and μ the dynamic viscosity of the fluid.

By using the expression given by Mednikov (1) for ε (see 4.3.1) all the results of figure 17 can be given in dimensionless form as shown on figure 19 where K_a^+ has been plotted against τ^+.

Fitting the points by a power function leads to the following expression :

$$K_a^+ = 0.031\ \tau^{+\ 0.471} \qquad (31)$$

for a τ^+ variation range between 10^{-3} and 1.

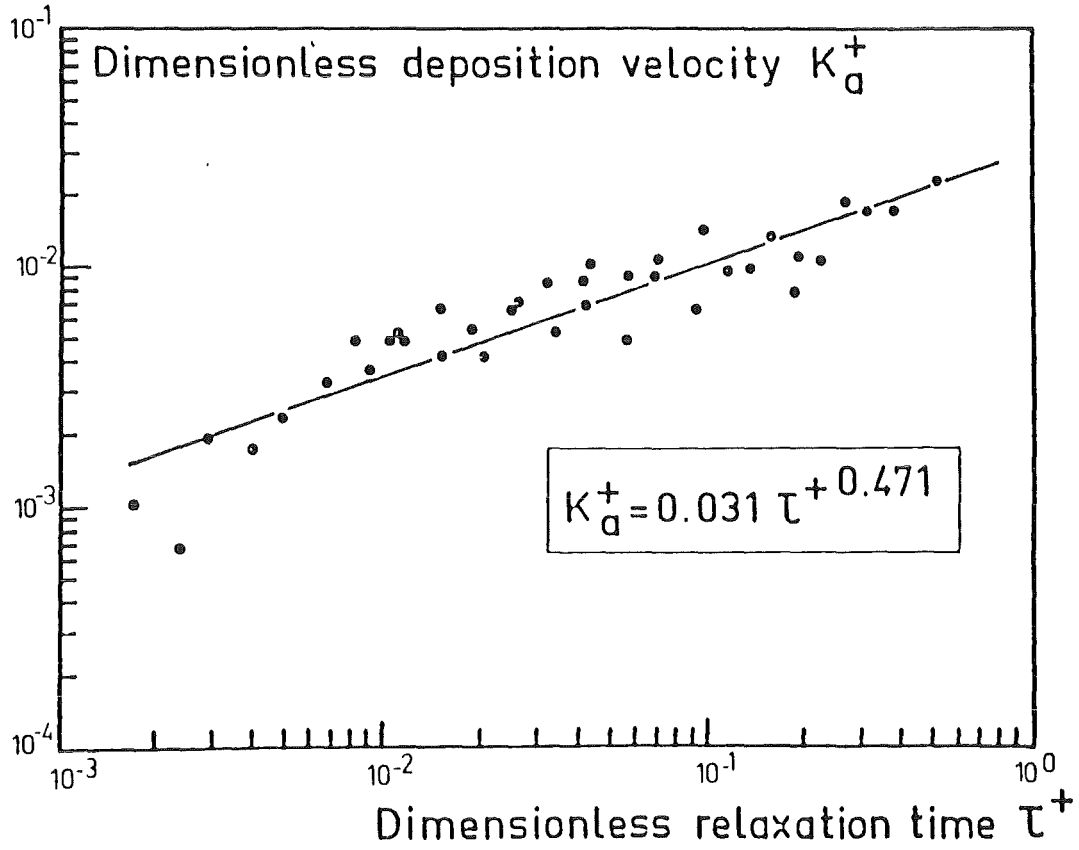

Figure 19 - Dimensionless deposition velocity versus dimensionless relaxation time

This dimensionless relation, obtained under restricted experimental conditions (constant tube geometry and fluid flow rate) remains to be confirmed for different tube geometries (variable diameter) and varying aeraulic conditions (different flow rates) ; after fitting with a correlation coefficient of 0.834 it offers a first empirical approach to acoustic deposition phenomena if we take for ε the expression given by E.P. MEDNIKOV / 1 /.

5. CONCLUSIONS

Two main phenomena occur when an aerosol pass through a volume exposed to an acoustic field :

- a mutual agglomeration of particles resulting in an increase in the median diameter of the aerosol and the corresponding standard deviation. These acoustic field effects begin to occur at around 140 dB but only became significant above 155 dB. The value of the acoustic frequency has little effect in the 500 to 2 000 Hz range. Particle should spent a few seconds in the agglomerator (1 to 3 seconds) depending on the numerical concentration of the aerosol. Moreover, whatever the nature of aerosol (liquid or solid) the behavior is very similar,

- a precipitation of particles on the wall of the volume ; this mechanism depends on, the size of this volume, fluid flow, level of turbulences induced by the acoustic field and particles inertia,

- the turbulence seems to appear between 152 to 153 db ; above 153 db, turbulence (which is revealed by fluctuating velocities) is developed in our system : the largest structures degenerate into smaller and smaller eddies to reach the Kolmogorov scale (about 100 μm in our system).

Above 158 dB the velocity fluctuations sharply increase and could represent up to 30 % of the acoustic wave oscillation velocity under high sound pressure level (163 dB).

REFERENCE

/ 1 / MEDNIKOV E.P.
"Acoustic coagulation and precipitation of aerosol"
a special research report
Trans. from Russian by C.V. LARRICK, consultant Bureau :
New York, (1965)

/ 2 / SHAW D.T.
"Acoustic Agglomeration of aerosols"
in Recent developments in Aerosol Science, Edited by D.T. SHAW,
Wiley Interscience, 279, (1978)

/ 3 / CHOU K.H., LEE P.S., SHAW D.T.
"Aerosols agglomeration in high intensity-acoustic fields"
J. Colloid Interface Sci., 83, 335 (1981)

/ 4 / BOULAUD D., DIOURI M., MADELAINE G.
"Parameters influencing the collection efficiency of solid aerosols in cascade impactors"
in Aerosol in Science Medicine and Technology, 9th Conference of the Gesellcharft für Aerosol Forschng (1981)

/ 5 / BOULAUD D., DIOURI M.
Méthodes de traitement des données expérimentales obtenues par impaction et par sédimentation
Rapport CEA-R-5177 (1982)

/ 6 / CHOU K.H., LEE P.S., WEGRZYN J., SHAW D.T.
"Aerosol deposition in acoustically induced turbulent flow"
Atmospheric Env., 16, 1513-1522 (1982)

/ 7 / BOUTIER A.
"L'anémométrie laser"
ONERA TP n° 153, (1979)

/ 8 / HINZE,
"Turbulence"
Mc Graw-Hill series in mechanical Engineering, (1959)

/ 9 / TAYLOR G.I.
Proc. Roy. Soc., 164, 476, (1938)

/ 10 / TAILLET J.
Personal communication (1986)

/ 11 / MALHERBE C.
"Etude du comportement d'un aérosol soumis à un champ acoustique"
Rapport CEA-R-5306, (1985)

PHYSICAL AND MATHEMATICAL MODELLING OF GRAVITATIONAL COAGULATION

Contribution to the Coagulation Workshop
held in Karlsruhe, FRG from March 16 to 18, 1988

Helmut Bunz

Introduction

Beside the Brownian coagulation the gravitional coagulation influences the behaviour of all particle size distributions dispersed in any arbitrary carrier gas whereas other effects as e.g. turbulence, electric forces and so on request the presence of certain conditions.
The basic physics involved is quite well understood and can mathematically be formulated at least for some particle size regimes. Only approximate solutions are available if the particles are similar in size or either very large or of intermediate size.
Comparing the different physical effects leading to coagulation the gravitional coagulation is of special importance for large particles ($d>10\mu m$) and for particles not too much different in size. Therefore, the most interest and research can be found in connection with cloud physics and the scavenging of aerosol particles by rain drops as for example the famous article by Fuks (1951).

The flow past a single sphere

Most approaches are bases on the description of the flow past a single sphere. Since the velocity of aerosol particles is usually far below the velocity of the sound the flow can be assumed to be incompressible. The relaxation time of a settling particle is quite small which means that the flow can additionally be regarded as stationary. The flow around a single settling sphere can, therefore, be described by the time independent Navier-Stokes equations for an incompressible flow.

$$\vec{u}\nabla\vec{u} = -\nabla p/\rho + \vec{f} + \nu\Delta\vec{u} \qquad (1)$$

The meaning of the different terms is as follows:
$u\nabla u$: inertial term or convective acceleration
accelaration of unit mass of flow by the (curved) convective field
$-\nabla p/\rho$: pressure gradient
$\vec{f}$: external field (e.g. gravity, electric fields etc.)
$\nu\Delta\vec{u}$: viscosity term
force on the volume element by the local shear stress
An additional equation is given by the continuity equation for an incompressible flow:

$$\nabla\vec{u} = 0 \qquad (2)$$

The Navier-Stokes equations (1) can be further simplified by defining the statical and the dynamical pressure.

$p = p_{stat} + p_{dyn}$ with $\nabla p_{stat}/\rho =: \vec{f}$

e.g. gravity $\Rightarrow \nabla p_{stat}$: buoyancy

Therefore, the force term can be removed (or be hidden in the pressure term).

Due to the condition (2) the flow field may be written as

$$\vec{u} = \nabla \times \vec{A} \quad \text{with } \vec{A} \text{ a vector potential} \tag{3}$$

Since the flow past a settling sphere is axisymmetric the vector potential has only an azimuthal component which is called stream function by definition. Working out the expression (3) the two (non-zero) velocity components u_r and u_θ can be written:

$$u_r = - (1/r^2 \sin\theta)\ \partial\psi/\partial\theta \tag{4a}$$

$$u_\theta = (1/r \sin\theta)\ \partial\psi/\partial r \tag{4b}$$

The equations (4a) and (4b) can be inserted into eq. (1) to yield a differential equation for the stream function ψ. This differential equation has to be solved for the appropriate boundary conditions:

1) $u_\theta = u_r = 0$ for $r = a$ with a: radius of the sphere. (5)

For simplicity it assumed that the sphere is at rest and the fluid is moving.

This non-slip or sticking boundary condition has to be modified for particles whose sizes are comparable to the mean free path length of the carrier gas and if two particles a very close together (in the order of the mean free path length).

2) In the infinity the flow has to be equal to an even flow in the direction of the gravity.

$$u_r = - u_\infty \cos\theta \tag{6a}$$

$$u_\theta = u_\infty \sin\theta \tag{6b}$$

The velocity u_∞ is the terminal settling velocity of the sphere.

The flow can be further characterized by the Reynolds number (R) to get even more simplified equations for the different flow regimes.

The magnitude of the two terms $\vec{u}\nabla\vec{u}$ (inertial acceleration) and $\nu\Delta\vec{u}$ (friction) has to be estimated and compared which leads automatically to the Reynolds number.

$$\frac{|\vec{u}\nabla\vec{u}|}{|\nu\Delta\vec{u}|} \approx \frac{u_\infty^2/a}{\nu u_\infty/a^2} = \frac{u_\infty a}{\nu} = R \qquad (7)$$

As examples some values of R for ρ = 1 g/cm^3 and air as carrier gas:
a = 1 μm: R = 7.5 10^{-6}
a = 10 μm: R = 7.5 10^{-3}
a = 51 μm: R = 1
a = 100 μm: R = 7.5

1) R » 1
The viscosity term $\nu\Delta u$ may be neglected which leads to the Navier-Stokes equations of a frictionless flow. The differential equation can be solved by a potential function:

$$\vec{u} = \nabla\phi \qquad (8)$$

The flow is, therefore, called potential flow and can be valid only in some distance from the particle or outside the boundary layer since it is not possible to fulfill the boundary conditions (5) (sticking condition at the particle surface) with a frictionless flow.

2) R ≈ 1
Analytical solutions for this (transition) regime are not known. Only some approximative solutions based on either the Stokes flow or on the potential flow or numerical solutions can be found in the literature (see e.g. Pruppacher and Klett, 1978).

3) R « 1
This case is most important for aerosol particles as most particles are within this flow regime. In this case the inertial term may be neglected in comparison to the viscosity term. The Navier-Stokes equation (1) can be simplified to the equation for a viscous or Stokes flow.

$$\nu\Delta\vec{u} = \nabla p/\rho \qquad (9)$$

Inserting the stream function ψ into (9) and solving the resulting partial differential equation leads to:

$$\psi_{St} = (1/4)u_\infty a^2 \sin^2\theta\,(2r^2/a^2 - 3r/a + a/r) \qquad (10)$$
$$u_r = -u_\infty \cos\theta\,(2r^2/a^2 - 3r/a + a/r) \qquad (11)$$
$$u_\theta = u_\infty \sin\theta\,(1 - 3a/4r - a^3/4r^3) \qquad (12)$$

Using the solutions (10) to (12) the pressure gradient along the surface of the particle and the resulting drag force on the particle can be calculated. The result is the well-known Stokes formula for the resistance of a sphere moving in a fluid.

Calculation of the collision efficiency

The collision efficiency is defined as the ratio between the real collision probability to the probability by pure geometric interception. By this definition the collision probability for the gravitional coagulation can be written as follows:

$$w_{Coll}(a_1,a_2) \sim \epsilon(a_1,a_2)\pi(a_1+a_2)^2|u_{\infty 1}-u_{\infty 2}| \qquad (13)$$

For most applications to aerosol particles the Reynolds number of the collecting particles is small against unity. Therefore Stokes-flow can be assumed for the flow past this particle. If in addition the collected particle is much smaller than the collecting particle it can further be assumed that the flow field is not influenced by the smaller particle. The method to calculate the collision efficiency consists of calculating the stream line passing the larger particle (number 1) at a distance of a_1+a_2 based on the solution of the stream function for the flow past a single sphere (eq. 10). The distance of this stream line from the axis of symmetry y_c is equal to the impact parameter of particles with a settling velocity of zero. If the settling velocity of the collected particle is neglected the ratio $(y_c/(a_1+a_2))^2$ gives the requested collision efficieny already, a method as it was applied by Fuks (1951). The distance y_c may be calculated using eq.(10):

$$\psi_{St}(a_1+a_2,\pi/2) = \psi_{St}(r,y_c/r)|_{r\to\infty} \qquad (14)$$

$$\Rightarrow y_c^2 = (a_1+a_2)^2 - (3/2)a_1(a_1+a_2) + (1/2)a_1^2/(a_1+a_2) \qquad (15)$$

To calculate now the total flux of small particles 2 to the collecting particle the flow of particles 2 into the lower hemisphere of the sphere with a radius of a_1+a_2 has to be calculated. Since the particle 2 does not influence the flow field the velocity of particle 2 in the system of particle 1 $\vec{v}_2$ may simply be calculated by:

$$\vec{v}_2 = \vec{u} - \vec{u}_{2\infty} \qquad (16)$$

Eq. (16) is called the superposition principle.

The flux of particles 2 in the system of particle 1 is given by $n_2 \cdot \vec{v}_2$ and the total flux in the hemisphere by intergrating over the particle flux. The integral consists of two terms, the first one the integral over $\vec{u}$,

the second one over $\vec{u}_{2\infty}$. Since the flow is imcompressible the first integral is equal to $\pi y_c^2 u_{1\infty}$. The second integral yields $\pi(a_1+a_2)^2 u_{2\infty}$.
The gravitional coagulation kernel can be calculated from the total particles flux by normalizing the flux by the particle concentration n_2.

$$K_G(a_1,a_2) = (1/n_2) \int n_2 \vec{v}_2 \, dS =$$
$$= \pi u_{1\infty}(1+p)^2 a_1^2 (1 - 3/2(1+1p) + 1/2(1+p)^3 - p^2) \qquad (17)$$
with $p = a_2/a_1$

Eq. (17) may be simplified if $p \ll 1$ can be assumed. This assumption was already made deriving eq. (17) since it was necessary to apply the superposition principle.

$\Rightarrow$

$$K_G(a_1,a_2) = (1/2)\pi u_{1\infty} a_1^2 p^2 = (1/2)\pi u_{1\infty} a_2^2 \qquad (18)$$

If eq.(18) fulfills certain limits it can formally be extended to $p \to 1$. The velocity $u_{1\infty}$ has to be replaced by the velocity $u_{1\infty}-u_{2\infty}$.

$\Rightarrow$

$K_G(a_1,a_2) \to 0$ for $p \to 0$
and
$K_G(a_1,a_2) \to 0$ for $p \to 1$ as the relative velocity approaches 0.

$\Rightarrow$

$$K_G(a_1,a_2) = (1/2)\pi a_2^2 (u_{1\infty}-u_{2\infty}) \qquad (19)$$

Using the definition eq.(13) the collision efficiency $\epsilon(a_1,a_2)$ can be derived from (19):

$$\epsilon(a_1,a_2) = (1/2)a_2^2/(a_1+a_2) = (1/2)p^2(1+p)^2 \qquad (20)$$

The difference of this formula to the so-called Fuks formula (Fuks, 1964) consists of replacing the factor 1/2 by 3/2. This difference is caused by neglecting the settling velocity of the smaller particle as already mentioned above.
If the two approaching particles are similar in size the assumption that the flow field is dominated by the larger particle and that the superposition principle can be applied is not longer valid. The Navier-Stokes equations have to be solved for a system influenced by two moving spheres (see e.g. Davis, 1972, Jonas, 1972 and Hocking, 1973). One of the problems arising is caused by applying the boundary conditions (5) for both spheres since these sticking conditions yield an inverse power law for the repelling force between the particles. Interacting by such a force the particles could never collide. Therefore to get the correct power law the boundary conditions have to be modified taking into account the slip at the particle surfaces. The power changes then from d^{-1} (with

d the distance between the particles) to a logarthmic law allowing the particles to colllide. Fortunately, the resulting collision efficiencies of these more sophisticated calculations (Davis, 1972) and the simple model presented above differ not too much. The formula (20) seems, therefore, be applicable for aerosol behaviour calculations.
If the Reynolds number of the collecting particles exceeds one the flow regime changes to a potential flow as already mentioned. In this case which is only important for large particles with low residence time and rain drops a back flow behind the collecting particle may cause a wake capture and the collision efficiency can even exceed one (Fig. 1 from Pruppacher and Klett, 1978).
For non-spherical particles only qualitative theoretical statements or experimental investigations can be made. Depending on the geometry of the particles an increase or a decrease of the collision efficiency is possible. In particular an increase of the efficiency can be expected if the porosity of the particle is large enaugh to allow the flow to penetrate the particle and to diminish, therefore, the hydrodynamic deflection.

Some applications to aerosol behaviour calculations

The gravitional coagulation frequency of a particle with a radius of 10 μm with smaller particles can be seen in Fig. 2 in comparison to the Brownian and the total (the sum) frequency. Only in a quite small size range the two frequencies are of comparable magnitude justifying the simple superposition of the two frequencies as the dominating size regimes are quite different. The gravitional coagulation is of special importance for the coagulation if the size of the collected particle exceeds about 1 μm. Smaller particles follow the flow around the collecting particle due to their small inertia and are collected with a lower probability. Their chance to be collected increases only due to their enhanced Brownian motion or in other words due to diffusion to the collecting particle.

To examine the effect of the gravitional coagulation some numerical experiments were performed with the aerosol behaviour code NAUA-Mod5 (Bunz et al., 1987). In these experiments which can unfortuantely not so easily be repeated in real experiments the Brownian or the gravitional coagulation were switched off and the results were compared to the results using the combination of both processes.
The initial particle size distribution is bimodal (Fig. 3), the two maxima at 0.1 μm and at 1 μm. Each mode represents a mass concentration of 1 g/m^3. The three final distributions (Fig. 4 to 6) are after 20000 sec

of time. Comparing the results of the calculations using the combined coagulation process and the Brownian coagulation only the size distribution differ only at the upper end due to less effective coagulation between the larger particles in the absence of gravitional coagulation. In the case of gravitional coagulation only the mode of the smaller particles is more or less uneffected and only the mode of the bigger particles changes slightly. In this case the transport of the smaller particles to the bigger ones is lacking and, therefore, the initiating event for an effective gravitional coagulation.

Conclusions

The gravitional coagulation can be quite well described by an analytical formula if the collecting particle is within the Stokes regime ($R \ll 1$ corresponding to $a < 30\ \mu m$) and the particle to be collected is small against the collecting particle. Comparison of this model to more sophisticated models solving the Navier-Stokes equations for two spheres show that the numerical results of these models do not differ too much from the results if the formula mentioned above are extended to regimes where the sizes of the two particles are comparable. Therefore, this formula seems to be sufficient for most applications as all aerosol particles with noticable residence time are within the Stokes regime. If, however, the scavenging of particles by rain or spray drop has to be considered the flow regime changes to a potential flow. For these cases and in particular for the transition regime ($R \approx 1$) no analytical formula are available but only some results of numerical solutions or of experiments.
The same is true for the collision efficiency and the corresponding gravitional coagulation frequency of non-spherical particles. Theoretical results can only be obtained for special geometries like ellipsoids or are only rough gesses. Otherwise the collision efficiencies have to be determined by experiments with the difficulty that those measured data are applicable for the specific aerosol only.

References:

Bunz H., Koyro M., Schöck W. (1987) "NAUA Mod5 und NAUA Mod5-M" KfK 4278, September 1987, Kernforschungszentrum Karlsruhe, FRG
Davis M.H. (1972) J. Atmos. Sci 29, 911
Fuks N.A. (1951) Dokl. Akad. nauk SSSR ("Geofizika") 81, 1043
Fuks N.A. (1964) "The Mechanics of Aerosols" Pergamon Press, Oxford
Hocking L.M. (1973) J. Engr. Math. 7, 207
Jonas P.R. (1972) Quart. J. Meteor. Soc. 98, 681
Klett J.D., Davis M.H. (1973) J. Atmos. Sci. 30, 107
Lin C.L., Lee S.C. (1975) J. Atmos. Sci. 32, 1412
Pruppacher H.R., Klett J.D. (1978) "Microphysics of Clouds and Precipitation" D. Reidel Publ. Comp. Dordrecht, Boston, London
Schlamp R.J., Grover S.N., Pruppacher H.R., Hamielec A.E. (1976) J. Atm. Sci. 33, 1747

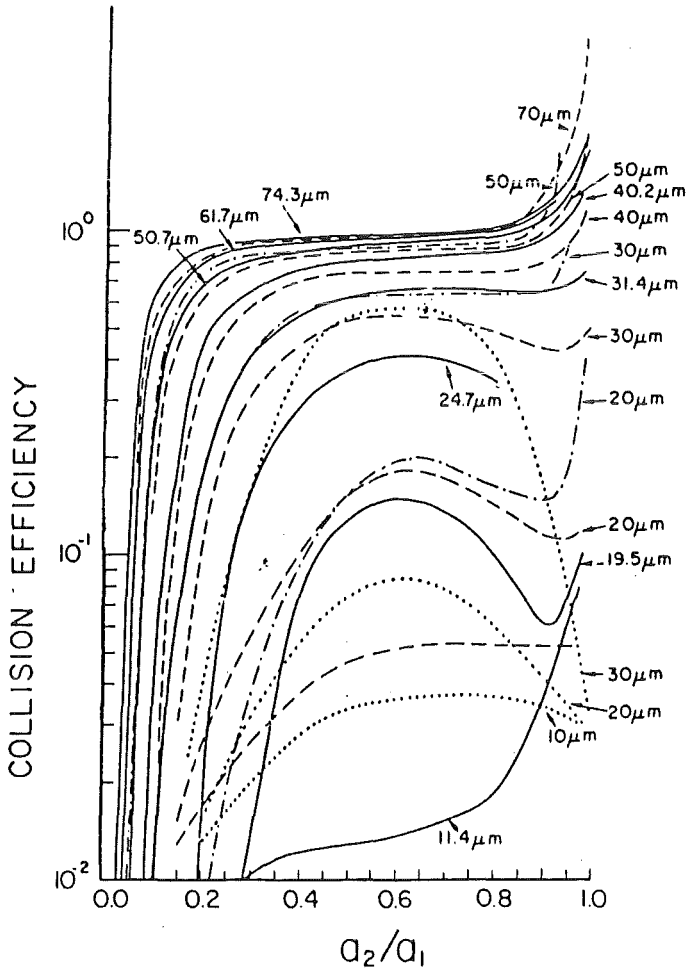

Fig. 1 Theoretical collision efficiencies of spherical water drops in calm air as a function of p-ratio and of collector drop radius (given by label of each curve); —— Schlamp *et al.* (1976), ---- Klett and Davis (1973), -·-·- Lin and Lee (1975), ····· Jonas (1972).

(from Pruppacher and Klett, 1978)

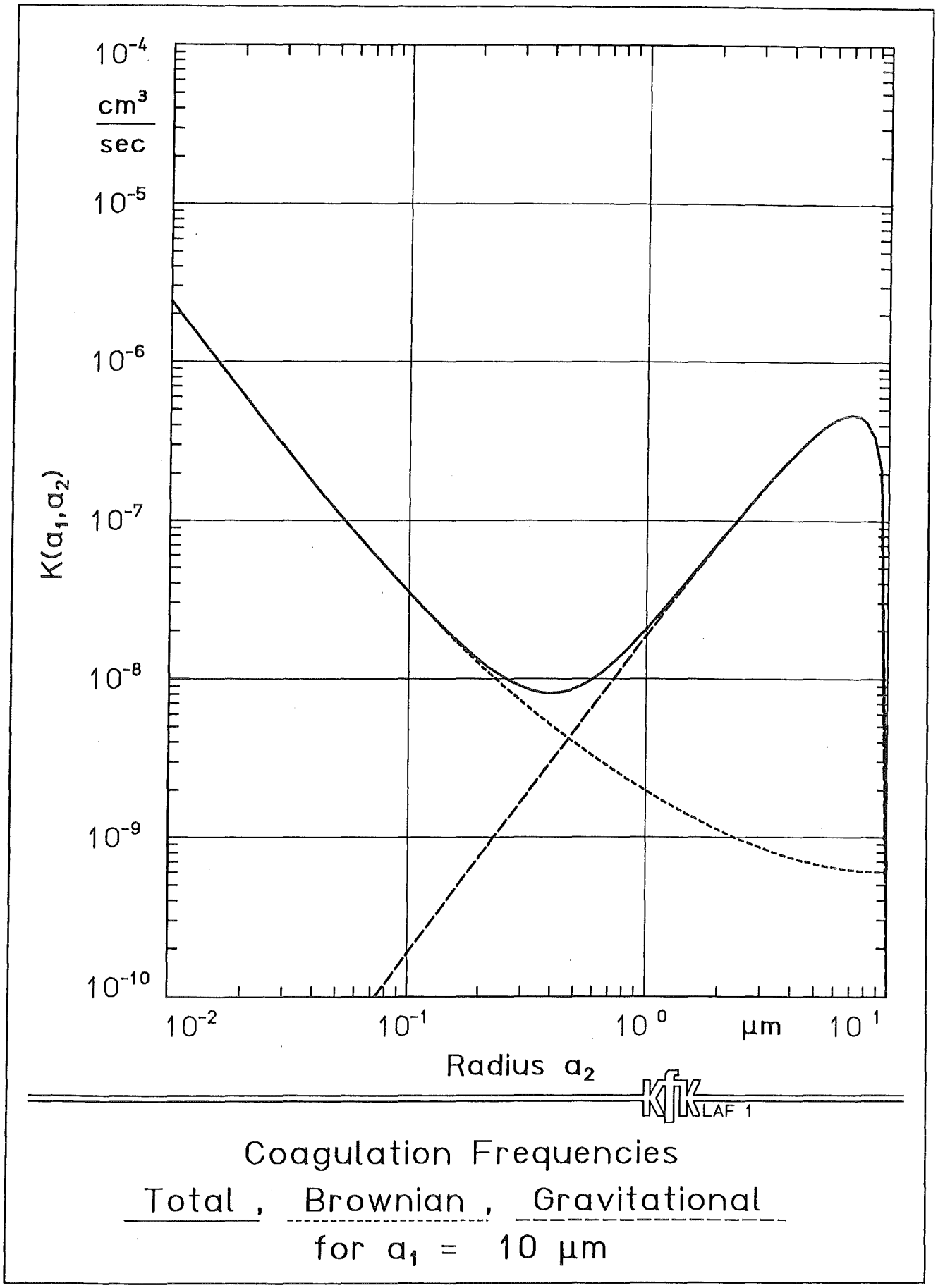

Fig. 2 Comparison of different coagulation frequencies

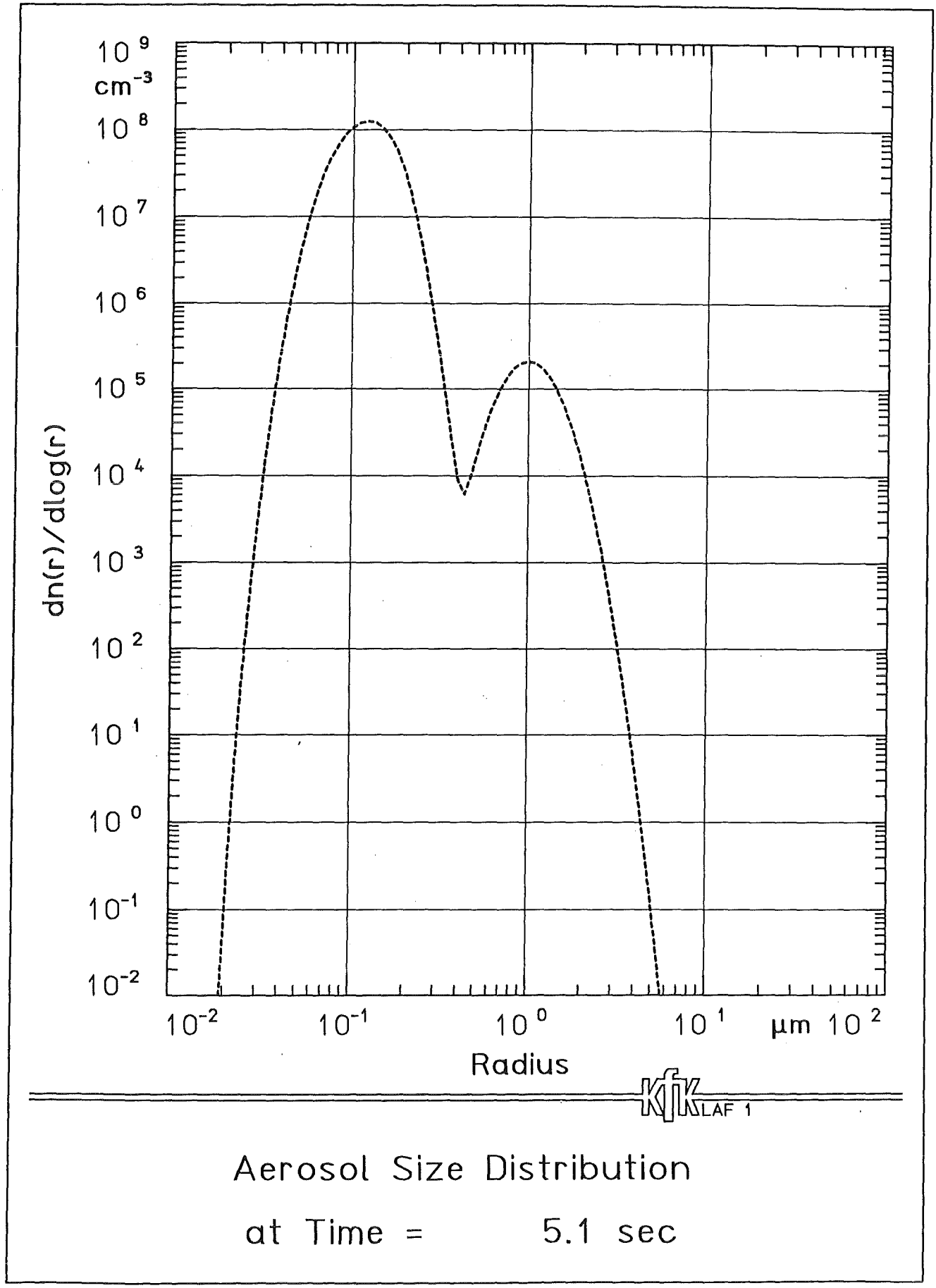

Fig. 3 Initial particle size distribution for model calculations

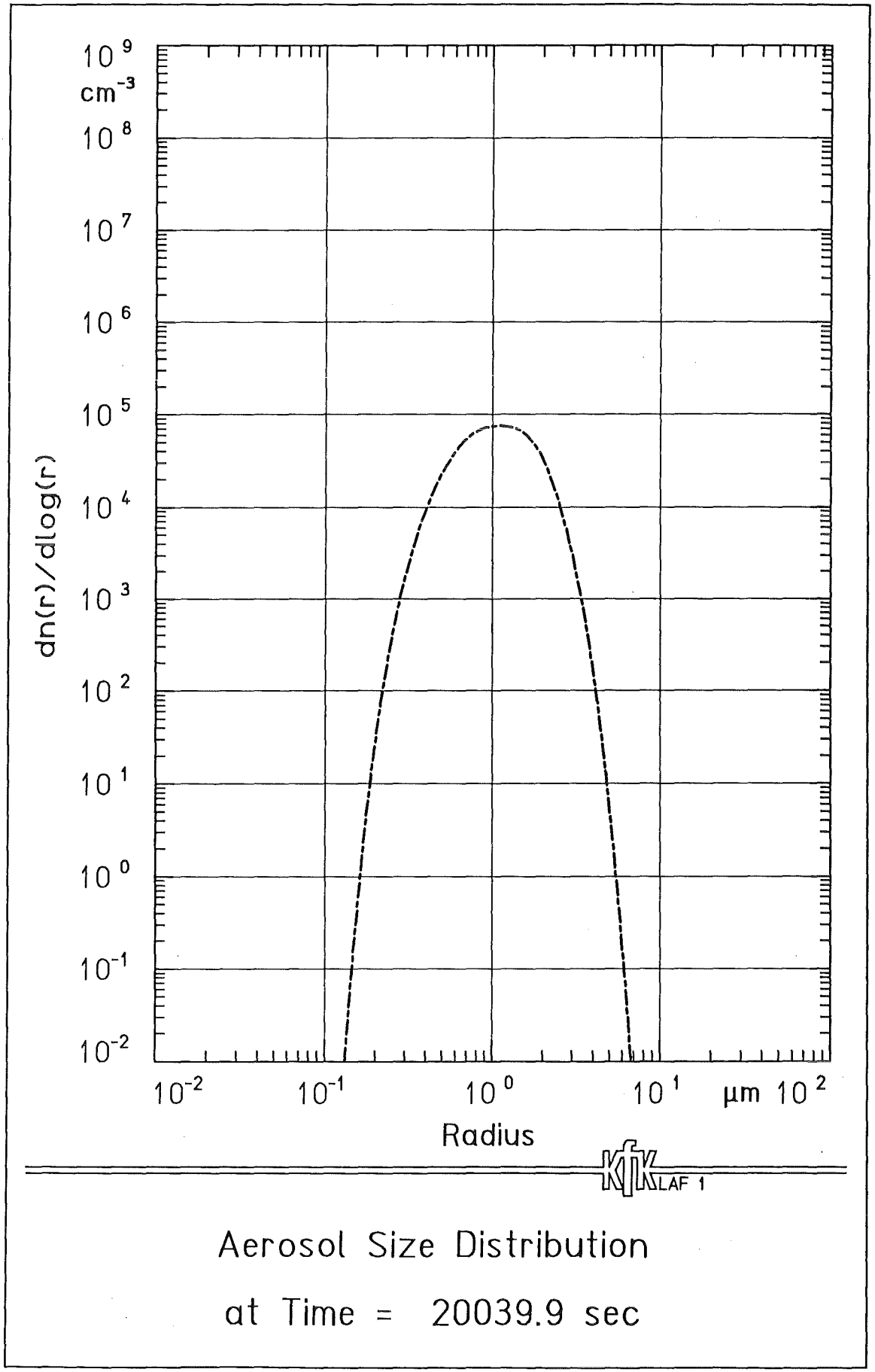

Fig. 4 Particle size distribution at 20000 sec with Brownian and gravitional coagulation

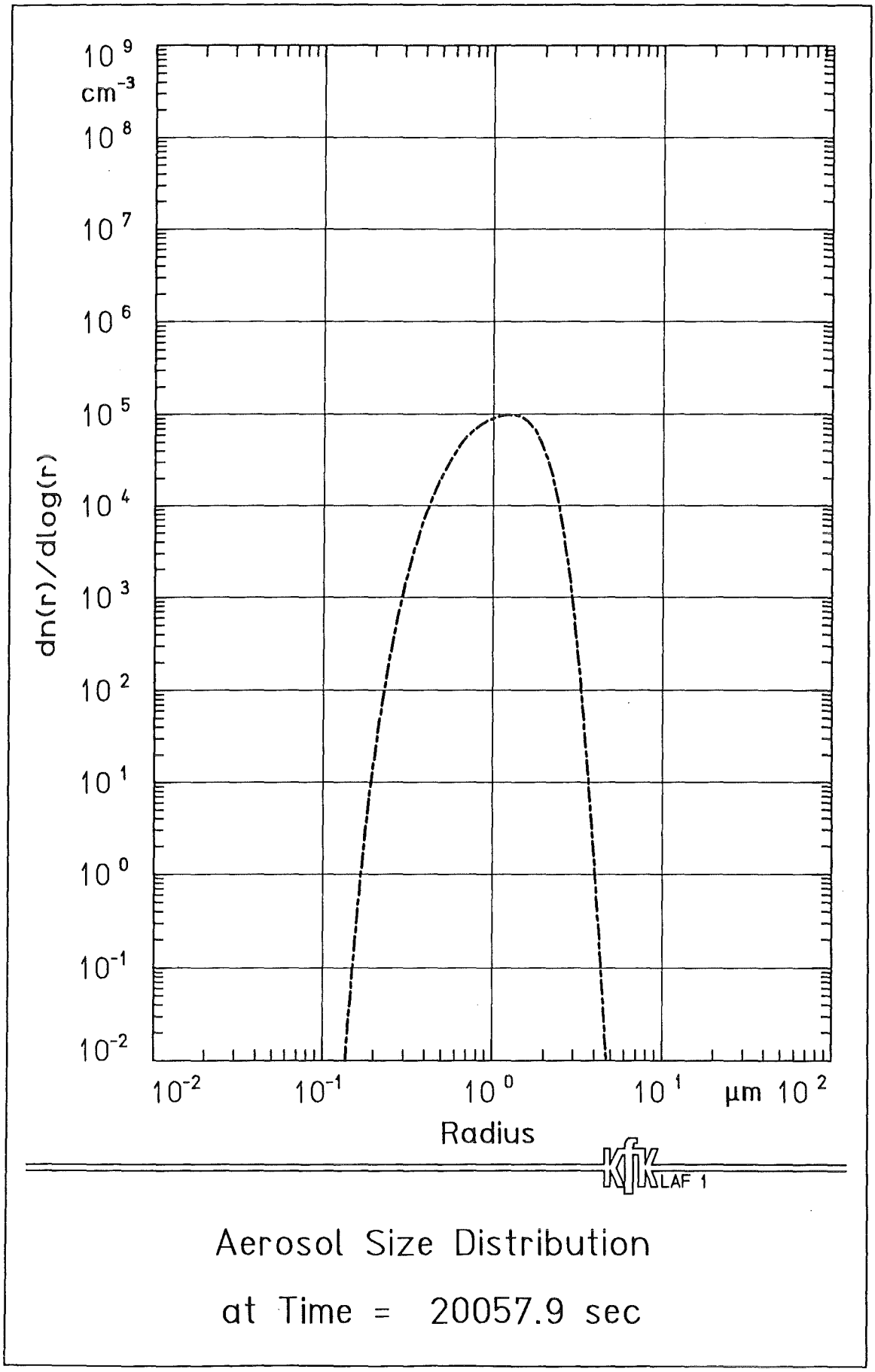

Fig. 5 Particle size distribution at 20000 sec with Brownian coagulation only

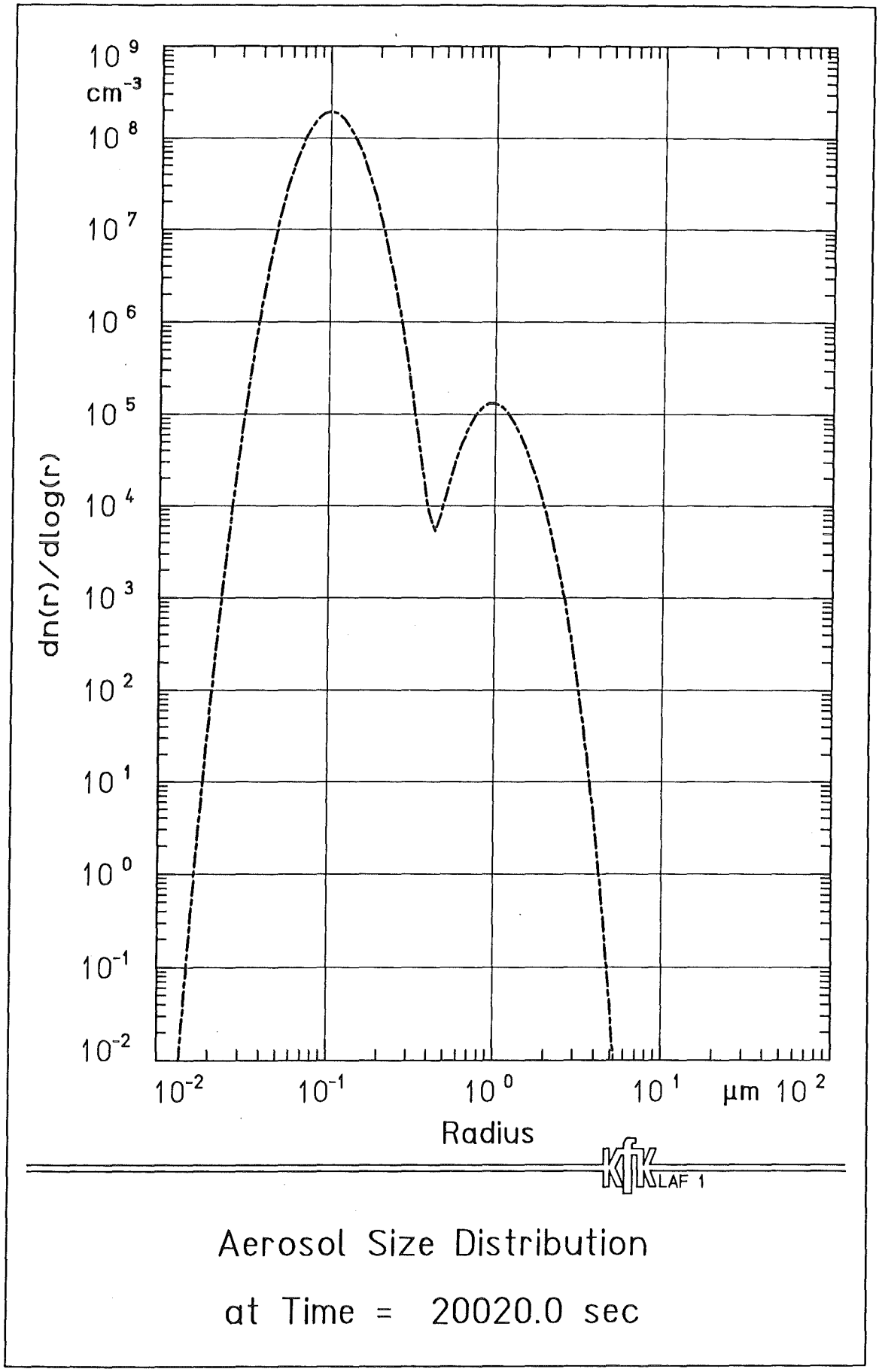

Fig. 6 Particle size distribution at 20000 sec with gravitional coagulation only

Coagulation Workshop
Nuclear Research Center Karlsruhe
March 16-18, 1988

Bipolar Coagulation of Asymmetric Particle Distributions

Theoretical Considerations

B. Eliasson and W. Egli
Asea Brown Boveri
Corporate Research
CH-5405 Baden, Switzerland

ABSTRACT

We present calculations of the coagulation rate of aerosol particles which have been charged with ions of both polarities. The classical theory for bipolar coagulation has been expanded to include distributions of polydisperse aerosols. We include a brief introduction explaining the reasons for the interest in this kind of work. We treat the general case of asymmetric particle distributions after giving a short description of the symmetric case of equal distributions of positive and negative charges. The numerical simulations are done with a measured fly ash distribution taken from the literature.

INTRODUCTION

In the field of electrostatic precipitation one of the problems which remains to be solved is the efficient precipitation of particles in the range from approximately 0.1 to 1 μm radius. In an electrostatic precipitator (ESP) the aerosol particles are charged and the pulled out of the stream by an applied field. As the size of the particle diminishes the maximum charge it can carry diminishes also. The rate at which a particle can be removed from the gas stream is a function of the migration velocity perpendicular to that stream. The migration velocity is a function of the particle charge, its mass and the frictional forces. If one plots the migration velocity vs. radius one gets a curve similar to the one shown in Fig. 1. The important thing is to note that the

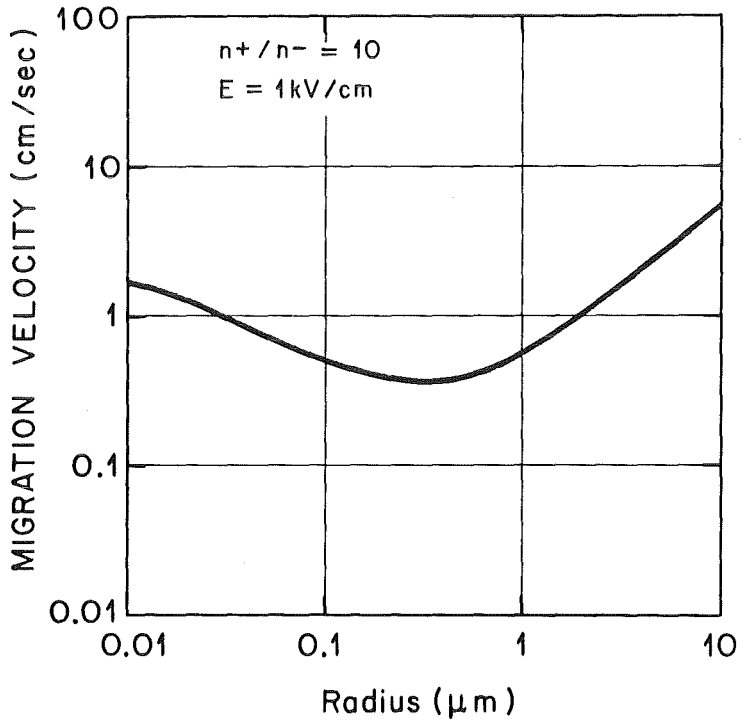

Fig. 1: A calculated plot of migration velocity vs. particle radius when both ionic polarities are present. The applied field is 1 kV/cm and the positive ion density (n^+) is 10 times the negative ion density (n^-).

migration velocity, w, has a minimum below 1 μm. This leads to a minimum in the efficiency of the ESP as one can see from the Deutsch approximation of the efficiency η of an ESP, viz.

$$\eta = 1 - \exp(-wA / Q) \qquad (1)$$

where A is the electrode area (cm^2) and Q the gas flow rate (cm^3/sec).

The problem depicted in Fig. 1 is an inherent problem and difficult to deal with. One possible way is to make the area A larger, i.e. make the precipitator higher or longer. There are limits though imposed on these parameters by the space available. Another limit is costs. The flow rate Q is given and cannot easily be changed. This leaves the migration velocity w as a parameter to be increased. One solution in this direction is the two-stage ESP. Here one charges in a first stage and precipitates in a second stage. This way one hopes to increase w by achieving better charging with a higher charging field in the first stage and applying a higher migration field in the second stage. A third possible solution which has been suggested is to change the size distribution of the aerosol particles in the gas flow, i.e. shift it to larger particles by coagulation. There is one important limitation here and that is time. Coagulation takes time and the time available is given because the average residence time of an aerosol particle in the ESP is given by

$$\tau_r = \frac{V}{Q} \tag{2}$$

where V is the volume of the ESP. Both V and Q are basically fixed and cannot be changed much. Typical values for τ_r are of the order of 1-10 seconds.

In a typical ESP all particles in the gas flow are charged by ions of the same polarity. Such particles, at least it they are of a similar size, repel each other and do not coagulate. If one wants to achieve efficient coagulation one has to do it in a coagulator before the precipitator itself.

Neutral or uncharged particles do coagulate due to collisions induced by their random or Brownian motion. Such processes are characterized by a collision cross section and a relative collision velocity. There is a third important parameter and that is the adhesion probability. This parameter describes the probability of the two particles sticking together after the collision. It is a function of e.q. the collision velocity v_{rel} and the material of the particles. The effective collision rate $\overline{k}$ of two particle densities of a certain size can be written as

$$\overline{k} = < h\, v_{rel}\ \sigma > \tag{3}$$

where $< >$ signifies an average over many collisions, h is the dimensionless probability of adhesion, v_{rel} the relative collision velocity and σ is the collision cross section. The influence of the adhesion probability h on the coagulation rate was investigated in Ref. [1].

The natural coagulation rate of neutral particles was first calculated by Smoluchowski [2]. If we assume that the adhesion coefficient is always h = 1 and that the cross sectional collision radius between particles i, with radius r_i, and particles j, with radius r_j, is $R = r_i + r_j$ then the coagulation rate k_{oij} is given by [3]

$$k_{oij} = \frac{2}{3}\frac{kT}{\eta}\left(2 + r_i / r_j + r_j / r_i\right) \tag{4}$$

where T is the gas temperature, k the Boltzmann constant and η the viscosity of the gas. This kind of coagulation, which is due to Brownian diffusion, is a very slow process. If we assume that the coagulation rate is independent of r and put $k_o = k_{oii}$, viz.

$$k_o = \frac{8}{3} \cdot \frac{kT}{\eta} \tag{5}$$

then as Smoluchowski has shown one can integrate the coagulation equations. In this case one can show that the sum of all particle densities $n_i(t)$ decreases with a time constant τ, such that

$$\tau = \frac{2}{k_o \cdot n_o} \tag{6}$$

and $\sum_{i=1}^{N} n_i(o) = n_o$ and $\sum_{i=1}^{N} n_i(\tau) = n_o / 2$ resp.

In air k_o is of the order of 610^{-10} cm^3/sec. Thus for technical particle densities in the range 10^4-10^7 cm^{-3} τ is of the order of hours or larger and thus $\tau >> \tau_r$.

One way to increase the coagulation rate is to introduce attractive electrical forces and charge some of the particles with positive ions and the remainder with negative ions. This will be referred to as bipolar coagulation and will be the subject of the remaining part of this report.

BIPOLAR COAGULATION

Fundamental studies of the coagulation rate of bipolarly charged particles were made by Fuchs [4]. He calculated a new coagulation rate coefficient which can be written with the aid of the Smoluchowski coagulation rate as

$$k_{ij} = f_{ij}\, k_{oij} \quad ; \quad f_{ij} = \alpha_{ij} / \left(\exp\left(\alpha_{ij}\right) - 1\right) \quad ; \quad \alpha_{ij} = q_i q_j / \left(4\pi\varepsilon_o (r_i + r_j) kT\right) \quad (7)$$

where q_i is the charge on a particle with radius r_i and one polarity and q_j is the charge of the opposite polarity on a particle with radius r_j. For bipolar charges f_{ij} can be of the order of 10^4 or larger for 1 μm particles. Thus the coagulation time, at least theoretically, can be reduced from hours to seconds. Fuchs assumed for his analysis that the particles had arbitrary charges but equal radii. In the above expression all inductive forces have been neglected. This implies that the above expressions are only valid as long as the charges do not differ by a very large factor. If the particles are of very unequal sizes or do have very unequal charges inductive forces become important. In this case even particles with charges of equal sign can attract each other because of induced charges [5]. The limit imposed upon the coagulation time is that it be less than τ_r. As we can only hope to reach that order of magnitude by bipolar coagulation we will devote the remainder of this report to that very phenomenon. We will estimate the effect of bipolar coagulation on various distribution functions, especially a function known to characterize the size distribution of fly ash from a coal power plant. In the following section we will assume that the above expressions are valid for the entire range of particle radii considered.

SYMMETRIC BIPOLAR COAGULATION

In this section we will assume that the aerosol is split up into two equal parts and that each half flows through a positive or respectively negative charging section (Fig. 2). In the following coagulator the particles coagulate during the time $\tau = \ell / v_f$ where ℓ is the length of the coagulator and v_f the flow velocity. After the coagulator section a second charging section might follow and thereafter a second coagulator etc.

We will use the definitions given in [3]. Thus we specify the particle density n(r,t) through

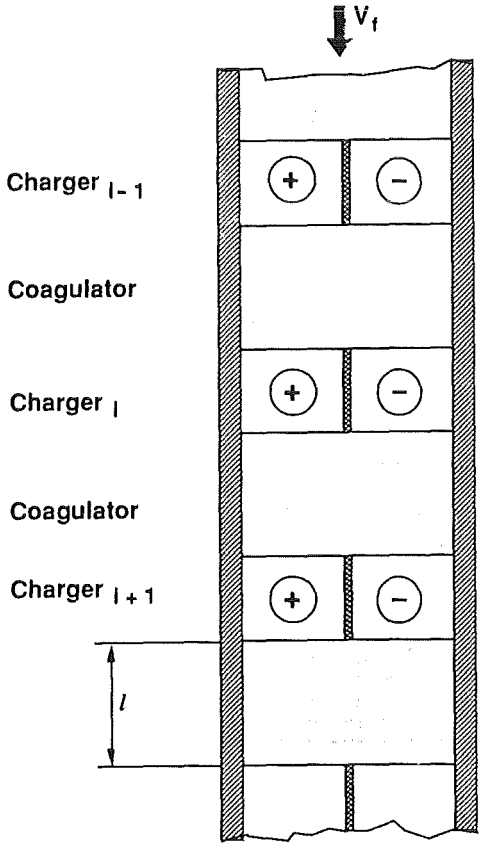

Fig. 2: A schematic diagram of the charging section.

the particle fraction density f(r,t) in such a way that the total particle density with radii between r and r + dr is given by

$$n(r,t) = n_0 \, f(r,t) \, dr; \qquad \int_0^\infty f(r,0)\, dr = 1 \tag{8}$$

where n_0 is the average particle density at time t = 0. Analogously we define a space charge fraction $f_\rho(r,t)$ and an average charge density ρ_0 at time t = 0 such that

$$\begin{aligned} \rho(r,t) &= n(r,t)\, q(r,t) \\ \rho(r,t) &= \rho_o \, f_\rho(r,t) dr \end{aligned} \tag{9}$$

where q(r,t) is the charge on an aerosol particle of radius r at time t. In case of field charging the saturation value q_{so} for unipolar charging is given by

$$q_{so} = p \cdot 4 \pi \varepsilon_o \cdot r^2 E \tag{10}$$

where E is the charging field, $p = 3 \varepsilon_r/(\varepsilon_r + 2)$ and ε_r is the dielectric constant of the particle.

The differential equations which describe the temporal behaviour of n and ρ are given in discrete form in [3] as

$$\frac{dn_j}{dt} = - n_j \sum_{i=1}^{\infty} k_{ij} \, n_i + \sum_{\substack{i=1 \\ m=j-i}}^{N<1} \beta_{im}^{j} \cdot k_{im} \cdot n_i n_m \tag{11}$$

$$\frac{d\rho_j}{dt} = - \rho_j \sum_{i=1}^{\infty} k_{ij} \cdot n_i \tag{12}$$

where

$$\beta_{im}^{j} = \frac{1}{2} \frac{r_j^3}{r_i^3 + r_m^3} \tag{13}$$

$$n_j(t) = n_o f(r_j, t) \Delta r_j \qquad (14)$$

In Fig. 2 of Ref. [3] we show an evaluation of the above equation for monodispere wax particles of average radius = 2 μm and a distribution width of 0.82 μm. The coefficient of adhesion h was assumed to be equal for 1. The calculations were compared to measured values and a rough agreement was found.

Calculations with realistic fly ash distributions and taking the variation of h with the relative impact velocity into account shows that the reduction in mass of particles below 1 μm is only of the order of 2 or 3. This is after 10 seconds and after going through 10 coagulations stages with typical particle concentrations as they are found in coal-burning power stations [3]. This is totally unsatisfactory considering that one is talking about calculations assuming idealized coagulation conditions and an unrealistic limit of 10 coagulation stages.

The reason for the relatively slow coagulation rate in case of symmetric charging can be understood by viewing Figs. 3. Fig. 3a which shows the fractional distribution f(r,t) as a function of time in case of natural coagulation for a distribution which was initially rectangular

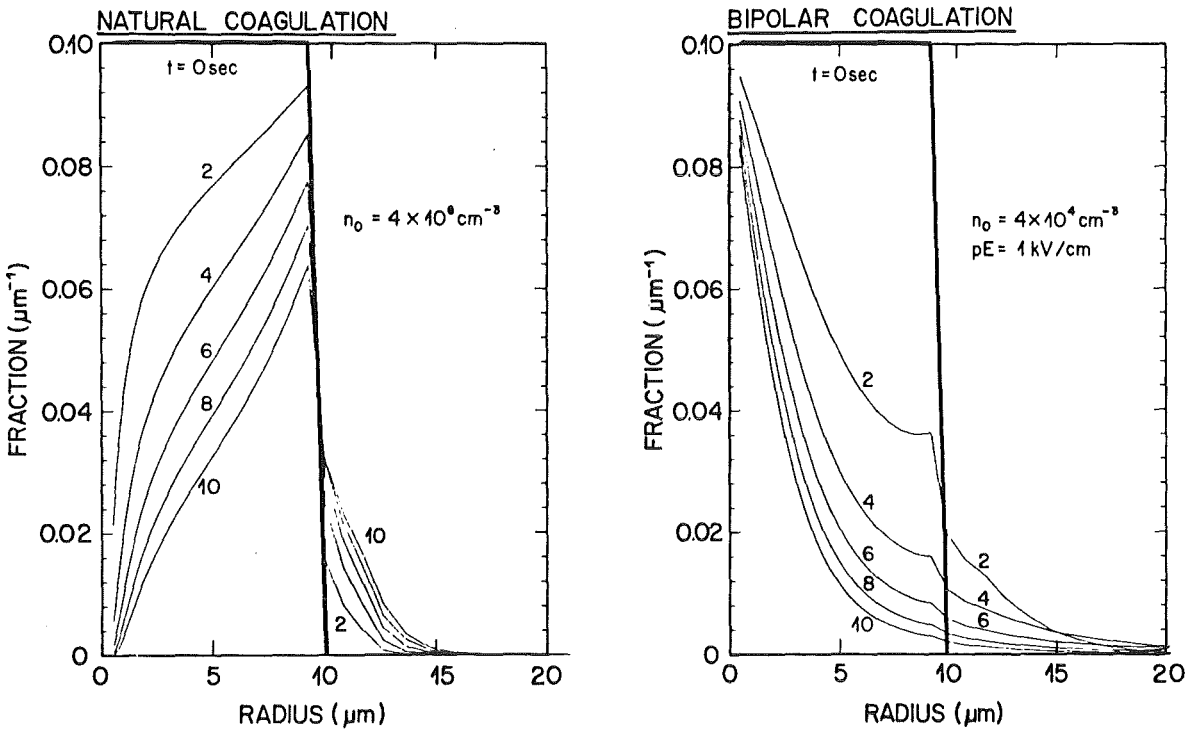

Fig. 3: The qualitative difference between natural (neutral) and bipolar coagulation as a function of time and radius. The initial average density n_0 was 10^4 higher ($4 \cdot 10^8$ cm^{-3}) in case of natural coagulation.

in the range 0.5 μm - 10 μm. Here the small particles disappear faster than the large particles due to the factor r_1/r_2. This is qualitatively what one would like to have. On the right in Fig. 3b, one has the same initial distribution at a factor of 10^4 lower density for the case of symmetric bipolar coagulation. Here one has the opposite behaviour to Fig. 3a. The large particles disappear much faster than the small particles. This is solely due to the factor α_{ij} which is proportional to r^3 for equal size particles, i.e. the large particles do coagulate among themselves and are thus less likely to coagulate with a small particle. This is the main reason for the relatively slow coagulation obtained with symmetric bipolar coagulation. The remedy for the situation is

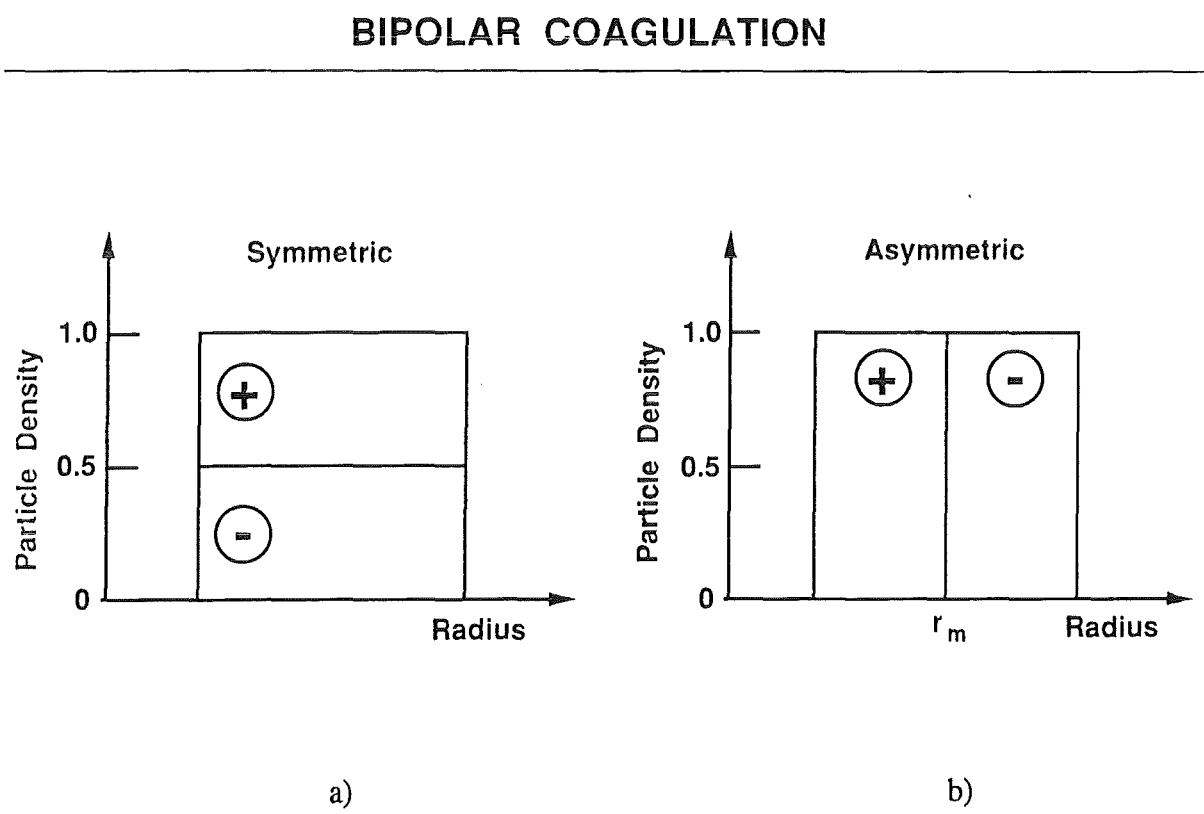

Fig. 4: A schematic diagram showing how the case of symmetric coagulation can be improved by using asymmetric charging.

obvious once one has understood what is shown in Fig. 3b. One has to keep the large particles from coagulating with other large particles. Whereas in symmetric bipolar coagulation all sizes have both positive and negative polarities in equal amounts (Fig. 4a), a better way would be to charge all large particles with the same polarity and likewise all small particles at the opposite polarity (Fig. 4b). This is what we want to attain with what we in the following call asymmetric bipolar coagulation.

ASYMMETRIC BIPOLAR COAGULATION

By asymmetric bipolar coagulation we refer to a situation where the density distribution of positive particles, n^+, is different from the negative, n^-. The two cases of symmetric and asymmetric bipolar coagulation are schematically compared in Fig. 5.

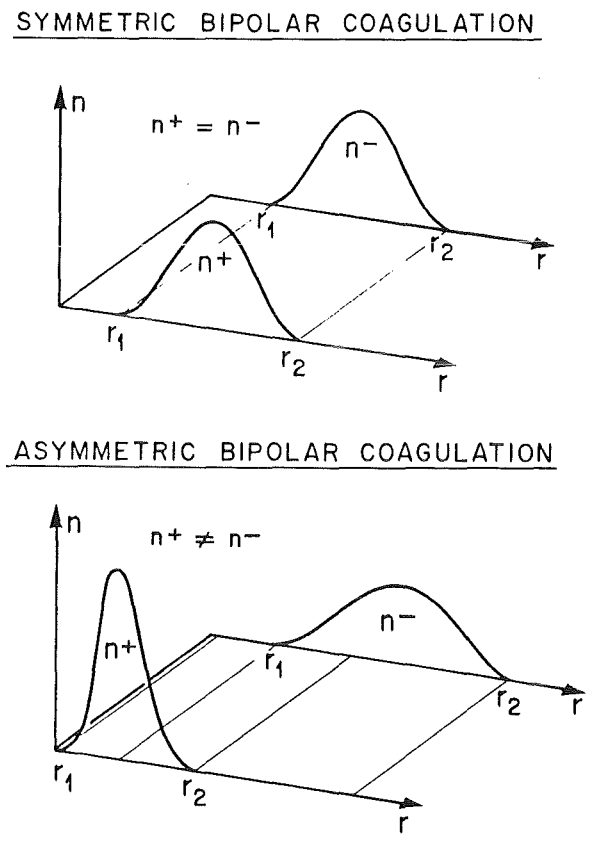

Fig. 5: A schematic comparison of symmetric and asymmetric bipolar charging.

In our case the original distribution is separated into two halves e.g. in a cyclone. Depending on the separation efficiency of the cyclone the two halves are more or less well separated. An ideal cyclone would separated the original distribution n(r) into two halves with a transition radius r_m such that

$$n\,(r) = n^+\,(r) + n^-\,(r) \tag{15a}$$

where

$$n^+\,(r) = n\,(r), \qquad n^-\,(r) = o \qquad \text{for } r_1 \le r \le r_m \tag{15b}$$

$$n^+\,(r) = o, \qquad n^-\,(r) = n(r) \qquad \text{for } r_m < r \le r_2 \tag{15c}$$

We denote such a separation as a (0/100) % separation. In a more realistic case there will be some negative particles at smaller radii and positive particles at larger radii. Such a separation we denote by (100-a/a) % and it is defined as

$$n^+(r) = \frac{a}{100}\, n(r), \qquad n^-(r) = \left(1 - \frac{a}{100}\right) n(r) \qquad \text{for} \quad r_1 \le r \le r_m \tag{16a}$$

$$n^+(r) = \left(1 - \frac{a}{100}\right) n(r), \quad n^-(r) = \frac{a}{100}\, n(r) \qquad \text{for} \quad r_m < r \le r_2 \tag{16b}$$

This situation is shown in Fig. 6. In this notation the symmetric case corresponds to a (50/50) % separation.

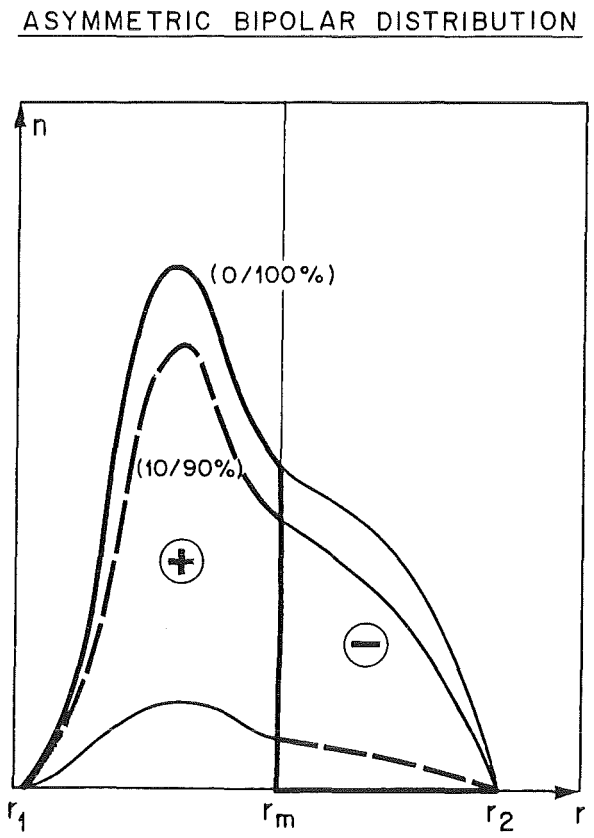

Fig. 6: Definition of the transition radius r_m and the general (100-a/a)% distribution.

The differential equations which govern the coagulation of the positive and negative particles differ considerably from the symmetric case. This is due to two main factors, viz.

a) particles can change classes, i.e. go from positive particles to negative particles or vice-versa and
b) the charge density corresponding to a radius r_j can now either decrease or increase whereas it could only decrease before.

These new rules are reflected in a somewhat more cumbersome system of equations which is given below:

$$\frac{dn_j^{\pm}}{dt} = -n_j^{\pm} \sum_{j=1}^{\infty} k_{ji}\, n_i^{\pm} + F_j^{\pm}$$

$$\frac{d\rho_j^{\pm}}{dt} = -\rho_j^{\pm} \sum_{j=1}^{\infty} k_{ji}\, n_i^{\pm} + G_j^{\pm}$$

where

$$R_j > 0: \quad F_j^{+} = 2N_j, \quad F_j^{-} = 0 \quad ; \quad G_j^{+} = 2R_j, \quad G_j^{-} = 0 \tag{17}$$

$$R_j < 0: \quad F_j^{+} = 0, \quad F_j^{-} = 2N_j \quad ; \quad G_j^{+} = 0, \quad G_j^{-} = 2R_j \tag{18}$$

$$R_j = 0: \quad F_j^{+} = F_j^{-} = N_j \quad ; \quad G_j^{+} = G_j^{-} = 0 \tag{19}$$

and

$$N_j = \sum_{\substack{i=1 \\ (m=j-i)}}^{N \le 1} \beta_{im}^{j}\, k_{im} \left(n_i^{+} n_m^{-} + n_i^{-} n_m^{+} \right) \tag{20}$$

$$R_j = \sum_{\substack{i=1 \\ (m=j-i)}}^{N \le 1} \beta_{im}^{j}\, k_{im} \left[n_i^{+} n_m^{-} \left(q_i^{+} - q_m^{-} \right) + n_i^{-} n_m^{+} \left(q_m^{+} - q_i^{-} \right) \right] \tag{21}$$

The test distribution we have used is the same one which was used in Ref. [3] and it was taken from [6]. It is shown in Fig. 7, i.e. its density, surface and mass. The total mass density was $n_0 = 7$ g/m^3. In Fig. 8 we compare the case of a symmetric bipolar coagulation (Fig. 8a)

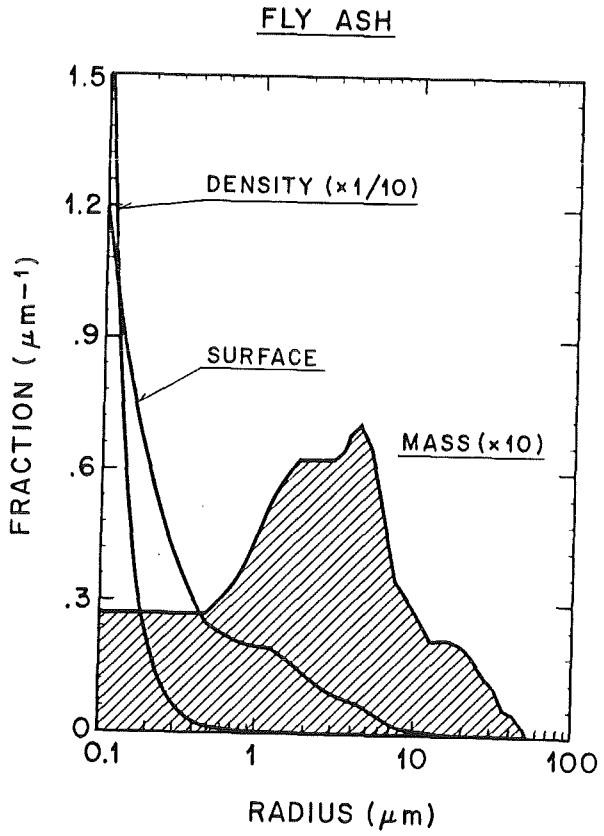

Fig. 7: The density, surface and mass distribution of fly ash taken from Ref. [6].

with the asymmetric case with $r_m = 2$ μm (Fig. 8b). The tremendous difference in the coagulation rate for small radii is very well visible. E.q. for r = 1 μm and the case shown in Fig. 8a the mass has hardly changed at all whereas in Fig. 8b the mass around 1 μm totally disappears within 10 sec.

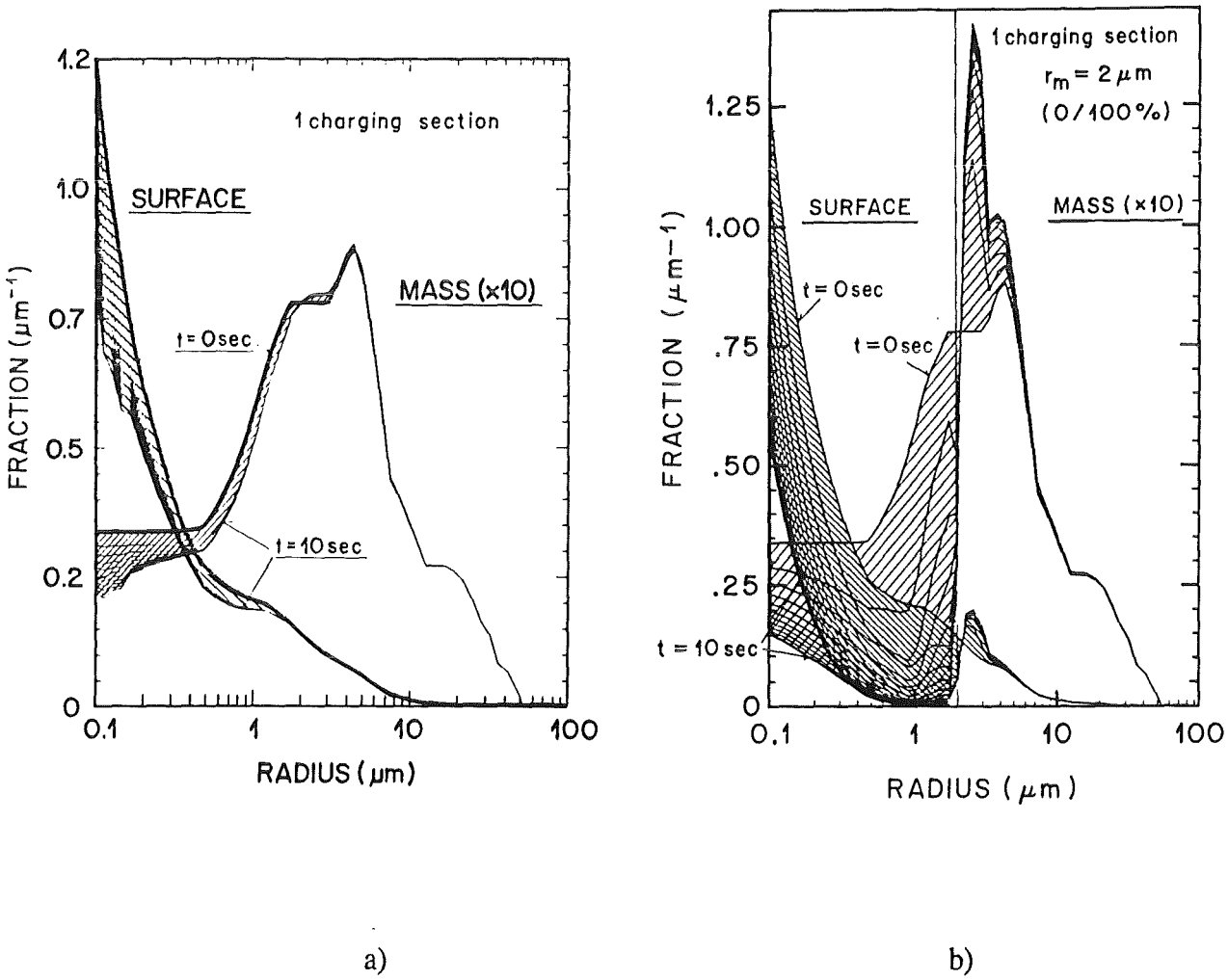

a) b)

Fig. 8: The effect of symmetric vs. asymmetric bipolar coagulation on the coagulation speed. Fig. 8a shows the change in the surface and mass distributions due to symmetric coagulation during 10 sec. Fig. 8b shows the same situation for (0/100)% asymmetric coagulation and $r_m = 2\mu m$.

In Fig. 9 we show the effect of changing the transition radius r_m on the mass distribution after a coagulation time of t = 10 sec.

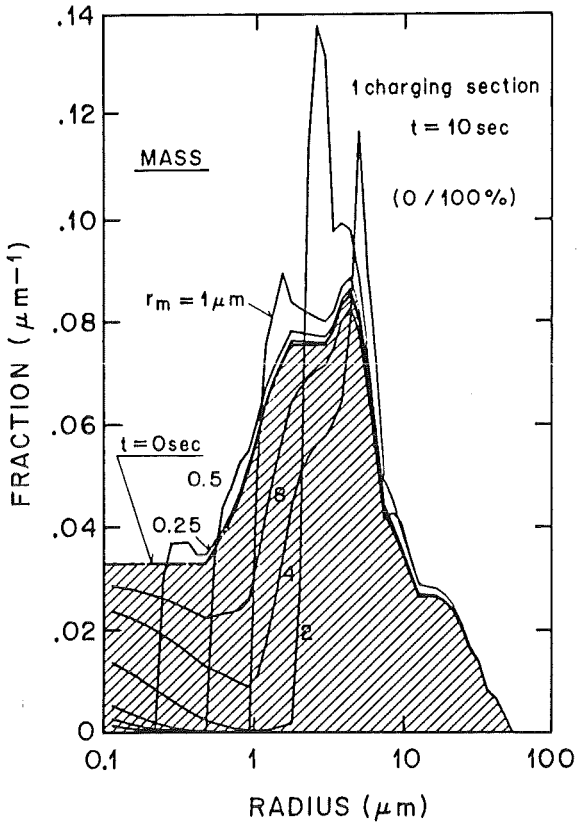

Fig. 9: The effect of the transition radius on the mass distribution after t = 10 sec and a single coagulation stage.

In Fig. 10 we compare the decrease in the average density < n > as a function of time for symmetric and asymmetric bipolar coagulation. After 10 seconds the asymmetric case with $r_m = 1$ μm leads to approximately 7 times lower average density than the symmetric case.

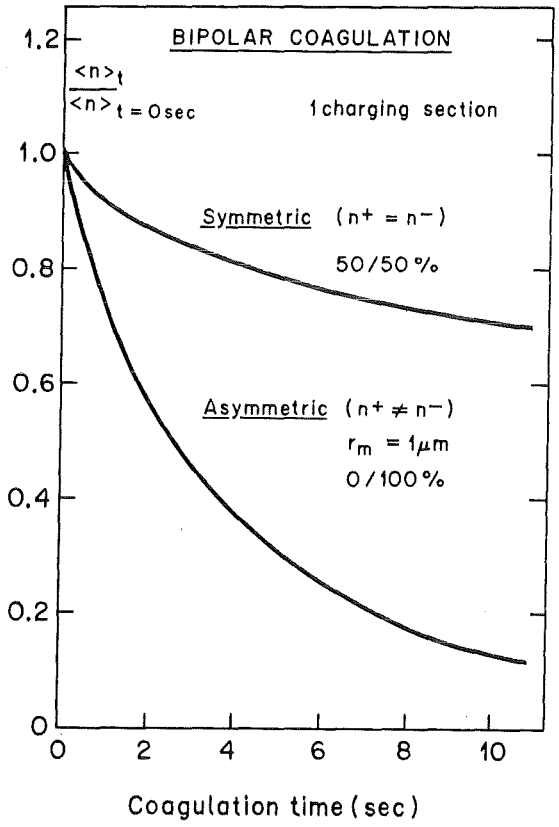

Fig. 10: The decrease in average density vs. time for the symmetric and asymmetric bipolar cases resp.

In Fig. 11 we compare the drop in average density after 10 seconds as a function of r_m. Four different curves have been plotted the parameter being the extent of asymmetry of the charging.

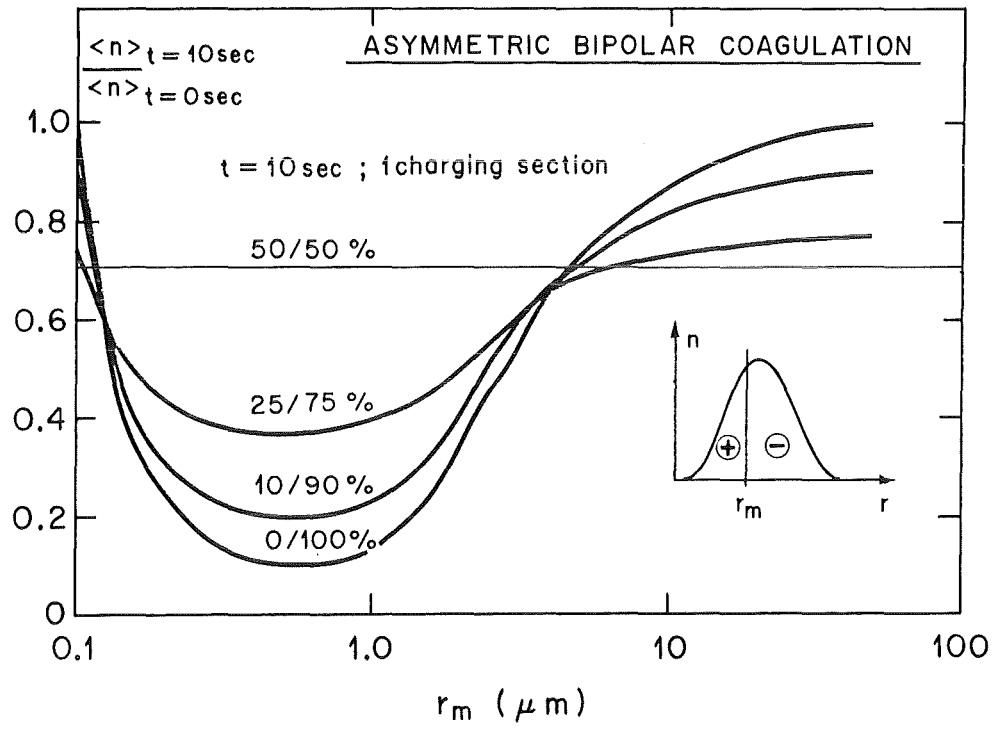

Fig. 11: The effect of the separation efficiency on the average density vs. the transition radius r_m. There is an optimum transition radius at approx. $r_m = 0.5$ μm.

For the fly ash distribution there is an optimum radius $r_m \cong 0.5$ μm. If r_m is too small or too large the results with asymmetric charging are inferior to symmetric charging. In the last figure 12 we show the results of measurements which are described in [3]. An equal mass mixture of spherical glass particles with $< r > = 6$ μm and quartz particles with $< r > = 1$ μm coagulated for

t = 4 seconds. In Fig. 12a a neutral mixture was run through the coagulator for 4 seconds. In Fig. 12b we see the result of symmetric bipolar coagulation with half of each kind with one polarity and the other halves at the other polarity. Then in Fig. 12c we see the effect of asymmetric coagulation with all glass spheres charged positive and all quartz particles charged negative. The improvement in the coagulation rate for the small particles is evident.

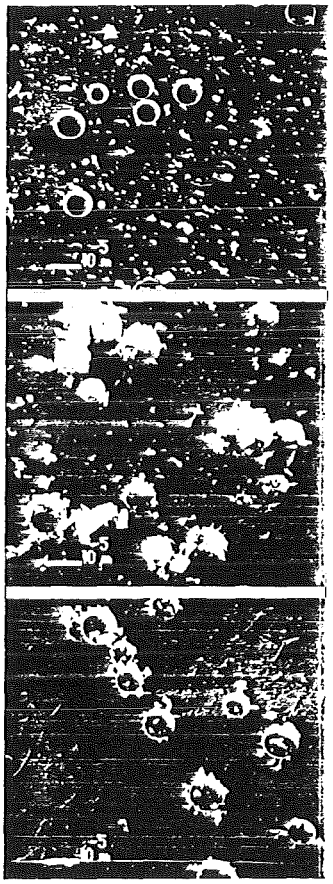

Fig. 12: Coagulation experiments with glass spheres ($< r > = 6\mu m$) and quartz particles ($< r > = 1\ \mu m$) in a single coagulation stage. The total mass was $7 g/m^3$, the coagulation time t = 4 sec. a) neutral particles, b) symmetric bipolar charging, c) asymmetric bipolar during (glass spheres positive, quartz particles negative).

CONCLUSIONS

We have shown how, at least theoretically, a fast coagulation of smaller particles with larger ones can be achieved by using asymmetric bipolar coagulation. By charging the smaller particles with one polarity and the larger ones with the opposite polarity one can shift the particle distribution to larger radii. Such a shifted particle distribution can then be separated more easily from the gas flow e.g. in an electrostatic precipitator.

ACKNOWLEDGEMENT

We would like to thank Dr. H. Jodeit for supplying the results of the coagulation measurements shown in Fig. 12.

REFERENCES

[1] B. Eliasson, W. Egli and H. Jodeit, "Coagulation of Bipolarly Charged Aerosols", Helvetica Physica Acta, 60, 1987, 859 - 866.

[2] M.V. Smoluchowski, "Drei Vorträge über Diffusion, Brownsche Molekularbewegung und Koagulation von Kolloidteilchen", Physik. Zeitschrift XVII, 1916, 557 - 99.

[3] B. Eliasson, W. Egli, J.R. Ferguson and H. Jodeit, "Coagulation of Bipolarly Charged Aerosols in a Stack Coagulator", J. Aerosol Sci, 18 (6), 1987, 869 - 72.

[4] N.A. Fuchs, "Über die Stabilität und Aufladung der Aerosole", Z. Physik, 89, 1934, 736-43.

[5] A. Russel "The Problem of Two Electrified Spheres"", Proc. Phys. Soc. London, 35, 1922, 10 - 29.

[6] G.B. Nichols et. al. "Particulate Collation Efficiency Measurements on Three Electrostatic Precipitators", EPA Report No. 600/2-75-056, October 1975.

Special Processes and Parameters in Coagulation

Chairman: K.R. Spurny

The fractal nature of agglomerates
- Review Paper -

by
A. Schmitt - Ott

"This manuscript was not made available
for printing"

COAGULATION BEHAVIOR OF NON-SPHERICAL AND OF MIXED AEROSOLS

W. Schöck, H. Bunz
Kernforschungszentrum Karlsruhe
Laboratorium für Aerosolphysik und Filtertechnik

Modelling of aerosol processes in general and of coagulation in particular always begins with the assumption that the aerosol is homogeneous and the particles are spherical. As long as these assumptions are valid predictions of aerosol behavior show good agreement with experimental observations in many cases, e.g. in a droplet aerosol [1]. However, with the exception of droplets, particles are mostly non-spherical, and aerosols are frequently inhomogeneous, i.e. composed of different species, they may be internally or externally mixed. The non-sphericity of the particles is usually taken into account by introducing correction factors, so called shape factors, into the model equations. Modelling of inhomogeneously composed aerosols can be done by different simplifying assumptions. In this article we give some examples for the present state of knowledge in these two areas of problems with respect to coagulation.

Shape factors in coagulation

A shape factor, by definition, relates a measurable property of a real particle to the theoretical property of an ideal particle. An ideal particle in this sense is always spherical and mostly has a density of 1 g/m^3. By this definiton it is also obvious that the shape factor problem only occurs when theory is involved, i.e. in aerosol behavior modelling of real aerosol systems where shape factors constitute a vast area of problems.

Relating measurable properties to properties of ideal spheres invokes immediately at least as many shape factors as there are measurement principles. For Brownian coagulation, the number of shape factors necessary to model the coagulation rates is two, at least: the dynamic shape factor κ and the coagulation shape factor f in the coagulation kernel:

$$K(r_1,r_2) = 4\pi \cdot kT \cdot f \cdot (r_1+r_2) \cdot \{B(r_1,\kappa) + B(r_2,\kappa)\} \qquad \text{Eq.(1)}$$

The dynamic shape factor κ corrects particle mobility $B(r,\kappa)$ for the influence of non-sphericity and/or porosity of the particle:

$$B(r,\kappa) = \frac{C(r)}{\kappa \cdot 6 \cdot \pi \cdot \eta \cdot r} \qquad \text{Eq.(2)}$$

κ is thus found in the equations for not only coagulation but nearly all aerosol processes. The coagulation shape factor f which accounts for the change in target size of coagulating particles is a parameter specifically introduced for coagulation.

Following the definition, shape factors have to be measured. When, as in coagulation, two shape factors simultaneously influence an aerosol process rate there are two possibilities to determine their values: either, to run through an iterative two parameter best fit procedure with a sufficiently large number of data from experiments with coagulating aerosols, or, to determine one of them (κ) by a separate measurement and then evaluate the other (f) from a direct coagulation experiment. Both methods have been used to determine the coagulation shape factor, a few examples will be given now.

Fitting to experimental data

Noticeable effects of coagulation on the overall aerosol behavior are only found in aerosols with high concentration. Up to date, the by far largest efforts to calculate the behavior of highly concentrated aerosols have been undertaken in nuclear aerosol behavior modelling. Most nuclear aerosols have high concentrations and irregular shapes, they are ideally suited for studying the effects of shape factors on aerosol behavior.

The first attempt to fit experimental data with Eq.(1) by varying κ and f was made in 1972 [2]. In Fig.1 four examples of calculated particle number concentration vs time are compared to the experimental values of an enclosed aerosol. The aerosol was generated by capacitor discharge vaporisation of a

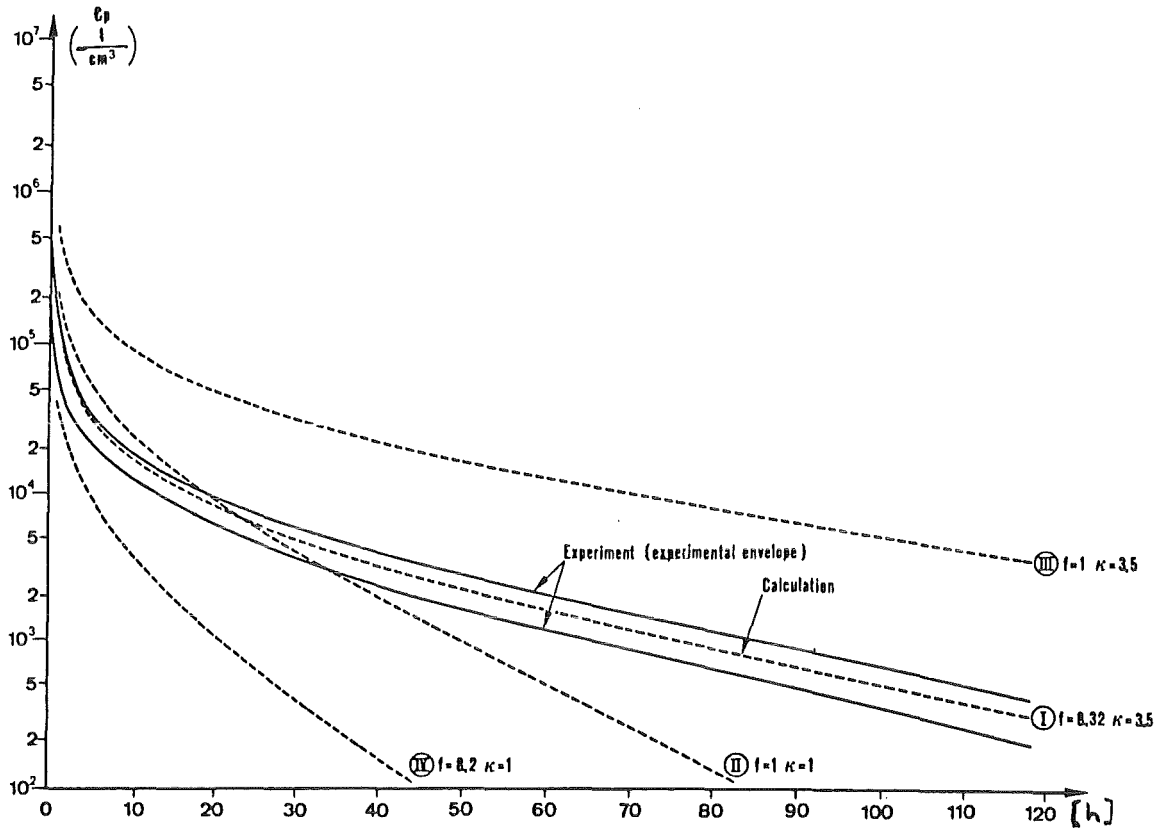

Figure 1 Particle number concentration vs time of a uranium dioxide aerosol: experiment and calculations with different sets of shape factors

UO_2-pellet, the maximum initial concentration was 20mg/m^3. The particles were fluffy aggregates composed of large numbers of very small primary particles. The authors found the best fit with the values of κ=3.5 and f=8.2.

Much higher experimental aerosol concentrations have been reached in sodium fire aerosol experiments. Fig.2 shows an example of such an experiment [3]. The peak mass concentration was 100 g/m^3 in a vessel of 850 m^3 volume. During the burning interval up to 2000 s no good agreement between experiment and calculation could be obtained, which is quite common for aerosols from fires. Thereafter, during the removal phase of the experiment, the best fit is achieved with κ=1.1 and f=1.5 ... 2 in this case. The lower values, as compared to Fig.1, reflect the fact that the sodium fire aerosol particles are more compact and composed of less and coarser primaries.

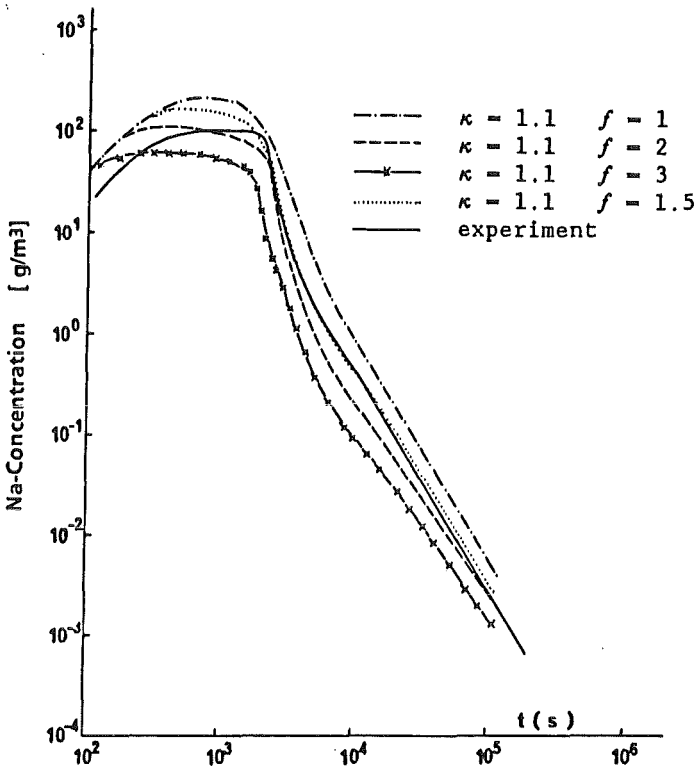

Figure 2 Mass concentration of a sodium fire aerosol: experimental data and calculations with different sets of shape factors

A systematic dependence on particle morphology can be seen as expected. For κ this dependence has been experimentally investigated by Kops [4] who developped an equation relating κ of a linear chain aggregate particle to the number n of primary particles of which the chain is composed.

$$\kappa = F(d_e) \cdot 0.3 \cdot n^{1/3}$$

where $F(d_e)$ is the Cunningham correction. Fig.3 shows the experimental results in graphic form. It has to be noted that this correlation was established only for aggregates with less than $5 \cdot 10^3$ particles. For branched chains and clusters the concept of effective density of particles proved to be more suitable, which uses the envelopping dimensions of the aggregate as the size and corrects for the aerodynamic properties by introducing an effective density of the aggregate.

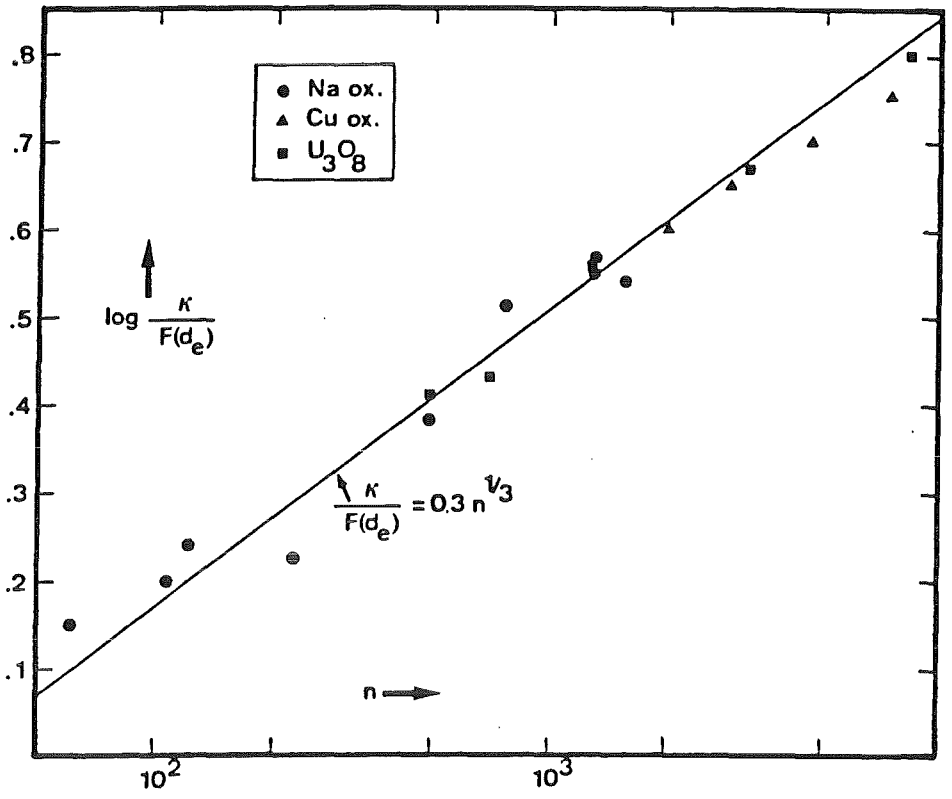

Figure 3 Correlation of shape factor κ with aggregate structure

Direct measurement of the coagulation shape factor

A more convincing method than the two parameter fitting described above is to measure the dynamic shape factor κ separately and then to do a coagulation experiment with the same aerosol to determine the coagulation shape factor f. A limited number of such time consuming experiments has been done by Zeller [5]. The dynamic shape factor was measured with a spiral centrifuge and the coagulation shape factor was evaluated from measurements of the size distibutions of fresh and aged aerosols in a coagulation tube. Coagulation tube experiments have been done earlier to measure coagulation rates [1]. A 6 m long vertical tube of the same kind was now used for the coagulation shape factor measurement, the apparatus is shown in Fig.4. Two sampling locations at the lower and upper end were used, both equipped with sampling filters SF, flow meters FM and regulating valves NV. The experiments were done with irregularly shaped particles of platinum oxide and uranium dioxide aerosols.

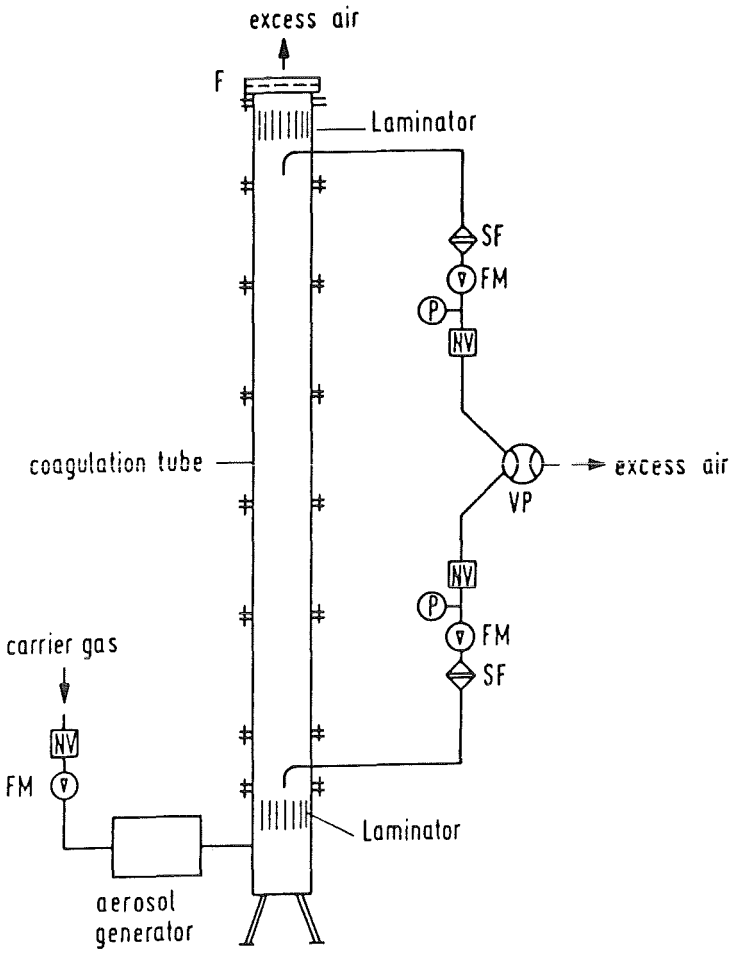

Figure 4 Coagulation tube, experimental setup

Fig.5 shows the measured values of κ as a function of particle size. Only a size averaged value of f could be determined which was f=1.8 for the platinum oxide aerosol and f=3.2 for the UO_2 aerosol.

Most interesting is that the values of the averaged dynamic shape factor and of the coagulation shape factors were approximately equal. Although (with the trivial exception of spherical particles) there is yet no convincing proof for the shape factors κ and f to be necessarily equal it appears somewhat plausible. Equal shape factors would greatly facilitate the prediction of aerosol behavior because dynamic shape factors are known in many cases or are at least much easier to measure than coagulation shape factors.

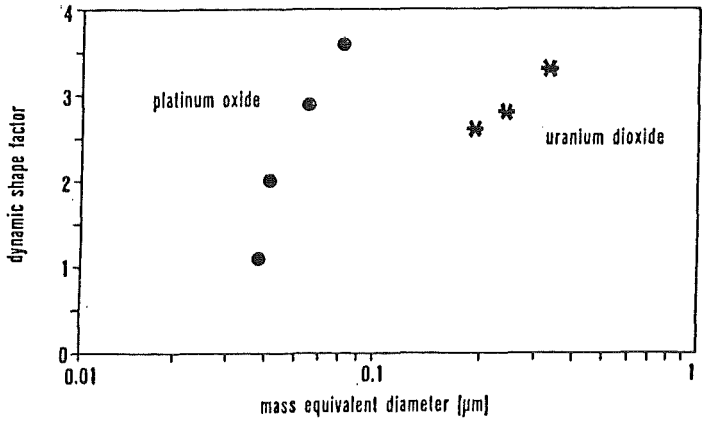

Figure 5 Experimental values of dynamic shape factor

Collision efficiency in gravitational coagulation

For gravitational coagulation the subject of discussion had been simply how to formulate the collision efficiency in the gravitational coagulation kernel. The recent theoretical work by Bunz [6] is becoming accepted now, this is described in another article in this volume and will not be discussed here. Yet, experimental work from which values of the collision efficiency could be determined to conclude this discussion finally is still missing.

Coagulation of mixed aerosols

One particular issue has been frequently discussed in connection with the behavior of highly concentrated aerosol systems, the so called coagglomeration issue. This deals with the question whether, in a mixed aerosol, coagulation processes between the components differ from coagulation of single component aerosols or not.

If one considers coagulation as a mechanical aerosol process there is no reason to believe that coagulation should be selective with respect to the particle material or composition. This means that by coagulation an aerosol which is initially externally mixed should be converted to an internally mixed aerosol. The final state of a homogeneous internally mixed aerosol should be reached sooner or later, depending only on coagulation rates and time.

On the other hand, experimental observations have been made which, on the first glance, seem to show the existence of persisting components which might not have taken part in the overall coagulation process. Fig.6 shows an example. The figure shows the measured mass concentrations vs time of an enclosed two-component aerosol consisting of a fine MnO and a coarse CsOH fractions which were generated in separate generators and during separate overlapping time intervals [7]. It is seen that the mass concentration vs time functions of the two fractions are not identical at late stages of the experiment. The MnO fraction remains airborne longer than the CsOH fraction.

This experimental result is of course not questioned. The subject of discussion is only whether the observed behavior is conflicting with the

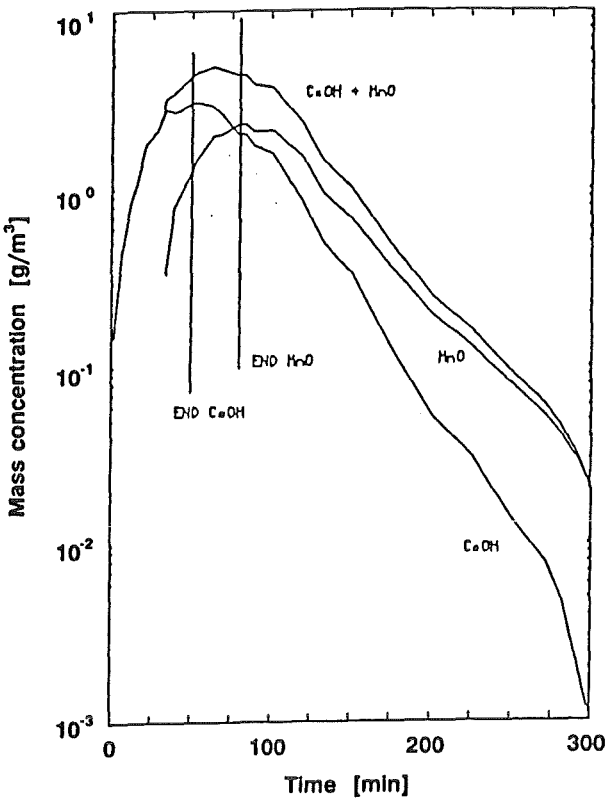

Figure 6 Time dependent behavior of a mixed aerosol of MnO and CsOH

existing coagulation theory and whether a 'persisting' MnO fraction existed which did not participate in the coagulation process for any reason. We will show qualitatively now that this is not the case and that the behavior shown in Fig.6 is in agreement with the assumption of non-selective coagulation among any components of a mixed aerosol.

A series of calculations was made with a modified version of the aerosol behavior code NAUA [8] which was able to track the components of a two-component aerosol.

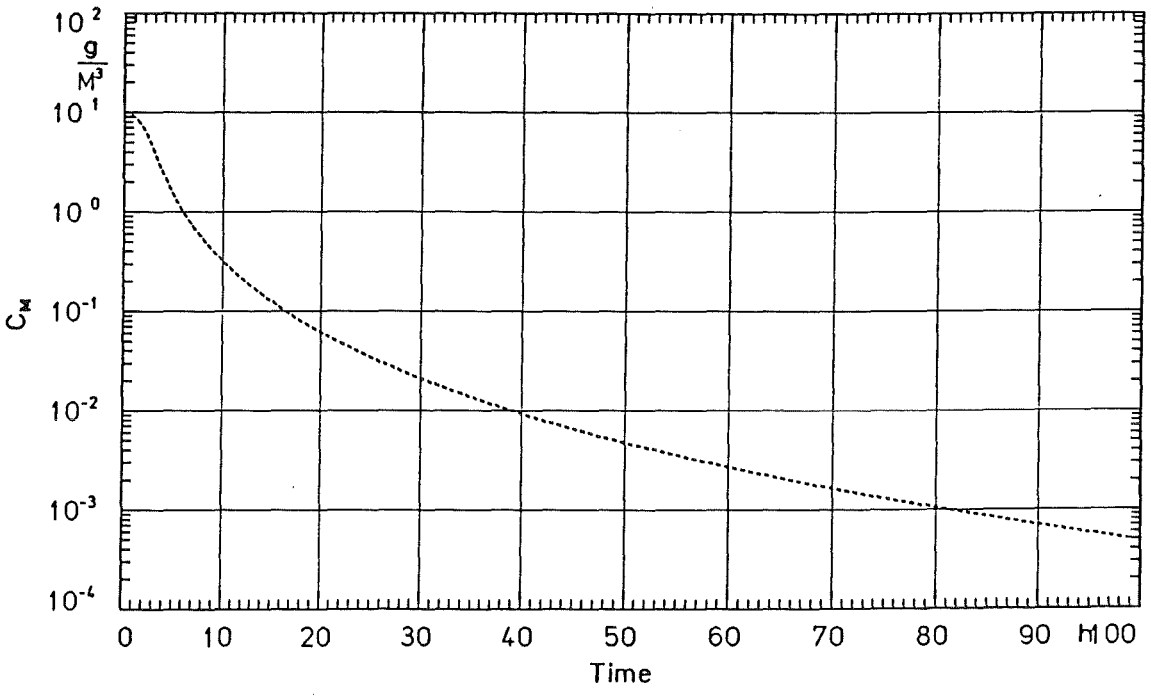

Figure 7 Behavior of a coagulating aerosol fine component only

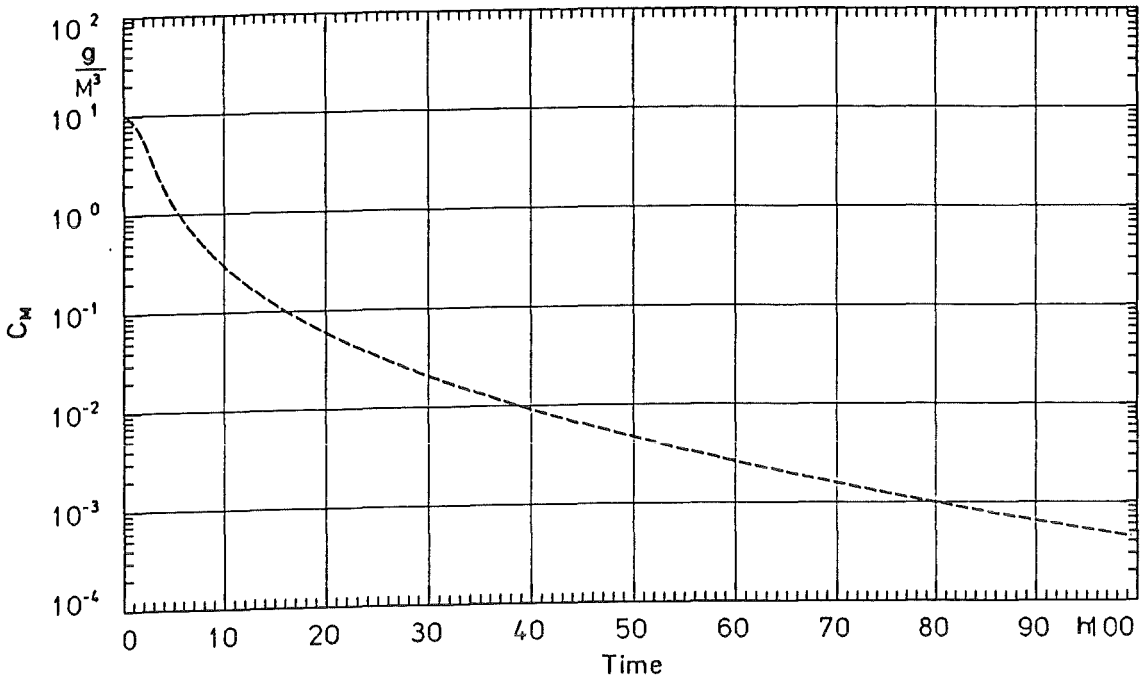

Figure 8 Behavior of a coagulating aerosol coarse component only

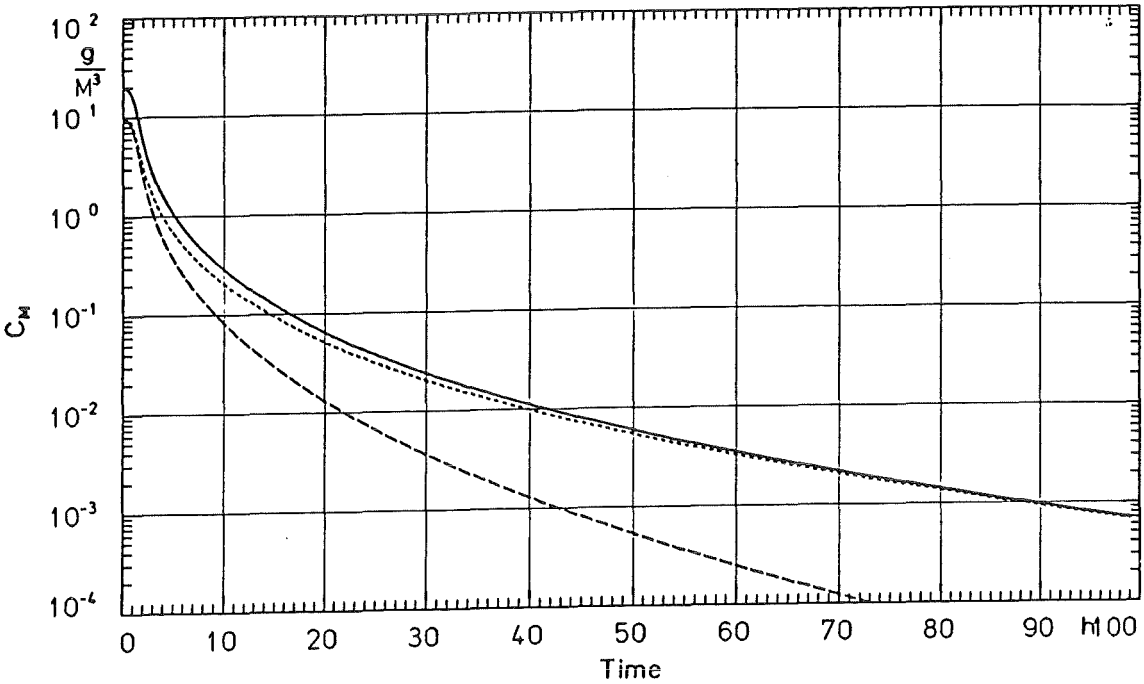

Figure 9 Behavior of a coagulating mixed aerosol with equal masses of fine (·····) and coarse (----) components, (——) = total aerosol

For these calculations the following assumption was made. Within a size class the composition of individual particles is not followed. Instead all particles in a size class are assumed to be equally composed. The composition may, however, change with size and with time. This simplifying assumption, of course, anticipates that no differences in coagulation behavior exist between particles of equal size but different composition, i.e. coagulation does not depend on composition but only on size distribution and concentration.

The calculations were done for a two component aerosol in an arbitrary cubic enclosure with a volume of 1000 m^3. In order to understand the difference, the behavior of a homogeneous aerosol has to be discussed first. In Fig.7 the mass concentration vs time is shown for a fine aerosol with an initial median diameter of 0.2 μm. Fig.8 shows the same for an initially coarse aerosol with 2 μm diameter. The initial mass concentration was 10 g/m^3 in both cases to assure strong coagulation effects. The curves in the two figures are practically indentical, the same is true (after a short time) for the size distributions which are not shown here. This is a well known property of highly concentrated aerosols in enclosures: an enclosed coagulating aerosol, after long enough time, asymptotically assumes a state which is independent of the initial state. 'After long enough time' depends on the coagulation rate, the higher the coagulation rate the sooner the asymptotic state will be reached. The curves in Figs.7 or 8 can be regarded as an upper envelope for any aerosol in that particular vessel, aerosol concentrations in that vessel can only be lower but not higher than the envelope values.

Now, in a third calculation, these two aerosols were mixed together and the partial concentrations of the two species are shown in Fig.9. Indeed, after some time the two concentrations are diverging as in Fig.6. But the important result is that the fine component is not persisting more than in the case when it is alone (Fig.7), in fact the curves for the fine component are identical in Figs.7 and 9. Instead the removal rate of the coarse species is enhanced by the presence of the fine species as compared to Fig.8.

Keeping in mind the fundamentals of coagulation this finding is not surprising. The coagulations rates in a bimodal aerosol, as was used here, are always much larger between the two modes than within both of the modes. Also

the product of a single coagulation between a fine and a coarse particle will be a coarse particle, larger than the initial coarse particle. Consequently at the beginning the fine particles are moved into the coarse mode making the coarse mode still coarser and increasing the sedimentation rate of the coarse mode. This effect is quite analogous to the wash-out effect by condensation. This means that the coarse mode disappears more quickly from the airborne state in the presence of a fine particle fraction than without that. The overall concentration of the aerosol follows the envelope function of the vessel, and since the coarse fraction has disappeared faster, the fine fraction's concentration approaches the envelope function asymptotically.

This explains the behavior of the two fractions in Fig.6 and in Fig.9 as well. The quick conclusion that the fine component may persist due to incomplete coagulation is proved to be not true. Instead, coagulation does not change the long term behavior of the fine component at all, but rather enhances the removal of the other component. The overall effect in a mixed aerosol is thus positive: while the fine fraction's behavior is not changed the coarse fraction is removed faster.

References

[1] P.E. Wagner, Brownian coagulation of aerosols in rarefied gases, J. Chem. Phys. 66, pp 638-646 (1977)

[2] H. Jordan, W. Schikarski, H. Wild, Nukleare Aerosole im geschlossenen System, KfK 1989 (1974)

[3] R. Jonas, Consideration of turbulent deposition in aerosol behaviour, KfK 4431 (1988)

[4] J.A.M.M. Kops, The aerodynamic diameter and specific surface area of branched chain-like aggregates, Thesis, University of Eindhoven (1976)

[5] W. Zeller, Direct measurement of aerosol shape factors, Aerosol Science and Technology 4, 45 (1985)

[6] H. Bunz, Physical and mathematical modelling of gravitational coagulation, this volume

[7] J.D. McCormack, R.K. Hilliard, J.M. Salgado, Final report of experimental results of LACE test LA4 - Late containment failure, LACE report TR-025 (1988)

[8] H. Bunz, M. Koyro, W. Schöck, NAUA Mod5 und Mod5-M zwei Computer-programme zur Berechnung des Aerosolverhaltens im Containmentsystem eines LWR nach einem Kernschmelzunfall, KfK 4278 (1987)

Application of Coagulation in Sciences and Technology

Chairman: H. Fissan

THE ROLE OF COAGULATION IN AEROSOL FORMATION TECHNOLOGY

Presentation at the
GAeF Workshop on Coagulation
March 16-18, 1988
KfK, Karlsruhe, West Germany

Sotiris E. Pratsinis

Department of Chemical and Nuclear Engineering
Center for Aerosol Processes
University of Cincinnati
Cincinnati, OH 45221-0171

May, 1988

INTRODUCTION

Aerosol technology is attractive for manufacture of particulate commodities (carbon blacks and pigments) and materials for high technology applications such as optical waveguides and advanced ceramics (Ulrich, 1984).

Aerosol processes do not require the several tedious operations and high liquid volumes of wet chemistry. Thus, the 'chloride' process has gradually substituted the 'sulfate' process in industrial scale manufacture of titania pigments (Solomon and Hawthorne, 1983). Aerosol processes can be used for production of highly pure materials. Hence, in lightguide fabrication technology aerosol ('vapor' deposition) processes phased out the double crucible process for manufacture of low loss fibers for telecommunications (Nagel et al., 1982; Kim and Pratsinis, 1988). Reactant mixing is achieved in much shorter time scales in aerosol than in wet chemistry processes. Aerosol processes are also energy efficient operations for manufacture of particulates. A typical example is the production of silicon for photovoltaic applications in which the power consumption per unit silicon mass can be an order of magnitude lower in an aerosol reactor than in the classic Siemens process (Alam and Flagan, 1986).

The focus of traditional aerosol science has been on the environmental impact of aerosols. Its goal has been to understand the physicochemical phenomena controlling the behavior of rather dilute suspensions in processes involving relatively long residence times. In contrast, the technology of aerosol formation aims in generation of extremely high particle concentrations at short process residence times. As a result, coagulation plays a key role in determining the characteristics of the product particles and the overall process yield.

This presentation reviews the role of coagulation in manufacture of

optical waveguides, ceramic powders and carbon blacks. Emphasis is placed on experimental and theoretical studies of current or potential aerosol formation technologies.

CARBON BLACKS

Carbon blacks are the oldest manufactured aerosols. Carbon blacks are made primarily by the oil furnace process. According to this process, an aromatic residual oil ("feedstock") is sprayed into a hot gas-air flame in a furnace where carbon black is formed as soot. The flue gas is rapidly quenched and the soot is collected by electrostatic precipitators, cyclones and bag house filters (Medalia and Rivin, 1976).

The control of particle size and size distribution of carbon blacks and the environmental implications (toxicity and visibility reduction) of released soot motivate the research of soot formation and growth. Although substantial progress has been made in understanding the fundamentals of fuel lean flames, the mechanism of soot formation in fuel rich flames such as those encountered in manufacture of carbon blacks has not been elucidated (Homann, 1984).

Studies of soot formation in laminar diffusion flames are especially important since these flames retain some of the key features (e.g. reactant mixing) of industrial processes for manufacture of carbon blacks. During hydrocarbon oxidation in laminar diffusion flames, soot particles are formed (incepted) by cyclization reactions at the fuel rich side of the flame. The soot particles grow by coagulation and surface reactions (material addition from the gas phase) and the total soot particle concentration decreases as its mass increases. At the end of the flame, the soot is depleted by oxidation but the flame temperature is rapidly reduced (quenched) and, thus, soot particles are produced. At the later part of the flame the total soot mass

certainly decreases while the total particle concentration may either remain intact when oxidation takes place at the soot particle surface (e.g. by OH radicals) or increase when O_2 diffuses into and disintegrates the particles (Santoro and Miller, 1987).

Soot particles are characterized by in situ laser scattering/extinction dissymmetry (D'Alessio et al., 1974), thermophoretic (Dobbins and Megaridis, 1987), fluorescence (Santoro and Semerjian, 1984) and microscopic analyses (Medalia and Heckman, 1969; Wersborg et al., 1972). Laser measurements of soot concentration and size are popular since they are nonintrusive and can be rapidly made though an assumption must be made for the shape of the soot size distribution to facilitate inversion of the optical data. Nevertheless, particle concentrations as high as 10^{13} particles/cm^3 and sizes down to 50 $\mathring{A}$ have been measured by lazer techniques.

Understanding the evolution of the soot size distribution as a function of time is important for proper inversion of light scattering/extinction data and for unraveling the effect of process variables (feedstock and oxidant flowrates) on the characteristics of carbon blacks. Wersborg et al. (1972) modeled soot generation in premixed flames in terms of nucleation, condensation and coagulation treating the soot particles as spheres of uniform size. This model was in good agreement with their data on soot from acetylene-oxygen flames when the coagulation rate was enhanced by a factor of 30. This enhancement was attributed to interparticle van der Waals forces.

Dobbins and Mulholland (1984) modeled particle formation and coagulation in the free molecule regime in terms of the leading moments of the soot size distribution which was approximated by a lognormal function. They found that solutions to the soot population balance equation in which monodisperse or fixed width distributions were used, resulted in distorted particle

concentrations along the flame axis. Megaridis and Dobbins (1988) extended this model to bimodal distributions and accounted for surface growth reactions. Their results were in qualitative agreement with experimental studies of soot formation in premixed toluene/ethylene flames. Pratsinis (1988) developed a model for particle inception, condensation (surface growth) and coagulation in the free molecule and continuum regimes approximating the aerosol size distribution by a unimodal lognormal function. He found that when surface growth and coagulation simultaneously take place the polydispersity of the product aerosol is lower than that obtained when only coagulation takes place.

Frenklach (1985) and Frenklach and Harris (1987) also developed moment models for soot aerosol dynamics. They achieved closure of the moment equations by a series of approximations on the coagulation and condensation (surface growth) kernels without assigning a specific shape (self preserving or lognormal) to the soot size distribution. Frenklach et al. (1984) developed a detailed kinetic model predicting the inception rate of soot particles. The moment models of Frenklach and Harris (1987) were in good agreement with the model of Harris et al. (1986). The latter model numerically solves the complete discrete population balance equation for 10,000 particle sizes. Although this is a brute force approach, its results are free of numerical artifacts arising from approximations of the shape of the soot size distribution. Of course, the major limitation of this model is its excessive computer time requirements: simulations of soot dynamics for 2 ms require 60 CPU minutes in a CRAY computer (Frenklach and Harris, 1987). As a result, this model is best suitable for the early stages of soot formation where there is substantial uncertainty on the distribution shape.

Kennedy (1984) modeled free molecular soot dynamics in stagnation point

diffusion flames utilizing a sectional representation of the aerosol size distribution (similar to the model by Gelbard and Seinfeld, 1979). Using the fuel atom fraction, he calculated the flame temperature and species composition profiles without resorting to computation of the detailed flame kinetics. Kennedy (1984) found that the calculated soot size distribution attained its self preserving form away from the flame front.

More recently the application of fractal theory is actively explored in modeling soot formation and growth. Samson et al. (1987) found that an agglomeration model for fractal growth reproduces more closely the measured soot particle images than a diffusion limited aggregation model.

All models of soot dynamics employ the kinetic theory for coagulation and surface growth. There has been strong emphasis on the shape of soot size distribution from both measurement and modeling points of view. Moment models provide consistent results with the current understanding of soot generation at reasonable computational speed at the expense of accuracy. The popularity of these models is justified since the approximations of the shape of the aerosol size distribution are insignificant compared to the ones associated with the estimation of soot inception rates, intermolecular forces, ionic effects and particle shape effects. Quantitative estimates for these phenomena are either obtained by comparison of model predictions with experimental data or simply neglected.

CERAMIC POWDERS

Ceramic powders of submicron size are used to make pigments, catalytic substrates, silicone rubbers, semiconductors, superconductors and other advanced ceramics. These powders are made by aerosol processes in flames, shock tubes, lazer beams, plasmas, furnaces, condensers-hydrolyzers and by expansion of supercritical solutions.

In flame reactors particles are formed by chemical reactions from their precursor vapors in open flames. Usually small amounts of fuel (e.g. CH_4) are present in the feed to sustain the reaction. Production of rutile (TiO_2) by oxidation of $TiCl_4$ in flame reactors (the "chloride process") is one of the largest manufacturing aerosol processes. George et al.(1973) investigated titania production in a premixed laminar flame reactor. They found that titania grew by coagulation to spherical particles having a self preserving size distribution.

Ulrich and his colleagues (1971, 1976, 1977, 1982) extensively studied silica formation in laminar premixed and turbulent jet flame reactors. The silica was produced in aggregates of spherical primary particles. They suggested that the anomalous high viscosity of silica made fusion the controlling growth mechanism for primary particles and collision the controlling growth mechanism for silica aggregates. They employed sampling and microscopic analyses as well as in situ lazer characterization of the silica aggregates. They developed a sectional model for simulation of the silica aggregate aerosol dynamics in the free molecule and continuum regimes. Utilizing the initial surface area and temperature drop as adjustable parameters, they obtained good agreement between their theory and data. They accounted for the irregular shape of the silica aggregates by enhancing the collision rate in the free molecule regime by 20% (bulkiness

factor, 1.2) based on the observations of Medalia and Heckman (1969).

Nishida et al. (1987 a,b) and Bolsaitis et al. (1987) independently prepared ultrafine ($0.01 < d_p < 0.5$ μm) oxide powders by oxidation of metallic vapors. They used electric furnaces to generate high purity Mg and Zn vapors. Oxide powders were formed by injecting the metal vapors through a nozzle into the oxidation region of the furnace. Bolsaitis et al. (1987) simulated ZnO powder production by the above process using the aerosol dynamics model of Gelbard and Seinfeld (1979). They found, however, substantial disagreement between the computed ZnO particle size distributions and the measured ones by an electrical aerosol analyzer. This was attributed to the irregular (chainlike) shape of the ZnO powders.

In furnace reactors, particles are formed by chemical reactions of precursor gases in externally heated reaction vessels. Eversteijn (1971) used these reactors to study the onset of silicon particle formation ("snow formation") during chemical vapor deposition of thin silicon films in epitaxial reactors. Suyama and Kato (1976 and 1985) studied TiO_2 production by $TiCl_4$ oxidation in vertical and horizontal furnaces. They found by a series of microscopic and x-ray diffraction analyses that low concentrations of dopants (as low as 2% of inlet $TiCl_4$) have a pronounced effect on the crystallinity and size distribution of the product powder. This is an important result for industrial scale production of TiO_2 where dopants such as $AlCl_3$ and $SiCl_4$ are used for manufacture of rutile and anatase particles, respectively (Mezey, 1966). Silicon nitride powders have been also made by gas phase reaction between NH_3 and SiH_4 in furnace reactors by Prochaska and Greskovich (1978). They found that reactant stoichiometry and reactor temperature determined the color and crystallization temperature of the product powder.

Lay and Iya (1981) developed a furnace reactor ('free space reactor') to make silicon particles by thermal decomposition of SiH_4 for low cost production of silicon for photovoltaic applications. Alam and Flagan (1986), Wu and Flagan (1987) and Wu et al.(1987) generated Si particles up to 10μm in size by thermally regulated SiH_4 decomposition and controlled Si nucleation and growth in two furnace aerosol reactors in series. They monitored product size distributions by conventional aerosol characterization instruments (optical particle counter, consensation nuclei counter and electrical aerosol analyzer) as well as microscopic (SEM and TEM) and x-ray diffraction analyses. By comparing reactor residence times to the characteristic collision times of the Si particles (seeds) from the first reactor with the newly formed molecular Si clusters in the second reactor, Wu and Flagan (1987) concluded that silicon growth took place by seed-cluster coagulation.

Thermal decomposition of organometallic vapors in furnace reactors was investigated for production of ultrafine powders ($d_p < 0.01\mu m$) by Mazdiyasni et al. (1965) in mixed flows, and by Komiyama et al.(1985) and Okuyama et al.(1986) in premixed laminar flows. Okuyama et al.(1986) investigated production of Al_2O_3, TiO_2 and SiO_2 particles by thermal decomposition of their organometallic (alkoxide) vapors in a furnace reactor. They measured the size, shape and composition characteristics of the product powders by real time aerosol instruments and microscopic/diffraction analyses at various reactor temperatures and inlet alkoxide vapor concentrations. Since in most experiments the decomposition reaction had not been completed in their furnace, the product particles were fine ($0.006 < d_p < 0.15$ μm) and had broad size distributions ($\sigma = 1.3 - 2$). They simulated their experiments using the computational scheme of Gelbard and Seinfeld (1979) by assuming plug flow in

the reactor and coagulation controlled particle growth. Fair agreement was obtained between theory and experiment when most of the inlet alkoxide vapor had been converted to oxide powder.

Nonoxide powders such as SiC, Si_3N_4 and Si have been made by heating precursor gases with a gas laser (Cannon et al., 1982; Flint et al., 1986). This process achieves complete reactant mixing, reduces reactor wall deposits and results in high purity powders with fairly narrow size distribution since it confines the reaction to a small region where high temperatures and sort residence times prevail. Knudsen (1987) at DOW has prepared ultrafine ($0.01 < d_p < 0.1$ μm), equiaxed, loosely agglomerated B_4C powders by CO_2 laser-driven pyrolysis of $BCl_3/H_2/CH_4$ mixtures. Flint et al. (1986) determined particle size and concentration by real time, nonintrusive laser scattering/extinction measurements (D'Alessio et al., 1974). They observed the particle concentration to decrease as a function of process residence time. This was attributed to a change of the Si refractive index or coagulation of newly formed Si or SiC particles. Knudsen (1987) and Flint et al.(1986) proposed nucleation and growth as the mechanisms for B_4C , Si and SiC particle growth. Rice (1987) at Exxon developed a 6-way cross lazer reactor for manufacture of SiC/Si_3N_4 and TiO_2 powders from organometallic precursor vapors. Fairly polydisperse powders with significant neck formation were produced in his reactor. By controlling the reactant gas composition it was possible to control reaction temperature and powder stoichiometry and crystallinity.

In plasma reactors, particles are formed by heating the reactant gases and promoting erdothermic reactions by an electric plasma. Young and Pfender (1985) reviewed generation of ceramic particles ($0.001 < d_p < 100$ μm) in a variety of plasma reactors during the last 40 years. Although temperature and

residence time distributions are well understood, very little is known about particle formation and growth in plasmas. A variety of carbide, nitride and boride powders has been produced in RF plasmas (Vogt et al., 1987). Precursor material can be fed in plasmas even in solid state. Recently, industry is actively involved in developing plasmas for ceramic powder production and processing (Smith et al., 1987; Sheppard, 1987). Particle production in plasmas is carried out empirically since particle size, composition and crystallinity are usually controlled by trial and error procedures. Recently Gershick et al. (1988) modeled particle production in RF plasmas by coagulation in one dimensional (plug) flow at constant cooling rate using the computational scheme of Gelbard and Seinfeld (1979). They simulated production of iron particles and found that the mean particle diameter was proportional to inlet iron vapor mole fraction and inversely proportional to plasma cooling rate. These computations were in fair agreement with the data of Yoshida and Akashi (1981) and followed observations of other particle generation studies with RF plasmas (Sheppard, 1987).

OPTICAL FIBERS

Aerosol processes are unique for production of materials with high purity. This is an attractive feature in lightguide fabrication technology. Optical fibers are made by a series of processes: fabrication of a preform glass rod by silica (and dopant) particle deposition, rod sintering, fiber drawing and coating (Rowell, 1986). The key process, with respect to composition and purity of the product fiber, is the fabrication of the preform rod. The goal of this process is to make a preform rod having a prescribed radial distribution of refractive index at the maximum process yield.

Preforms are made by external and internal particle deposition

processes. The outside vapor deposition (OVD) and vapor-phase axial deposition (VAD) processes are the external processes. They involve deposition of vapor and particles onto horizontal or vertical substrates from combustion of $SiCl_4$, $GeCl_4$ and other precursor gases. Glass particles are formed at the combustion zone of the gas burner and deposit as aggregates on the surface of the substrate (glass boule). Miller et al.(1987) concluded that during OVD or VAD particle deposition at the substrate takes place by thermophoresis. The flame generated particles are too large for molecular diffusion and too small for impaction to be important. Rosner and Park (1988) investigated the external processes for preform fabrication by analyzing transport of hot aerosols around cold wedges. They found that the particle deposition rate onto the wedge is higher than that predicted by classic thermophoretic calculations because high mass loadings of particles modify the gas stream velocity and temperature by an effect similar to 'massive suction' in single phase laminar boundary layer flows. Both Brownian and shear induced coagulation have a pronounced effect on the size distribution of the silica deposits (Park and Rosner, 1987).

Modified chemical vapor deposition (MCVD) and plasma chemical vapor deposition (PCVD) constitude the internal processes for preform manufacture. According to these processes, O_2, $SiCl_4$ and dopant vapors flow through a rotating quartz tube that is externally heated by a slowly, axially traversing, oxyhydrogen torch (or plasma). Inside the tube, the reactant gases are oxidized forming particles that either deposit to the tube walls or exit the tube with the process gases. Aside from oxidizing the reactants, the heat from the traversing torch also fuses the deposited particles forming a glassy layer in the interior of the substrate tube (Nagel et al.,1982).

MacChesney et al.(1974) invented the MCVD process for fabrication of

lightguide preforms. Thermophoresis is the dominant mass transport mechanism as it has been proven experimentally by Simpkins et al.(1979) and theoretically by Walker et al.(1979 and 1980). Rapid coagulation of the freshly formed oxide clusters in the torch area of the preform reduces the importance of Brownian diffusion in favor of thermophoresis (Pratsinis and Kim, 1989). Morse and Cipolla (1984) found that the deposition efficiency (process yield) in MCVD can be substantially improved by increasing and maintaining the temperature gradient inside the preform tube by axial lazer heating of the process gases. Kim and Pratsinis (1988) developed a detailed model of the MCVD process accounting for both gas phase kinetics and silica aerosol dynamics along the preform tube. They identified process conditions in which the MCVD deposition efficiency is limited by either mass transfer or chemical reaction.

A major challenge in multicomponent MCVD is to understand the relationship between glass particle size composition and process conditions. This is important because it has been observed that during sintering of the multicomponent particulate deposits small particles lose GeO_2 far more rapidly than large particles. The above relationship is also important for improvement of the current low process yields (~50%). As the fiber optics market becomes tighter this can be a critical issue from both economical and environmental viewpoints (especially for some of the toxic dopants).

CONCLUDING REMARKS

Aerosol processes are frequently utilized for manufacture of particulates with high purity, chemical homogeneity, small and uniform particle size and shape. Particulate commodities such as pigments and carbon blacks as well as materials for high technology applications such as optical fibers and advanced

ceramics are currently made by aerosol processes on an industrial scale. Specific product requirements and engineering innovation has led to the development of a multitude of aerosol processes for material manufacture.

Historically aerosol processes phased out wet chemistry processes in industrial scale particulate operations. Typical examples are the dominance of the 'chloride' over the 'sulfate' process for manufacture of pigmentary titania and the success of dry scrubbing over the wet scrubbing processes for removal of pollutants from flue gases. The same trend is expected to develop for manufacture of ceramic powders that are currently made by sol-gel processes. There is a wide range of progress stages for production of ceramic powders by aerosol processes. Production of titania and silica powders by flame reactors is a well established industrial aerosol operation. On the other hand, production of non-oxide powders (carbides, borides and nitrides) by aerosol processes is at its developmental stage. Various systems such as plasmas, lazers, expansion of supercritical solutions are currently explored. Research in this area aims in inventing new processes for production of powders with specific characteristics and in understanding the fundamentals of existing processes for better monitoring and control of powder production. Invention of real time aerosol instruments and construction of comprehensive models for powder production constitute the key goals of this research.

Aerosol processes constitute one of the key operations in manufacture of optical waveguides. They determine the overall process yield and the distribution of refractive index across the fiber. There is good understanding of the physicochemical phenomena taking place during preform fabrication. Research in this area aims in developing quantitative models and control instruments for optimal operation of existing industrial units and

design of new highly efficient ones.

A paucity of general correlations between process variables and particulate characteristics, places serious limitations to the development, design, scale up and control of industrial aerosol operations. One of the encountered difficulties is the lack of standard instruments for real time particulate measurements. Conventional aerosol instruments such as electrical aerosol analyzers and optical particle counters find limited application in monitoring particulate production on an industrial scale. These instruments require high dilution and transport of the sample away from its environment for measurement at room temperature.

Basic studies of soot formation in flames have led to the invention of nonintrusive optical techniques for real time characterization of highly concentrated aerosols. These techniques are already used in laboratory studies for production of ceramic powders and have high potential to be used for monitoring industrial aerosol production. Research is needed to characterize generation of irregular particulates and to trace the early stages of particle formation by these instruments.

Formation of particulates is described by moment, sectional and detailed solutions of the population balance equation. The results of these calculations serve two purposes. First, they relate process variables to particulate characteristics and second they are used to extract particulate size distributions from light scattering and extinction data. All models seem to perform reasonably well at least with respect to integral properties of the size distribution. Poor knowledge of specific physical phenomena (e.g. particle inception rates, van der Waals forces etc.) does not allow, however, precise model predictions from first principles. Quantitative estimates for these phenomena are usually obtained by fitting model calculations with

experimental data.

Coagulation is one of the most important physicochemical phenomena in industrial aerosol processes. Advances in experimental techniques and theoretical schemes (Euclidean or fractal) for studying coagulation of highly concentrated aerosols with non-spherical particle shape will greatly benefit the emerging aerosol formation technology.

REFERENCES

Alam, M.K., Flagan, R.C., Aerosol Sci. Technol. 5, 237 (1986).

Bolsaitis, P.P., McCarthy, J.F., Mohiuddin, G., Elliot, J.F., Aerosol Sci. Technol. 6, 225 (1987).

Cannon, W.R., Danforth, S.C., Flint, J.H. Haggerty, J.S., Marra, R.A., J. Amer. ceram. Soc. 65, 324 (1982).

D'Allesio, A., Di Lorenzo, A., Sarofim, A.F., Beretta, F., Masi, S., Venitozzi, C. 15th Symp. (Int.) on Combustion, 1427 (1974).

Dobbins, R.A., Mulholland, G.W. Combust. Sci. Technol. 40, 175 (1984).

Dobbins, R.A., Megaridis, C.M. Langmuir 3, 254 (1987).

Flint, J.H., Marra, R.A., Haggerty, J.S. Aerosol Sci. Technol. 5, 249 (1986).

Frenklach, M., Harris, S.J. J. Colloid Interface Sci. 118, 252 (1987).

Frenklach, M. J. Colloid Interface Sci. 108, 237 (1985).

Frenklach, M., Clary, D.W., Gardiner, Jr., W.C., Stein, S.E. 20th Symp. (Int.) in Combustion, 887 (1984).

Gelbard, F., Seinfeld, J.H. J. Colloid Interface Sci. 68, 363 (1979).

George, A.P., Murley, R.D., Place, E.R. Faraday Symposia 7, 63 (1973).

Girshick, S.L., Chiu, C.-P., McMurry, P.H. Plasma Chem. Plasma Process. 8 in press (1988).

Harris, S.J., Weiner, A.M., Ashcraft, C.C. Combust. Flame 64, 65 (1986).

Homann, K.H. 20th Symp. (Int.) on Combustion, 857 (1984).

Kennedy, I.M. 20th Symp. (Int.) on Combustion, 1095 (1984).

Kim, I.M., Pratsinis, S.E. AIChE J. 34, June (1988).

Knudsen, A.K. in Ceramic Powder Science (Adv. in Ceramics) 21, 237 (1987).

Komiyama, H., Kanai, T., Inoue, H. Chem. Lett. 1283 (1984).

Lay, J.R., Iya, S.K. 15th IEEE Photovoltaic Specialists Conference, 565 (1981).

MacChesney, J.B., O'Connor, P.B. and Presby, H.M. Proc. IEEE 62, 1278 (1974).

Mazdiyasni, K.S., Lynch, C.T., Smith, J.S. J. Amer. Ceram. Soc. 48, 372 (1965).

Medalia, A.I., Rivin, D., in Characterization of Powder Surfaces, (Parfitt, G.D., Sing, K.S.W) Academic, London, 1976.

Medalia, A.I., Heckman, F.A. Carbon 7, 567 (1969).

Megaridis, C.M., Dobbins, R.A. Combust. Sci. Technol. in press (1988).

Mezey, E.J., in Vapor Deposition (Powell, C.F., Oxley, J.H., Bocher, Jr. J.M. eds), Wiley New York, 1966.

Miller, T.J., Potkay, E., Yuen, M.J. AIChE Symp. Series 83(258), 1 (1987).

Morse, T.F. and Cipolla, J.W. J. Colloid Interface Sci. 97, 137 (1984).

Nagel, S.R., MacChesney, J.B., Walker, K.L. IEEE J. Quant. Elec. QE-18, 459 (1982).

Nishida, A., Veki, A., Yoshida, K. Ceramic Powder Science (Advances in Ceramics) 21, 265 (1987a).

Nishida, A., Yoshida, K., Igaroshi, H., Kobayashi, W. Ceramic Powder Science (Advances in Ceramics) 21, 271 (1987b).

Okuyama, K., Kousaka Y., Tohge N., Yamamoto, S., Wu, J.J., Flagan, R.C., Seinfeld, J.H. AIChE J. 32, 2010 (1986)

Park, H.M., Rosner, D.E. Chem. Eng. Sci. submitted for publication (1987).

Pratsinis, S.E., Kim, K.-S. J. Aerosol Sci. 20 (2), in press (1989).

Pratsinis, S.E. J. Colloid Interface Sci. in press (1988).

Prochazka, S., Greskovich, C. Amer. Ceram. Soc. Bull. 57, 579 (1978).

Rice, G.W. Ceramic Powder Science (Advances in Ceramics) 21, 229 (1987).

Rosner, D.E., Park, H.M. Chem. Eng. Sci., in press, 1988.

Rowell, J.M. Scientific American, October, 147 (1986).

Samson, R.J., Mulholland, G.W., Gentry, J.W. Lanmuir 3, 272 (1987).

Santoro, R.J., Semerjian, H.G., Dobbins, R.A. Combust. Flame 51, 203 (1983)

Santoro, R.J., Semerjian, H.G. 20th Symp. (Int.) on Combustion, 997 (1984).

Santoro, R.J., Miller, J.H., Langmuir 3, 244 (1987).

Sheppard, L.M. Adv. Mater. Proc. 4, 53 (1987).

Simpkins, P.G., Greenberg-Kosinski, S., MacChesney, J.B. J. Appl. Phys. 50, 5676 (1979).

Smith, F.N., Liu, J., Becker, A. Meyer, T.N. Aerosols '87 Pilat, M.J., Davis, E.J. eds., American Association for Aerosol Research, 143 (1987).

Solomon, D.H., Hawthorne, D.G. Chemistry of Pigments, Wiley, 1983.
Suyama, Y., Kato, A. J. Amer. Ceram. Soc. 59, 146 (1976).

Suyama, Y., Kato, A. J. Amer. Ceram. Soc. 68, C-154 (1985).

Ulrich, G.D., Combust. Sci. Technol. 4, 47 (1971).

Ulrich, G.D., Riehl, J.W. J. Colloid Interface Sci. 87, 257 (1982)

Ulrich, G.D., Subramanian, N.S. Combust. Sci. Technol. 17, 119 (1977).

Ulrich, G.D., Milnes, B.A., Subramanian, N.S. Combust. Sci. Technol. 14, 243 (1976).

Ulrich, G.D. Chem. Eng. News 62(32), 22 (1984).

Visca, M., Matijevic, E. J. Colloid Interface Sci. 68, 308 (1979).

Vogt, G.J., Phillips, D.S., Taylor, T.N. Ceramic Powder Science (Adv. in Ceramics) 21, 203 (1987).

Walker, K.L., Homsy, G.M., Geyling, F.T. J. Colloid Interface Sci. 69, 138 (1979).

Walker, K.L., Geyling, F.T., Nagel, S.R. J. Am. Ceram. Soc. 63, 552 (1980).

Wersborg, B.L., Howard, J.B., Williams, G.C. 14th Symp. (Intl) on Combustion, 929 (1972).

Wu, J.J., Flagan, R.C. J. Appl. Phys. 61, 1365 (1987).

Wu, J.J., Nguyen, H.V., Flagan, R.C. Langmuir 3, 266 (1987).

Young, R.M., Pfender, E., Plasma Chem. Plasma Process. 5, 1 (1985).

Yoshida, T., Akashi, K. Trans. Japan Instit. Metals 22, 371 (1981)

Coagulation of particles during long-range transport over sea

by

B. Schneider

"This manuscript was not made available for printing"

Summary of the final discussion

Summary of the Final Discussion of the Coagulation workshop

Coagulation process	Open problems	almost clarified
Brownian	Theory and experiments in the transition regime Experiments on non-equally sized particles Experiments on solid particles Coagulation of particles with unequal chemical composition Calibration of measuring instruments (e.g. CNC) Theory and experiments with irregular particles Experiments with highly concentrated aerosols and variable refractive index for monitoring by optical techniques Coalescence efficiency	Brownian coagulation in the limiting regimes Kn $\ll$ 1 (continuous) and Kn $>>$ 1 (free molecule) can be calculated and is understood. Discrepancies are still possible for the free-molecule regime. The Knudsen number Kn is not a feasible parameter to characterize coagulation in the free-molecule regime.
v. d. Waals	Much improved retardation treatment is necessary. V. d. Waals forces should more accurately be characterized by material properties like electrical and magnetic susceptibility. Local dissipation. Influence of size and shape on V. d. Waals forces is not yet understood.	Qualitative importance of forces on the coagulation rates in the free-molecule regime is agreed Free-molecule coagulation of electrolytes V. d. Waals interaction between completely characterized (e.g. known frequency dependent polarizability) materials can be calculated but not including size and shape effects.
Acoustic	Interaction between hydrodynamic and orthokinetic mechanism should be examined. Experimental data from in-situ measurements are necessary. AIT/hydrodynamic interaction.	AIT-initiation and characterization Orthokinetic mechanism (AIT = Acoustic Induced Turbulence)

Coagulation process	Open problems	almost clarified
Turbulence	Fill-up factor stochastic factor (non-uniformity of turbulence) collision efficiency	Energy dissipation rate as characteristic parameter
Other interaction forces	Electrostatic as well diffusiophoretic influence on coagulation rates should be examined to yield a solution for all boundary conditions.	
Gravitation	Analytical solution for cases with a Reynolds-number (R) of collecting particle in the order of $R \approx 1$ and $R > > 1$ are not yet available also if the ratio of particle radii r_2/r_1 is between 0.1 and 1. More experimental data for particles between 5 and 50 µm are necessary. Closed solution for whole particle size range is still missing.	For the case of $R < < 1$, $r_2 < < r_1$ and for spherical particles an analytical solution can be achieved. Qualitatively the process is also understood for the other range of R.
Shape factors	More information to the effects of shape factors on all types of coagulation processes are necessary. There is still no theory of shape factors available. Application of fractal analysis can possibly help to characterize particle shapes. Experiments (aerosol generation) can rarely be reproduced. No standards are available. Experiments with particles having a non-spherical but well-defined geometry.	Methods to measure shape factors are available Many values have been measured
General problems in Coagulation	Coagulation may be influenced by the flow characteristics. Coupled effects between coagulation and other aerosol processes. Coupling of different coagulation mechanisms.	

List of Participants

List of participants:

(1)	Barry, K.R.	NNC Ltd. Chelford Road Knutsford, Cheshire WA16 68Z United Kingdom
(2)	Boulaud, D.	IPSN/DPT/SPIN CEN-Fontenay-aux-Roses B.P: No. 6 F-92265 Fontenay-aux-Roses CEDEX
(3)	Bunz, H.	Kernforschungszentrum Karlsruhe LAF 1 Postfach 3640 D-7500 Karlsruhe 1
(4)	Egli, W.	ABB Forschungszentrum Ch-5400 Baden-Dättwill
(5)	Eliasson, B.	ASEA Brown Boveri Research Center (CRB) Ch-5404 Baden
(6)	Fißan, H.	Uni-Duisburg Bismarckstr. 90 D-4100 Duisburg
(7)	Holländer, W.	Fraunhofer-Institut f. Toxokologie u. Aerosolforschung Nikolai-Fuchs-Str. 1 D-3000 Hannover 61
(8)	Jonas, R.	Kernforschungszentrum Karlsruhe LAF 1 Postfach 3640 D-7500 Karlsruhe 1
(9)	Jordan, S.	Kernforschungszentrum Karlsruhe LAF 1 Postfach 3640 D-7500 Karlsruhe 1

(10)	Koch, W.	Fraunhofer-Institut f. Toxokologie u. Aerosolforschung Nikolai-Fuchs-Str. 1 D-3000 Hannover 61
(11)	Magill, J.	Europäisches Institut für Transurane Postfach 2340 D-7500 Karlsruhe 1
(12)	Majerowicz, A.	Institut für Experimentalphysik Universität Wien Strudlhofgasse 4 A-1090 Wien
(13)	Marlow, W.H.	Dept. of Nucl. Engineering Texas A & M University College Station, Texas USA 77843-3133
(14)	Mätzing, H.	Kernforschungszentrum Karlsruhe LAF 1 Postfach 3640 D-7500 Karlsruhe 1
(15)	Meier, U.	Kernforschungszentrum Karlsruhe LAF 1 Postfach 3640 D-7500 Karlsruhe 1
(16)	Metzig, G.	Kernforschungszentrum Karlsruhe LAF 1 Postfach 3640 D-7500 Karlsruhe 1
(17)	Miller, H.	Kernforschungszentrum Karlsruhe IRB Postfach 3640 D-7500 Karlsruhe 1

(18)	Mitchell, J.P.	Building A50/01 AEE Winfrith Dorchester Dorset DT2 80H, United Kingdom
(19)	Nichols, A.L.	Chemistry Division AEE Winfrith Dorchester Dorset DT2 80H, United Kingdom
(20)	Pickering, S.	Europäisches Institut für Transurane Postfach 2340 D-7500 Karlsruhe 1
(21)	Ramsdale, S.A.	SRD/UKAEA Wigshaw Lane Culcheth Warrinton WA3 4NE United Kingdom
(22)	Schikarski, W.	Kernforschungszentrum Karlsruhe LAF 1 Postfach 3640 D-7500 Karlsruhe 1
(23)	Schmidle, K.H.	ABB Forschungszentrum Ch-5400 Baden-Dättwill
(24)	Schmidt, H.	Kernforschungszentrum Karlsruhe IRB Postfach 3640 D-7500 Karlsruhe 1
(25)	Schmidt-Ott, A.	Uni-Duisburg Bismarckstr. 90 D-4100 Duisburg
(26)	Schneider, B.	GKSS-Forschungszentrum Geesthacht Max-Planck-Str. 1 D-2054 Geesthacht
(27)	Schöck, W.	Kernforschungszentrum Karlsruhe LAF 1 Postfach 3640 D-7500 Karlsruhe 1

(28)	Schrödel, E.	GRS Schwertnergasse 1 D-5000 Köln 1
(29)	Schwientek, G.	Babock-BSH Postfach 326 D-6430 Bad Hersfeld
(30)	Seidl, W.	Meteorologisches Insitut der Universität München Theresienstraße 37 D-8000 München 2
(31)	Shaw, D.T.	330 Bonner Hall State University of New York at Buffalo Laboratory for Power and Environmental Studies Amhert N.Y. 14051, USA
(32)	Smith, M.R.	NNC Ltd. Warrington Road Risley, Cheshire WA3 68Z, United Kingdom
(33)	Stauch, B.	Kernforschungsanlage Jülich ISF Postfach 1913 D-5170 Jülich
(34)	Spurny, K.R.	Fraunhofer-Institut D-5948 Schmallenberg 1
(35)	Vonka, V.	ECN P.O. Box 1 NL-1755 ZG Petten
(36)	Wagner, P.E.	Institut für Experimentalphysik Universität Wien Strudlhofgasse 4 A-1090 Wien

(37) Wagner-Ambs, M. Kernforschungszentrum Karlsruhe
LAF 1
Postfach 3640
D-7500 Karlsruhe 1